Central spin models: Quantum integrability and hyperfine induced spin dynamics

D I S S E R T A T I O N

zur Erlangung des
DOKTORGRADES DER NATURWISSENSCHAFTEN (DR. RER. NAT.)
der Fakultät für Physik
der Universität Regensburg

vorgelegt von

Björn Erbe

aus

Emden

im Jahr 2011

Die Arbeit wurde angeleitet von: Prof. Dr. John Schliemann
Das Promotionsgesuch wurde eingereicht am: 17.01.2011
Das Promotionskolloquium fand statt am: 20.7.2011

Prüfungsausschuß:

Vorsitzender:	Prof. Dr. Dominique Bougeard
1. Gutachter:	Prof. Dr. John Schliemann
2. Gutachter:	Prof. Dr. Jaroslav Fabian
weiterer Prüfer:	Prof. Dr. Vladimir Braun

Publication list

[1] B. Erbe and J. Schliemann
Perturbative regimes in central spin models
in preparation

[2] B. Erbe and J. Schliemann
Hyperfine induced electron spin and entanglement dynamics in double quantum dots: The case of separate baths
in preparation

[3] B. Erbe and J. Schliemann
Swapping and entangling hyperfine coupled nuclear spin baths
arXiv:1101.6011, submitted to Europhys. Lett.

[4] B. Erbe and J. Schliemann
Unexpected systematic degeneracy in a system of two coupled Gaudin models with homogeneous couplings
J. Phys. A: Math. Theor. **43**, 492002 (2010) (Fast Track Communication).

[5] B. Erbe and J. Schliemann
Different types of integrability and their relation to decoherence in central spin models
Phys. Rev. Lett. **105**, 177602 (2010).

[6] B. Erbe and J. Schliemann
Hyperfine induced spin and entanglement dynamics in double quantum dots: A homogeneous coupling approach
Phys. Rev. B **81**, 235324 (2010).

[7] B. Erbe and H.-J. Schmidt
Binary trees, coproducts, and integrability
J. Phys. A: Math. Theor. **43**, 085215 (2010).

Remarks: Publications [1]-[6] have been worked out during the PhD studies. Publications [3]-[6] are part of the present thesis.

Contents

1 Introduction

In 1896 Pieter Zeeman investigated the influence of a magnetic field on the spectral lines of sodium and found them to be broadened [1–3]. Using the laws of classical electrodynamics, Lorentz theoretically predicted a splitting of the spectral lines in triplets [4]. In 1902 Zeeman and Lorentz were jointly awarded the Nobel prize in physics for the discovery of this *Zeeman effect*. However, already in 1898 Preston, Michelson and Cornu had found further splittings in the spectral lines of sodium and cadmium, which could not be explained by the classical theory of Lorentz. The discovery of this *anomalous Zeeman effect* [4] can be regarded as the first experimental signature of one of the most fascinating intrinsic properties of a particle - *its spin*.

Further experimental evidence for the existence of the spin degree of freedom was provided in 1922 by the famous experiment of Stern and Gerlach [5, 6]. Here a beam of silver atoms is sent through an inhomogeneous magnetic field. The magnetic moment of the atoms couples to the magnetic field. Due to the inhomogeneity, the atoms experience a force deflecting their trajectory. Classically, the magnetic moment can have an arbitrary orientation. Consequently, a continuous distribution has to be expected on the detector. However, one finds two clearly separated peaks, as corresponding to the spin of the $5s$ electron of a silver atom.

The first theoretical treatment of the spin was provided by Pauli in 1927 [7]. However, it was Dirac who unveiled the full nature of the spin in 1928 by combining quantum mechanics with the special theory of relativity in what is known as the *Dirac equation* today [8, 9].

Since then, the spin degree of freedom has become subject to one of the broadest and most intensively studied fields of research in physics. The present thesis is part of this field and deals with so-called *central spin models*. The Hamiltonian of a general central spin model reads:

$$H_{\mathrm{CSM}} = \sum_{i=1}^{N_{\mathrm{c}}} \vec{S}_i \cdot \sum_{j=1}^{N} A_j^{(i)} \vec{I}_j + \sum_{i<j} J_{\mathrm{ex}}^{(ij)} \vec{S}_i \cdot \vec{S}_j \tag{1.1}$$

The first term describes the coupling of a set of N_{c} central spins $\vec{S}_i$ to a bath of N other spin degrees of freedom $\vec{I}_j$. The second term accounts for interactions within the system of central of spins. Often an additional Zeeman term

$$H_{\mathrm{z}} = B \sum_{i=1}^{N_{\mathrm{c}}} S_i^z \tag{1.2}$$

is considered, where we have assumed $\vec{B} = (0, 0, B)^T$ without loss of generality. Throughout the present thesis, we consider the spins to be dimensionless so that the coupling constants $A_j^{(i)}, J_{\mathrm{ex}}^{(ij)}$ and the parameter B have dimension of energy.

The interest in central spin models is threefold:

- The so-called Liouville-Arnol'd theorem of classical mechanics states that if a Hamiltonian system with n degrees of freedom has n involutive integrals of motion which are functionally independent, its Hamiltonian equations of motion can be solved via quadratures [10]. Such a system is called *integrable*. Despite for huge effort, so far it has not been achieved to adapt the concept of integrability to the quantum mechanical framework satisfactorily. Apart from being of high interest on its own right, a quantum mechanical notion of integrability could eventually lead to a better understanding of quantization [11].

  Central spin models came into the focus of the field of quantum integrability with the work of Gaudin, published in the early seventies [12]. He demonstrated that for central spin models with a single central spin only, today known as the Gaudin model, the problem of finding the eigenstates and eigenvalues can be reduced to the solution of set of coupled non-linear equations. The existence of such a *Bethe ansatz* [13–17] is one of the commonly accepted definitions of quantum integrability. Since Gaudin's seminal contributions, it has turned out that central spin models offer one of the few playgrounds to study *all* aspects of quantum integrability known so far and, in particular, their relation. This has the potential to eventually lead to an, at least, more comprehensive understanding of quantum integrability. If there is no danger of confusion or the need to stress the quantum mechanical context, in the remainder of the present thesis we refer to quantum integrability simply as integrability.

- In quantum mechanics the state of a physical system is not unique. If a system for example has two possible states, it can not only be in the one or the other but also in both of them at the same time. Having such a two level system in mind, it is a somewhat intuitive idea to use this quantum mechanical property for computational tasks. About 15 years ago, the first important examples of *quantum algorithms* came up and demonstrated that operations of key importance can be carried out amazingly fast employing quantum mechanics [18–20]. Immediately, the implementation of quantum algorithms became subject to enormous theoretical as well as experimental effort. The central challenge in this context results from the fact that physical systems are typically not well-isolated from their environment. However, the interaction with the environmental degrees of freedom destroys the superposition of states described above. This process is called *decoherence*.

  As a natural two level system, a spin of length (1/2) is an obvious candidate for serving as the quantum bit ("qubit"). One of the most promising approaches in this context was proposed by Loss and DiVincenzo in 1998, suggesting to use the spin of electrons confined in semiconductor quantum dots as qubits [21]. Here a decohering environment is constituted by the nuclear spins of the host material. These interact with the spins utilized as the qubits via the *hyperfine interaction*, which is described by a Hamiltonian of central spin type [22, 23]. However, in recent years the idea gained importance to turn vice into virtue by regarding the hyperfine interaction in semiconductor quantum dot spin qubits as a way to efficiently access the nuclear spins. Indeed, it more and more turns out that totally new solid state quantum information perspectives arise from the hyperfine interaction [24–29].

  In both of these contexts it is of key interest to understand the hyperfine induced spin

dynamics. Here it has to be distinguished between the case of a strong and the case of a weak magnetic field (1.2) as compared to the strength of the hyperfine interaction. The first case has been investigated intensively and is well-understood to a large extent [30–35]. However, it is still an unsolved problem how to treat the weak field limit correctly [36, 37].

- As indicated in the first point, there are various notions of quantum integrability. However, what they all have in common is that they are associated with strong and scarce mathematical properties. It is therefore highly interesting to investigate how integrable quantum models differ from those which are non-integrable or, in other words, to which extent physical properties are determined by the integrability of the respective models. In recent years, various results have been presented, relating integrability to transport properties [38, 39], to quantum phase transitions [40] and, in particular, to decoherence properties [41–46].

To varying degrees, all of the aforementioned aspects are subject to the present thesis. In the first part we focus on the first and the last point of the above list and investigate very basic properties of central spin models on an abstract level. In Chapter 2 we give a brief introduction to the field of integrability and review some results concerning central spin models, which are of importance for the following considerations. Then, in Chapter 3, we introduce a new, or rather enhanced, notion of quantum integrability. From this we derive an explicit and, to a certain extent, analytical relation between integrability and decoherence for central spin models with more than a single central spin. This result is not only of direct interest but also justifies the newly introduced definition of quantum integrability. Here, as throughout the thesis, it is the decay of the components of $\left\langle \vec{S}_i(t) \right\rangle$ which is analyzed in order to describe the decoherence process [36, 37, 47]. In Chapter 4 we specify a model of two coupled Gaudin models with all coupling constants being equal to each other ("homogeneous"), which we revisit in the second part of the thesis. We numerically study the spectral properties of the model and find the spectrum to exhibit systematically degenerate multiplets. Systematic degeneracies are extremely scarce. Hence, the result is interesting on its own right. Apart from that, we briefly discuss possible applications in solid state quantum information processing. The degenerate subspace is constructed analytically.

After studying basic properties of central spin models in the first part of the thesis, the second part is devoted to concrete physical considerations in the context of solid state quantum information processing. Here we consider two exchange coupled electron spins confined in semiconductor quantum dots and evaluate the hyperfine induced spin dynamics for the case of a weak magnetic field applied to the electron spins. As so far no well-controlled perturbative treatments are known for this limit, we focus on the special case of a *zero* magnetic field and resort to *exact* methods. In Chapter 5 we briefly introduce the hyperfine interaction and its role in the context of solid state quantum information processing using quantum dot spin qubits. Then, in Chapter 6, we consider the two exchange coupled electron spins to interact with the *same* bath of nuclear spins via homogeneous couplings. We then investigate analytically the electron spin and entanglement dynamics. In particular we derive a scaling law for the decoherence time. In Chapter 7 we come back to the two bath model introduced in Chapter 4. Here we try to turn vice into virtue by investigating to what extent it is possible to swap and entangle the two nuclear spin baths. From this point of view the two electron spins act as an effective coupling between the baths. We consider the two baths to be strongly polarized in opposite directions initially and then analyze under

which circumstances the magnetization of each bath is reversed. Surprisingly, it turns out that a nuclear swap is possible for *weakly coupled* nuclear spin baths of *realistic size*, but not for smaller ones. We indicate that under the same circumstances it should also be possible to fully entangle the baths. Interestingly, there is clear evidence that the occurrence of systematically degenerate multiplets, described in Chapter 4, has a dynamical signature.

The results of the second part of the present thesis give the first detailed study of the hyperfine induced spin dynamics in a weak magnetic field situation. In particular they do not only refer to the adverse aspects of the hyperfine interaction but also give a clear impression to what extent it is possible to *use* it as a resource of solid state quantum information processing. We close the thesis with a summary and an outlook on further important questions.

Part I

Quantum integrability and its relation to physical properties

2 Basics of central spin models

In the preceding chapter we introduced the so-called central spin models. Following the outline presented there, in the first part of this theses we focus on central spin models from a rather abstract point of view and investigate very basic properties. In a first step, presented in Chapter 3, we investigate in detail their integrable structure and relate our findings to the physical phenomenon of decoherence. Then, in Chapter 4, we consider a special example of a central spin model, consisting of two coupled Gaudin models with homogeneous couplings. We numerically and analytically study the spectral properties of the model and find a new example for a systematic degeneracy.

In the next three sections we briefly present basics, necessary for the following considerations. We begin with the background for Chapter 3. In Section 2.1 we point out the lack of a clear mathematical definition of quantum integrability and introduce the Bethe ansatz for the Gaudin model as one of the commonly accepted approaches to integrability in the quantum mechanical framework. In Section 2.2 we then review random matrix theory as a tool to detect the existence of a Bethe ansatz. Finally, in Section 2.3 we revisit the systematic degeneracy of the hydrogen atom as an interesting preliminary with respect to the results to be presented in Chapter 4.

2.1 Quantum integrability and the Bethe ansatz for the Gaudin model

The Liouville-Arnol'd theorem states that if a system with n degrees of freedom has n involutive integrals of motion which are functionally independent, its Hamiltonian equations of motion are solvable via quadratures [10]. Such a system is called integrable. As already mentioned in the introduction, despite for huge effort, so far it has not been achieved to adapt the concept of integrability to the quantum mechanical framework satisfactorily. At the present time there are two commonly accepted definitions: A quantum mechanical system is called integrable (i) if there is a Bethe ansatz [13–17] or (ii) if the system has a complete set of commuting operators [48–52] sharing "suitable" properties (to be further explained in Chapter 3). Note that integrability in classical mechanics does not require the solvability of the quadratures. In this sense both of the aforementioned approaches are in direct analogy with classical mechanics.

In the following we introduce the Bethe ansatz for the Gaudin model, which is an important preliminary for the next chapters. As explained in Chapter 1, the Gaudin model corresponds to the Hamiltonian (1.1) for $N_\mathrm{c} = 1$ and explicitly reads

$$H_\mathrm{G} = \vec{S} \cdot \sum_{j=1}^{N} A_j \vec{I}_j, \tag{2.1}$$

where $\vec{S}$ denotes the central spin and $\vec{I}_j$ denote the bath spins. The spin lengths S and I_j are arbitrary.

There are two approaches to the Bethe ansatz. The original one, introduced by Bethe for the XXX-Heisenberg chain [13, 14], today is referred to as the *coordinate* Bethe ansatz. Here a parameter-dependent ansatz for creation and annihilation operators relative to a known eigenstate, usually called the pseudo vacuum, is made. Then the parameters, the so-called Bethe ansatz roots, are determined so that successive application of the creation and annihilation operators to the pseudo vacuum produces the whole set of eigenstates. This is done by the elimination of "unwanted terms", which are non-eigenstate contributions coming from the application of the Hamiltonian. The resulting relations for the Bethe ansatz roots are referred to as the Bethe ansatz equations. In this procedure the ansatz for the creation and annihilation operators has to be guessed. The *algebraic* Bethe ansatz [15–17] now systemizes this guessing by interpreting the off-diagonal elements of the so-called monodromy matrix as the creation and annihilation operators. Drinfel'd embedded this approach in a mathematical framework, which led to the development of quantum group theory [53, 54]. This seminal work earned him the Fields medal in 1990 [55].

The pseudo vacuum for the Gaudin model is given by the highest weight vector $|0\rangle = |S\rangle|I_1 \dots I_N\rangle$. Here we used the notation $|S, m_S\rangle = |m_S\rangle$, with m_S being the S^z quantum number, and analogously for I_j, which is considered throughout the present thesis. The ansatz for the respective annihilation operators reads:

$$F(\omega) = \omega S^- + \sum_{j=1}^{N} \frac{A_j \omega}{A_j - \omega} I_j^- \tag{2.2}$$

For the related algebraic Bethe ansatz the reader is referred to Reference [17]. The eigenstates of the Gaudin model result from the operator (2.2) as

$$\begin{aligned} |N_\mathrm{D}\rangle &= \prod_{i=1}^{N_\mathrm{D}} F(\omega_i)|0\rangle \\ &= \prod_{i=1}^{N_\mathrm{D}} \left(\omega_i S^- + \sum_{j=1}^{N} \frac{A_j \omega_i}{A_j - \omega_i} I_j^- \right) |0\rangle \end{aligned} \tag{2.3}$$

and the eigenvalues are given by

$$E\left(\{\omega_1, \dots, \omega_{N_\mathrm{D}}\}\right) = -S \sum_{i=1}^{N_\mathrm{D}} \omega_i + S \sum_{j=1}^{N} I_j A_j. \tag{2.4}$$

The Bethe ansatz equations, determining the Bethe ansatz roots ω_i, then read:

$$S + \sum_{j=1}^{N} \frac{A_j I_j}{A_j - \omega_i} - \sum_{k=1, k\neq i}^{N_\mathrm{D}} \frac{\omega_k}{\omega_k - \omega_i} = 0 \tag{2.5}$$

Here N_D is the number of spin flips compared to $|0\rangle$. The proof of Equation (2.5) is presented in excellent form in References [12, 56]. In the following we therefore only very briefly illustrate the elimination of the unwanted terms for the case $N_\mathrm{D} = 1$, which is of particular importance in the following chapter.

The state $|1\rangle = F(\omega)|0\rangle$ explicitly reads:

$$|1\rangle = \omega\sqrt{2S}|S-1\rangle|I_1 \dots I_N\rangle + \sum_{j=1}^{N} \frac{A_j\omega}{A_j-\omega}\sqrt{2I_j}|S\rangle|I_1 \dots (I_j-1)\dots I_N\rangle \tag{2.6}$$

The rather cumbersome expression resulting from the application of the Hamiltonian (2.1) to the state (2.6) can be rewritten in the following form:

$$H_{\mathrm{G}}|1\rangle = \left(-S\omega + S\sum_{j=1}^{N} A_jI_j\right)|1\rangle \tag{2.7}$$

$$+ \underbrace{\left(\omega^2 S\sqrt{2S} + \omega^2\sqrt{2S}\sum_{j=1}^{N}\frac{A_jI_j}{A_j-\omega}\right)|S-1\rangle|I_1 \dots I_N\rangle}_{\text{unwanted terms}} \tag{2.8}$$

Obviously, $|1\rangle$ is an eigenstate of H_{G} provided the Bethe ansatz root ω is chosen in a way that the unwanted terms vanish. This yields the relation

$$S + \sum_{j=1}^{N}\frac{A_jI_j}{A_j-\omega} = 0, \tag{2.9}$$

which is exactly Equation (2.5) for the case $N_{\mathrm{D}} = 1$. It is important to note that the Bethe ansatz also works if a Zeeman term H_{Z}, as given in Equation (1.2), is added to H_{G}. Applying H_{Z} to $|1\rangle$, we get:

$$BS^z|1\rangle = BS|1\rangle \underbrace{-\sqrt{2S}\omega B|S-1\rangle|I_1 \dots I_N\rangle}_{\text{unwanted terms}} \tag{2.10}$$

Hence, adding $(-B/\omega)$ to Equation (2.9) yields the Bethe ansatz equation for the Hamiltonian $(H_{\mathrm{G}} + H_{\mathrm{Z}})$ on the subspace $N_{\mathrm{D}} = 1$, which generalizes to $(-B/\omega_i)$ in Equation (2.5). Interestingly, Gaudin also defined operators

$$H_i = A_i\vec{S}\cdot\vec{I}_i - \sum_{j=1,j\neq i}^{N}\frac{A_iA_j\vec{I}_i\cdot\vec{I}_j}{A_i-A_j} \tag{2.11}$$

for $i = 1, \dots N$ which together with H_{G} form a complete set of commuting operators. That the Hamiltonian (2.1) and the operators (2.11) are indeed mutually commuting can be verified by direct calculation. As most of the related reviews and publications omit an explicit proof, we briefly sketch it here. In order to abbreviate the calculations, in the following expressions we denote $\vec{S} = \vec{S}_1$ and

$$\vec{I}_j = \vec{S}_{N_{\mathrm{c}}+j} \tag{2.12a}$$

$$A_j = A_{N_{\mathrm{c}}+j}. \tag{2.12b}$$

Here we referred to an arbitrary number of central spins because the notation (2.12) is applied a second time in Chapter 3. If we set $A_1 = \infty$, the Hamiltonian (2.1) can be included in the set (2.11) up to a trivial minus sign. Explicitly the operators read:

$$H_i = \sum_{j\neq i}\frac{A_iA_j\vec{S}_i\cdot\vec{S}_j}{A_j-A_i} \tag{2.13}$$

We now have to evaluate the commutator

$$[H_k, H_l] = \sum_{m\neq k}\sum_{n\neq l} \frac{A_k A_m}{A_m - A_k}\frac{A_l A_n}{A_n - A_l}\left[\vec{S}_k\cdot\vec{S}_m, \vec{S}_l\cdot\vec{S}_n\right]. \tag{2.14}$$

Using the operator identity

$$[A\cdot B, C] = A\cdot[B,C] + [A,C]\cdot B, \tag{2.15}$$

we get

$$\begin{aligned}
[H_k, H_l] &= \sum_{n\neq l} \frac{A_k A_l}{A_l - A_k}\frac{A_l A_n}{A_n - A_l}\varepsilon_{abc} S_k^a \cdot S_l^c \cdot S_n^b && \text{(2.16a)}\\
&+ \sum_{n\neq k,l} \frac{A_k A_n}{A_n - A_k}\frac{A_l A_n}{A_n - A_l}\varepsilon_{abc} S_k^b \cdot S_l^a \cdot S_n^c && \text{(2.16b)}\\
&+ \sum_{n\neq k} \frac{A_k A_l}{A_k - A_l}\frac{A_k A_n}{A_n - A_k}\varepsilon_{abc} S_k^c \cdot S_l^b \cdot S_n^a, && \text{(2.16c)}
\end{aligned}$$

where ε_{abc} denotes the Levi-Cevita symbol and we used the Einstein notation. Noting that

$$\varepsilon_{abc} S_k^a \cdot S_l^c \cdot S_k^b + \varepsilon_{abc} S_l^b \cdot S_k^c \cdot S_l^a = 0, \tag{2.17}$$

it is possible to exclude the case $n = k$ in the sum (2.16a) and $n = l$ in the sum (2.16c) so that we can rewrite Equation (2.16) as a single sum:

$$\begin{aligned}
[H_k, H_l] &= \sum_{n\neq k,l} \left[\frac{A_k A_l^2 A_n}{(A_k - A_l)(A_l - A_n)} - \frac{A_k^2 A_l A_n}{(A_k - A_l)(A_k - A_n)}\right.\\
&+ \left.\frac{A_k A_l A_n^2}{(A_k - A_n)(A_n - A_l)}\right]\varepsilon_{abc} S_k^a \cdot S_l^c \cdot S_n^b. && \text{(2.18)}
\end{aligned}$$

It is now easy to see that the term in brackets is equal to zero for any choice of the coupling constants A_j.

2.2 Quantum integrability and random matrix theory

In statistical mechanics physical quantities are calculated as the average over an ensemble of systems governed by the same Hamiltonian, but with different initial states. However, there are situations in which e.g. not even the Hamiltonian is known. The concept of random matrix theory was introduced by Wigner in 1951 as an approach to solve problems like these in the context of nuclear physics [57–59]. In contrast to statistical mechanics, here ensembles of Hamiltonians, represented by hermitian matrices with random entries, are considered. It is by no means obvious how to realize this concept. In the following we consider what is today referred to as the classical random matrix theory. The classical random matrix theory is based on the observation that Hamiltonians can be divided into three groups:

1. Time-reversal invariant systems with rotational symmetry and time-reversal invariant systems with integer spin and broken rotational symmetry
2. Systems with broken time-reversal symmetry
3. Time-reversal invariant systems with half-integer spin and broken rotational symmetry

In Case 1 there are basis systems (*apart* from the system of eigenstates) with respect to which the Hamiltonian matrices are real and symmetric, whereas in Case 3 basis systems can be chosen so that the Hamiltonian matrices are quaternion real (for details the reader is referred to References [58, 59]). We denote the set of real and symmetric matrices by $\mathcal{M}_1$, the set of hermitian matrices by $\mathcal{M}_2$ and the set of quaternion real matrices by $\mathcal{M}_3$. The subset of unitary transformations which satisfy $\mathcal{M}_{1,3} \to \mathcal{M}_{1,3}$ are the orthogonal or symplectic transformations respectively.

The classical ensembles are now defined as tuples $(\mathcal{M}_i, P_i)$, where $P_i : \mathcal{M}_i \to [0,1]$ are probability densities. The probability densities are arbitrary, up to the requirement of invariance under orthogonal, unitary and symplectic transformations, respectively. Here invariance means that two matrices A and A' which are related due to $A' = T^+AT$, with T being one of the aforementioned transformations, have to be assigned the same probability $P_i(A)dA = P_i(A')dA'$. This is clear because the two matrices A and A' have to be considered as representations of the *same* Hamiltonian with respect to different basis systems. Usually the probability distributions P_i are chosen as simple Gaussian distributions with parameters depending on the different cases $i = 1, 2, 3$. With respect to this choice the three cases are referred to as the Gaussian orthogonal ensemble, the Gaussian unitary ensemble and the Gaussian sympletic ensemble, respectively.

It is now a natural question about which quantities random matrix theory can produce meaningful results. In other words: Which are the properties of the set of matrices $\mathcal{M}_i$ that are generic with respect to the associated set of physical systems given by Case i *and* independent of the concrete choice of the probability density P_i? Usually these properties are called universal. It is assumed that average properties are not universal, whereas fluctuations are. Indeed, random matrix theory turned out to be extremely successful in describing fluctuations.

Since its beginning in the fifties, random matrix theory has undergone substantial progress, eventually leading to totally new fields of research. Beyond the most remarkable developments is the relation between spectral statistics and integrability. Here one has to distinguish between "quantum signatures of chaos" and "quantum chaos". The basis of the first field is the so-called Bohigas-Giannoni-Schmidt conjecture [57, 59, 60]. It roughly states that the so-called nearest-neighbor level distribution, which is further explained below, of a system with an integrable classical analogue follows a Poisson distribution, whereas the statistics of a model with a non-integrable classical counterpart exhibits level repulsion towards the result associated with the respective Gaussian ensemble. The second approach utilizes the same argument for the existence of a Bethe ansatz [42–44, 61]. Neither of the two conjectures has been proven, still both of them yield excellent results, which suggests that they are closely related to each other. In the following we entirely focus on the second approach and review some recent results for central spin models presented in Reference [61]. These are of crucial importance for the work presented in the following section.

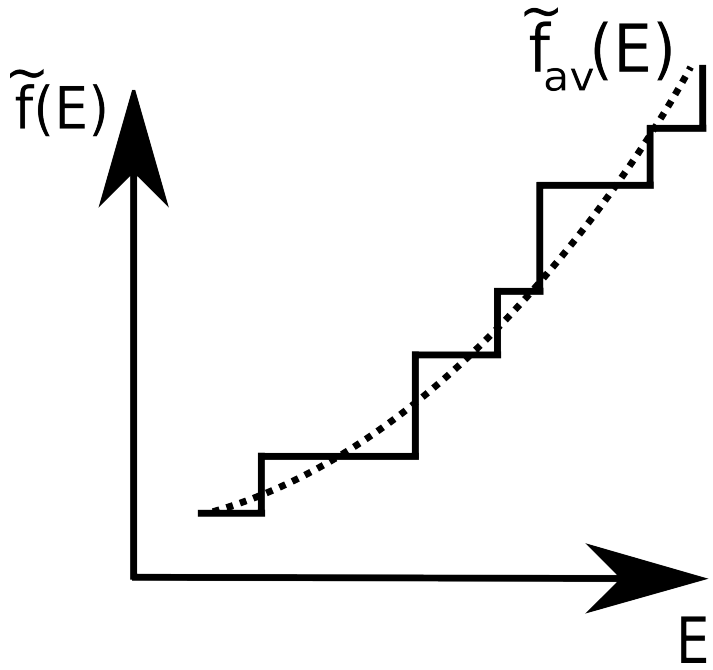

Figure 2.1: Sketch of the cumulative spectral function $\tilde{f}(E)$. The cumulative spectral function results from the integration of the spectral function $f(E)$. As $f(E)$ is a product of Dirac delta distributions, $\tilde{f}(E)$ is a step function. It fluctuates around a smooth function $\tilde{f}_{\mathrm{av}}(E)$, depicted by the dotted line. Within the unfolding procedure this smooth part is linearized, yielding a constant mean level density.

Here the Hamiltonian (1.1) is investigated for $J_{\mathrm{ex}}^{(ij)} = 0$ and $S_i = I_j = 1/2$. A large number of random realizations of the coupling constants is considered. For each realization the coupling constants are chosen from a uniform distribution in $[0, 1]$ and normalized afterwards $\sum_{j=1}^{N} A_j^i = 1$. Obviously, the Hamiltonian (1.1) conserves the total spin $\vec{J} = \vec{S} + \vec{I}$ with $\vec{S} = \sum_{i=1}^{N_{\mathrm{c}}} \vec{S}_i$ and $\vec{I} = \sum_{i=1}^{N} \vec{I}_j$. The eigenvalues are calculated on subspaces of fixed J via exact numerical diagonalization. Here J is the quantum number associated with $\vec{J}^2$. Then the nearest-neighbor level distribution, denoted by $p(s)$, is calculated as an average over the nearest-neighbor level distributions of all the realizations. The nearest-neighbor level distribution gives the probability of two consecutive energy levels having a distance s from each other.

In this context we have to keep in mind that random matrix theory is only significant with respect to fluctuations. In order to compare the results of the above approach with the random matrix theory predictions, the fluctuations of the spectra have to be isolated. This procedure is usually referred to as the unfolding. To this end the spectral function is defined

$$f(E) = \prod_{i=1}^{\dim(\mathcal{H})} \delta(E - E_i), \tag{2.19}$$

where $\dim(\mathcal{H}) = 2^{N_{\mathrm{c}}+N}$ denotes the dimension of the Hilbertspace, $\delta(E)$ is the Dirac delta distribution and E_i are the energy eigenvalues. The spectral function integrated due to

$$\tilde{f}(E) = \int_{-\infty}^{E} dE' f(E') \tag{2.20}$$

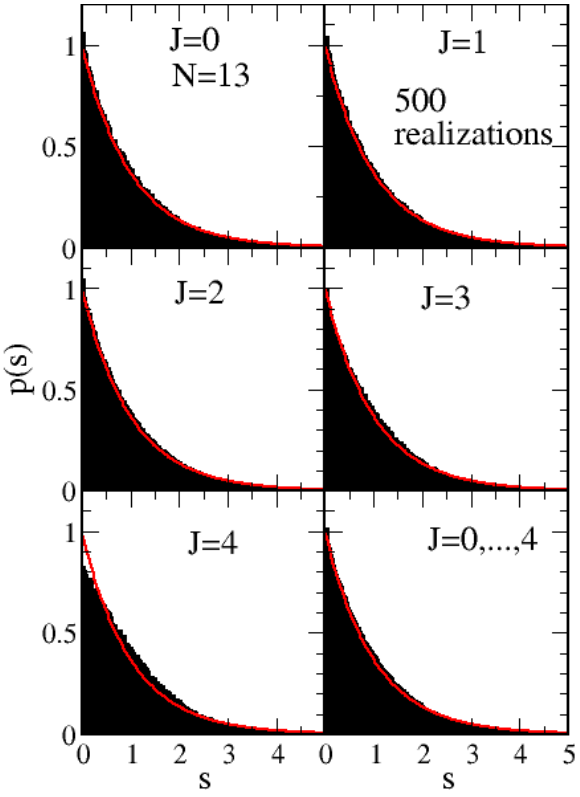

Figure 2.2: Nearest-neighbor level distributions $p(s)$ for 500 realizations of the Gaudin Hamiltonian (2.1) with $S_i = I_j = 1/2$. The number of bath spins is $N = 13$. The coupling constants are chosen from a uniform distribution in $[0, 1]$ and are normalized afterwards $\sum_{j=1}^{N} A_j^i = 1$. The different panels show the distributions for different subspaces of fixed J. In the bottom right panel all distributions are joined together. As expected for a model with a Bethe ansatz, the distributions clearly follow a Poisson distribution, marked by the red line. Reprinted figure with permission from [61]. Copyright (2010) by the American Physical Society.

is called the cumulative spectral function. As the spectral function is a product of Dirac delta distributions, $\tilde{f}(E)$ is a step function. In Figure 2.1 this step function is depicted schematically. Obviously, $\tilde{f}(E)$ can be decomposed in a smooth part $\tilde{f}_{\mathrm{av}}(E)$ and a fluctuating contribution $\tilde{f}_{\mathrm{fl}}(E)$:

$$\tilde{f}(E) = \tilde{f}_{\mathrm{av}}(E) + \tilde{f}_{\mathrm{fl}}(E) \tag{2.21}$$

If the energy eigenvalues are now rescaled due to $E_i \to s_i = \tilde{f}_{\mathrm{av}}(E_i)$ (obviously yielding a dimensionless variable), the smooth part of the transformed cumulative spectral function $\tilde{f}(s)$ simply reads $\tilde{f}_{\mathrm{av}}(s) = s$. Hence, the average level density, resulting as the derivative of $\tilde{f}_{\mathrm{av}}(s)$, is constant. This means that the rescaled spectrum only contains fluctuations. Decomposing $\tilde{f}(E)$ as given in Equation (2.21) is a non-trivial task in general. However, the numerical data presented below has turned out to be qualitatively invariant towards the concrete choice of the unfolding procedure.

In Figure 2.2 the nearest-neighbor distribution $p(s)$ is plotted for 500 realizations of the Gaudin model (2.1) with $N = 13$ bath spins. Subspaces of different total spin squared J are considered. In the bottom right panel the distributions of the different subspaces are joined together [57]. As expected for a model with a Bethe ansatz, $p(s)$ follows a Poisson

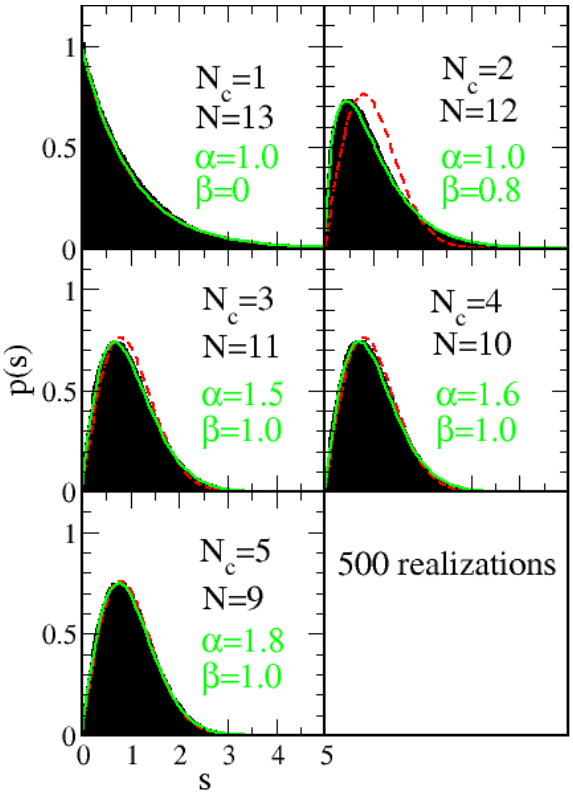

Figure 2.3: Joint nearest-neighbor level distributions $p(s)$ for 500 realizations of the Hamiltonian (1.1) with $S_i = I_j = 1/2$ and $J_{\mathrm{ex}}^{(ij)} = 0$. Different numbers of central spins N_{c} are considered. The total number of spins is fixed to $N_{\mathrm{c}} + N = 14$. The coupling constants are chosen from a uniform distribution in $[0, 1]$ and are normalized afterwards $\sum_{j=1}^{N} A_j^i = 1$. The red dotted curves show the Wigner surmise. With increasing N_{c} the distributions clearly approach the Wigner surmise. This indicates that for central spin models with more than a single central spin no Bethe ansatz exists. The transition from the Poisson distribution for $N_{\mathrm{c}} = 1$ to the Wigner surmise for $N_{\mathrm{c}} = 5$ is quantified by fits to a generalized Brody distribution with parameters α and β. Reprinted figure with permission from [61]. Copyright (2010) by the American Physical Society.

distribution as given by the red curve. Representing the Hamiltonian (1.1) with respect to the standard product basis $|S_1^z \dots S_{N_c}^z\rangle|I_1^z \dots I_N^z\rangle$ yields real and symmetric matrices. Consequently, in the non-integrable case the nearest-neighbor level distribution is expected to follow the distribution corresponding to the Gaussian orthogonal ensemble, called Wigner surmise. In Figure 2.3 the joint level distributions are shown for an increasing number of central spins. Obviously, $p(s)$ approaches the Wigner surmise with increasing N_c. For five central spins $p(s)$ already nearly perfectly coincides with the Wigner surmise.

The data presented in Figures 2.2 and 2.3 clearly indicate that there is no Bethe ansatz for central spin models with more than a single central spin. As mentioned above, this result is of great importance in what follows.

2.3 Degeneracies and symmetries: The hydrogen atom revisited

It is well-known that the energy levels of a quantum system usually tend to repel each other and degeneracies are exceptional events [62]. Hence, there are only extremely few examples of systems with degenerate eigenstates and *even less*, whose eigenstates are *systematically* degenerate. Systematic degeneracies result from the symmetries of the model. Let us for example consider a Hamiltonian H having two symmetries A and B, which do not commute with each other. The common eigenstates of either H and A or H and B can be labeled by the eigenvalues and we e.g. have $H|E,a\rangle = E|E,a\rangle$ with a being some eigenvalue of A. Now obviously $HB|E,a\rangle = EB|E,a\rangle$ with $|E,a\rangle$ and $B|E,a\rangle$ being linearly independent as $[A,B] \neq 0$, which means that there is some higher dimensional degenerate subspace [63]. If the operators A and B commute with each other, it is not necessary but still possible that the spectrum of the Hamiltonian exhibits degeneracies. Famous examples for systems with systematic degeneracies are given by the hydrogen atom [64], the n-dimensional harmonic oscillator [65], and the Haldane-Shastry model [48, 66]. In all three cases the degeneracies are due to hidden symmetries requiring a dedicated analysis. In the following we briefly review the degeneracies of the hydrogen atom, which are interesting with respect to the results presented in Chapter 4.

The Hamiltonian of the hydrogen atom reads

$$H_{\mathrm{H}} = \frac{\vec{p}^{\,2}}{2m_{\mathrm{e}}} - \frac{1}{4\pi\varepsilon_0}\frac{e^2}{r}, \tag{2.22}$$

where $\vec{p}$ denotes the momentum operator and m_{e} is the electron rest mass. The charge of the electron is denoted by $(-e)$ and ε_0 is the electric constant. This Hamiltonian can be rewritten in terms of the orbital angular momentum $\vec{L}$:

$$H_{\mathrm{H}} = -\frac{\hbar^2}{2m_{\mathrm{e}}}\frac{1}{r^2}\partial_r\left(r^2\partial_r\right) + \frac{1}{2m_{\mathrm{e}}r^2}\vec{L}^{\,2} - \frac{1}{4\pi\varepsilon_0}\frac{e^2}{r} \tag{2.23}$$

Note that $\vec{L}^{\,2}$ has exclusively angular dependence. The common eigenfunctions of $\vec{L}^{\,2}$ and L^z are the spherical harmonics $Y_{Lm_L}(\vartheta,\varphi)$, where L denotes the $\vec{L}^{\,2}$ and m_L is the L^z quantum number. Using a separation ansatz consisting of $Y_{Lm_L}(\vartheta,\varphi)$ and a radial function $u = u(r)$ yields an equation for $u(r)$ alone - the radial equation. This is solved by a power series ansatz, provided it is truncated after some finite order. If the respective order is denoted by

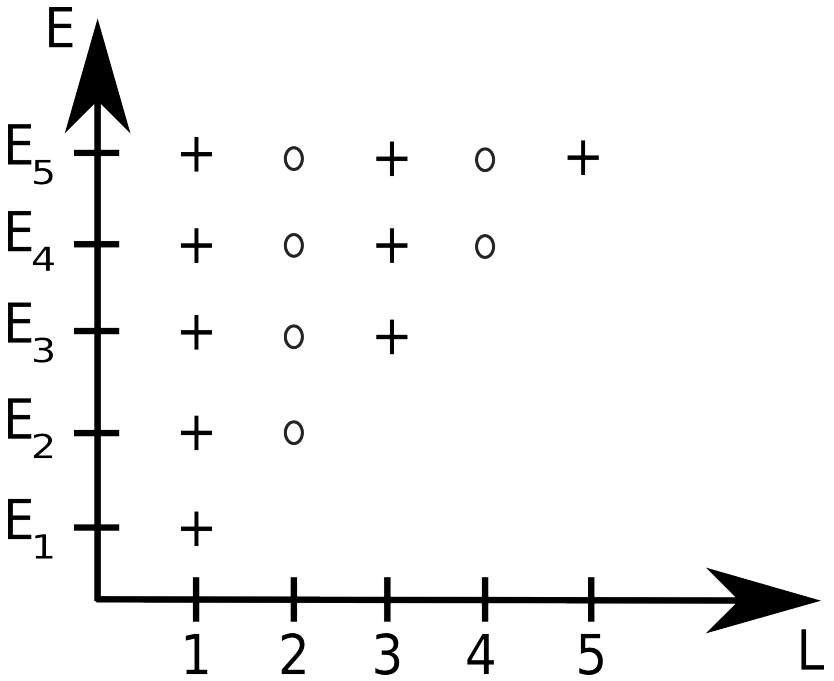

Figure 2.4: Sketch of the hydrogen spectrum. The eigenenergies are plotted against L. The cross (circle) indicates positive (negative) parity of the respective multiplet. The spectrum exhibits degenerate multiplets of consecutive angular momentum L and alternating parity. These "accidental" degeneracies result from the quantum mechanical Runge-Lenz vector $\vec{R}$.

i_{trunc}, we get

$$n = i_{\mathrm{trunc}} + l + 1 = l + 1, l + 2, l + 3 \ldots \tag{2.24}$$

and consequently

$$E_n = -\frac{E_{\mathrm{R}}}{n^2} \tag{2.25}$$

with E_{R} being the Rydberg energy. Obviously, the energy eigenvalues do not depend on L so that the spectrum, schematically shown in Figure 2.4 as a plot against L, exhibits the well-known degeneracies. Let $\tau_{\vec{r}}$ denote the inversion operator $\psi(\vec{r}) \to \psi(-\vec{r})$. Obviously, $\tau_{\vec{r}}$ has the eigenvalues (± 1), to which we refer as positive (negative) parity. In polar coordinates the inversion reads $r \to r, \theta \to \pi - \theta, \phi \to \pi + \phi$ [63]. Consequently, the parity of a multiplet is exclusively determined by the parity of $Y_{Lm_L}(\vartheta, \varphi)$. Here one finds:

$$\tau_{\vec{r}} \cdot Y_{Lm_L}(\vartheta, \varphi) = (-1)^L Y_{Lm_L}(\vartheta, \varphi) \tag{2.26}$$

In Figure 2.4 the cross (circle) indicates positive (negative) parity of the respective multiplet. Obviously, the spectrum shows degenerate multiplets of consecutive angular momentum L and alternating parity.

For a long time this degeneracy was believed to be accidental, meaning not to depend on any symmetry. However, Pauli demonstrated that there is a hidden symmetry [64], which is given by the direct quantum mechanical analogue of the Runge-Lenz vector:

$$\vec{R} = \frac{1}{2m_{\mathrm{e}}} \left(\vec{p} \times \vec{L} - \vec{L} \times \vec{p} \right) - \frac{1}{4\pi\varepsilon_0} e^2 \frac{\vec{r}}{r} \tag{2.27}$$

This makes the symmetry group of the hydrogen Hamiltonian into $SO(4)$ and yields the "accidental" degeneracies of the Hamiltonian. As usually not considered in standard textbooks, we briefly demonstrate that $\vec{R}$ commutes with H_{H}. Using (2.15), in a first step we note that

$$\begin{aligned}\left[\vec{L}^{\,2}, p_i\right] &= [L_j \cdot L_j, p_i] \\ &= i\hbar\left(\varepsilon_{jik} L_j \cdot p_k + \varepsilon_{jik} p_k \cdot L_j\right) \\ &= i\hbar\left(-\varepsilon_{ijk} L_j \cdot p_k + \varepsilon_{ikj} p_k \cdot L_j\right). \end{aligned} \tag{2.28}$$

Hence, $\vec{R}$ can be rewritten as

$$\vec{R} = \frac{\left[\vec{L}^{\,2}, \vec{p}\right]}{2 i m_{\mathrm{e}} \hbar} - \frac{1}{4\pi\varepsilon_0} e^2 \frac{\vec{r}}{r}. \tag{2.29}$$

Using again (2.15) and

$$[H_{\mathrm{H}}, \vec{p}] = \frac{1}{4\pi\varepsilon_0} e^2 i\hbar \frac{\vec{r}}{r^3}, \tag{2.30}$$

it follows with (2.23) that

$$\begin{aligned}\left[H_{\mathrm{H}}, \vec{R}\right] &= \frac{\left[H_{\mathrm{H}}, \vec{L}^{\,2} \cdot \vec{p}\right]}{2 i m_{\mathrm{e}} \hbar} - \frac{\left[H_{\mathrm{H}}, \vec{p} \cdot \vec{L}^{\,2}\right]}{2 i m_{\mathrm{e}} \hbar} - \frac{1}{4\pi\varepsilon_0}\left[H_{\mathrm{H}}, \vec{e}_r\right] \\ &= \frac{\left[\vec{L}^{\,2}, [H_{\mathrm{H}}, \vec{p}]\right]}{2 i m_{\mathrm{e}} \hbar} - \frac{1}{4\pi\varepsilon_0} e^2 \left[H_{\mathrm{H}}, \vec{e}_r\right] \\ &= \frac{1}{4\pi\varepsilon_0} \frac{e^2}{2 m_{\mathrm{e}} r^2}\left[\vec{L}^{\,2}, \vec{e}_r\right] - \frac{1}{4\pi\varepsilon_0} e^2 \left[H, \vec{e}_r\right] = 0. \end{aligned} \tag{2.31}$$

Here we introduced $\vec{e}_r = \vec{r}/r$ in order to stress the exclusively angular dependence. Note that $[\vec{R}, \vec{L}^{\,2}] \neq 0$. As explained above, this means that there has to be a degeneracy necessarily. Considering a degenerate subspace, we can rescale $\vec{R} \to \sqrt{-m_{\mathrm{e}}/2E}\,\vec{R} = \vec{R}_{\mathrm{E}}$ (note that $E < 0$). Then we have the following commutation relations between the generators of the symmetry group of H_{H}

$$\left[L^i, L^j\right] = i\hbar\varepsilon_{ijk} L^k \tag{2.32a}$$

$$\left[R^i_{\mathrm{E}}, R^j_{\mathrm{E}}\right] = i\hbar\varepsilon_{ijk} L^k \tag{2.32b}$$

$$\left[R^i_{\mathrm{E}}, L^j\right] = i\hbar\varepsilon_{ijk} R^k_{\mathrm{E}}, \tag{2.32c}$$

which defines a realization of the $SO(4)$. We will see that the degeneracy to be reported in Chapter 4 shows a lot of similarities to the degeneracy of the hydrogen atom.

3 Different types of integrability and their relation to decoherence in central spin models

Parts of this chapter have been published in collaboration with John Schliemann in Reference [67].

In the Sections 2.1 and 2.2 we introduced the basic concepts of quantum integrability. In particular we emphasized that so far quantum integrability lacks a clear mathematical definition and the related research concentrates on either (i) the existence of a Bethe ansatz or (ii) the existence of complete sets of mutually commuting operators (CSCO).

In investigations mainly focused on the first type of integrability, evidence has been found that it is related to transport properties [38, 39], to quantum phase transitions [40], and to decoherence [41–46]. Here systems of the form

$$H = H_{\mathrm{cs}} + H_{\mathrm{cs}\leftrightarrow\mathrm{b}} + \ldots \text{further terms} \tag{3.1}$$

have been considered, where H_{cs} denotes the Hamiltonian of a central system and $H_{\mathrm{cs}\leftrightarrow\mathrm{b}}$ a coupling term between the central system and a bath. Mainly two roads have been followed. On the one hand, the influence of chaotic or regular baths on the decoherence of the central system has been investigated [41, 42]. On the other hand, the decoherence properties of the central systems of models which are integrable or non-integrable have been studied [43–46]. The usual procedure within such considerations is to evaluate numerically the level statistics of the respective system in the sense of Section 2.2 and to relate a possible change in the statistics to a change of other properties of the system happening at the same point.

Also as a basis for the second part of the present thesis, in this chapter we investigate integrability and its relation to decoherence in central spin models with more than a single central spin. Here we refrain from the definitions (i) and (ii) and instead consider a quantum system to be integrable if it is possible to compute *all* eigenstates and eigenvalues of the respective Hamiltonian using operations with less complexity than the direct diagonalization of the Hamiltonian matrix [68]. In this context we refer to the computational complexity. The complexity of the exact diagonalization of a Hamiltonian matrix for example grows exponentially with the system size. This very strict notion of quantum integrability contains (i) and (ii) as possible sources of integrability.

In Sections 3.1 and 3.2 we first study the integrable structure of central spin models. In particular we show that there is a transition between integrability ensured by Bethe ansatz and integrability ensured by CSCO. Differing from the previous investigations mentioned above, in Section 3.3 we then open a new route by applying a strong magnetic field to the central spin system and analyzing its reaction with respect to decoherence. In the non-integrable case as well as in the case of integrability ensured by Bethe ansatz the strong magnetic field leads, as generally expected, to highly coherent central spin dynamics, whereas in the remaining case decoherence still takes place. In contrast to previous work we relate

the latter observation *explicitly* to the *type* of integrability and interpret the result from two different points of view. Obviously, this does not only teach us something about the relation between integrability and physical phenomena. It also gives new insights into quantum integrability itself, as the definition introduced above turns out to be "productive" in the sense that it leads to the aforementioned relation between integrability and decoherence.

3.1 Integrable and non-integrable central spin models

In the present section we investigate which of the central spin models (1.1) are integrable and which are not. To this end it is convenient to rewrite the original Hamiltonian in terms of sums and differences between the coupling constants

$$\begin{aligned} H_{\mathrm{CSM}} &= \sum_{i=1}^{N_\mathrm{c}} \vec{S}_i \cdot \sum_{j=1}^{N} A_j^{(i)} \vec{I}_j + \sum_{i<j} J_{\mathrm{ex}}^{(ij)} \vec{S}_i \cdot \vec{S}_j \\ &= \left(\sum_{i=1}^{N_\mathrm{c}} \vec{S}_i \right) \cdot \sum_{k=1}^{N} \left(\frac{1}{N_\mathrm{c}} \sum_{j=1}^{N_\mathrm{c}} A_k^{(j)} \right) \vec{I}_k \\ &+ \sum_{i=1}^{N_\mathrm{c}} \sum_{j=i+1}^{N_\mathrm{c}} \left(\vec{S}_i - \vec{S}_j \right) \cdot \sum_{k=1}^{N} \frac{1}{N_\mathrm{c}} \left(A_k^{(i)} - A_k^{(j)} \right) \vec{I}_k \\ &+ \sum_{i<j} J_{\mathrm{ex}}^{(ij)} \vec{S}_i \cdot \vec{S}_j, \end{aligned} \tag{3.2}$$

where in the following we consider $J_{\mathrm{ex}}^{(ij)} = J_{\mathrm{ex}}$ and $N_\mathrm{c} > 1$. For later convenience we define $A = N_\mathrm{c}^{-1} \sum_{k=1}^{N} \sum_{j=1}^{N_\mathrm{c}} A_k^{(j)}$. The first term is nothing else than a Gaudin model [12] with a central spin replaced by a sum over a set of spins, whereas the second term acts as a perturbation, vanishing whenever $A_k^{(i)} = A_k^{(j)}$.

Let us consider the aforementioned case of a vanishing perturbation. Here the central spins can couple to different values of the total central spin squared. On each of the respective subspaces we are left with a usual Gaudin model. As explained in Section 2.1, for the Gaudin model there is a Bethe ansatz, which reduces the problem of finding the eigensystem of a Hamiltonian to the solution of a set of typically non-linear equations. Hence, it has to be expected that integrable central spin models satisfy $A_k^{(i)} = A_k^{(j)}$, whereas the model (3.2) should be non-integrable in general. Obviously, the latter is explicitly verified by the data presented in Section 2.2, where the spectral properties of central spin models with $J_{\mathrm{ex}}^{(ij)} = 0$ have been studied. It has been demonstrated that for more than a single central spin the nearest-neighbor level distribution exhibits level repulsion towards the Wigner surmise. This indicates that there is no Bethe ansatz for those central spin models, clearly suggesting that there is no possibility to reduce the computational complexity of the diagonalization of the Hamiltonian. Note that this result will not change if non-zero couplings $J_{\mathrm{ex}}^{(ij)}$ are considered. We will come back to an integrable case of two central spins with $A_i^{(1)} = A_i^{(2)}$ below.

3.2 Different types of integrability

In the present section we focus on models fulfilling $A_k^{(i)} = A_k^{(j)} = A_k$ and investigate by which structures integrability can be ensured. In particular we demonstrate that for homogeneous couplings $A_i = A_j$ integrability can never result from the Bethe ansatz, but is always ensured by CSCO.

In Section 3.1 we explained that for $A_k^{(i)} = A_k^{(j)}$ there is a Bethe ansatz for the Hamiltonian (3.2). Considering the Bethe ansatz equations instead of the direct diagonalization of the Hamiltonian matrix reduces a problem of exponential complexity to one of polynomial complexity. Hence, the Hamiltonian (3.2) with $A_k^{(i)} = A_k^{(j)}$ is integrable in the sense of our definition provided the Bethe ansatz equations (2.5) yield the correct number of solutions $\{\omega_1, \ldots, \omega_{N_\mathrm{D}}\}$. However, this strongly depends on the inhomogeneity of the couplings A_k. Indeed, for $A_k = (A/N) \Leftrightarrow A_j^{(i)} = (A/N)$ the Bethe ansatz equations can never yield all eigenstates and eigenvalues. This becomes clear already on the subspace with only one spin flip, $N_\mathrm{D} = 1$. Here the Bethe ansatz equation (2.9) becomes

$$S + \frac{A}{A - N\omega} \sum_{j=1}^{N} I_j = 0, \tag{3.3}$$

which obviously gives only a single solution. Therefore integrability ensured by Bethe ansatz breaks if all couplings become identical. We now show that in this case integrability is ensured by CSCO. In order to construct the respective operators we apply the so-called binary tree formalism [49]. On the first sight this seems to be unnecessary because Gaudin also gave the set of operators introduced in Equation (2.13) which together with the Hamiltonian of his central spin model form a CSCO [12]. Indeed, these operators, which do not play any role concerning the construction of the eigenstates and eigenvalues of the Gaudin model, obviously become ill-defined in the homogeneous coupling limit.

We restrict ourselves to a special case of the binary tree formalism [49] directly adapted to our model: Let T be a binary tree with n leaves as shown in Figure 3.1 for $n = 6$. A binary tree consists of a set of nodes, each of which is connected to exactly two following nodes, except for the leaves. If we distinguish between a left and a right "child" p_1 and p_2 connected to a node p, we arrive at a natural ordering of the leaves. We denote the leaves a node $p \in T$ is connected to as $L(p)$. The node connected to all leaves is called the root, denoted by r in the following. Now we associate every leaf i with a spin $\vec{S}_i$ and define $H_p = \left(\sum_{i \in L(p)} \vec{S}_i\right)^2$ and $H_r^z = \sum_{i \in L(r)} S_i^z$. It is simple to see that for all $p \in T$ these operators commute. As every binary tree with n leaves has $(n-1)$ nodes apart from the leaves, we thus arrive at exactly n non-trivial, mutually commuting operators, which indeed form a CSCO. In Section 2.1 it was mentioned that CSCO have to share "suitable" properties. What makes the operators constructed above suitable is the fact that they are complete for all spin lengths. In fact, for any system it is possible to find a CSCO by e.g. considering the eigenbasis of the respective Hamiltonian and choosing a sufficient number of diagonal matrices with only one entry different from zero. We investigated such systems for the simple model of two Heisenberg coupled spins and found that they consist of more than two operators and lose the property of being complete when the spin length is changed. We suppose that sets of commuting operators can only be complete for any spin length if the number of operators is equal to the number of spins. Surprisingly, up to our knowledge such a statement has not been made so far.

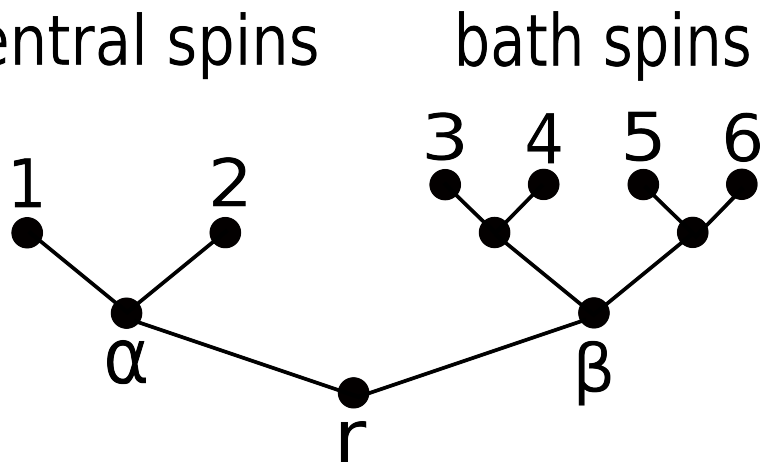

Figure 3.1: Binary tree with $n = N_\mathrm{c} + N = 2 + 4 = 6$ leaves. In order to embed the Hamiltonian of an arbitrary central spin model with homogeneous couplings into a CSCO using the binary tree formalism, two binary trees α, β with N_c and N leaves respectively must be grafted together. The Hamiltonian results as given in Equation (3.4).

Now we show how to embed the Hamiltonian of an arbitrary central spin model with homogeneous couplings in a CSCO. To this end we consider two binary trees α and β with N_c and N leaves respectively. Grafting them together as shown in Figure 3.1, we arrive at a new binary tree with $N_\mathrm{c} + N$ leaves. If we use the notation (2.12), the Hamiltonian of the associated homogeneous coupling model can be written in terms of elements of the CSCO resulting from the binary tree formalism as

$$H_\mathrm{CSM} = \frac{A}{N}(H_r - H_\beta) + \left(\frac{J_\mathrm{ex}}{2} - \frac{A}{N}\right) H_\alpha. \tag{3.4}$$

Note that the number of central and bath spins as well as their lengths are arbitrary and that there is no further restriction to α and β so that indeed there are numerous CSCO in which H_CSM can be embedded. Furthermore, it should be mentioned that by adding $J_b H_\beta$ to Equation (3.4) we can easily include a homogeneous interaction of strength J_b between the bath spins. It is simple to find the common eigenstates of the respective CSCO [49, 69]:

$$|\{S_{p\in T_L}\}, S_r^z\rangle = \sum_{S^z_{p\in T_r}} \left(\prod_{p\in T_L} \langle S_{p_1}, S_{p_2}, S^z_{p_1}, S^z_{p_2} | S_p, S^z_p\rangle \right) |S_1^z, \ldots, S^z_{N+2}\rangle \tag{3.5}$$

Here $T_L = T \setminus L(r)$, $T_r = T \setminus r$ (here $\setminus$ denotes the mathematical "without") and S_p denotes the quantum number associated with H_p. The complexity for calculating the Clebsch-Gordan coefficients is polynomial [70] and hence the approach indeed yields integrability. The eigenvalues read:

$$\begin{aligned} E(\{S_{p\in T_L}\}, S_r^z) &= \frac{A}{N}\left(S_r(S_r+1) - S_\beta(S_\beta+1)\right) \\ &+ \left(\frac{J_\mathrm{ex}}{2} - \frac{A}{N}\right) S_\alpha(S_\alpha+1) \end{aligned} \tag{3.6}$$

3.3 Relation between integrability and decoherence

Now we relate our above findings to the phenomenon of decoherence. The product of two spin operators consists of "flip-flop" terms involving ladder operators and a coupling of the z components:

$$\begin{aligned} H_{\mathrm{CSM}} &= \underbrace{\frac{1}{2}\sum_{i=1}^{N_\mathrm{c}}\sum_{j=1}^{N} A_j^i \left(S_i^+ \cdot I_j^- + S_i^- \cdot I_j^+\right)}_{=H_{\mathrm{ff}}} + \frac{J_{\mathrm{ex}}}{2}\sum_{i<j}\left(S_i^+ \cdot S_j^- + S_i^- \cdot S_j^+\right) \\ &+ \sum_{i=1}^{N_\mathrm{c}}\sum_{j=1}^{N} A_j^i S_i^z \cdot I_j^z + J_{\mathrm{ex}}\sum_{i<j} S_i^z \cdot S_j^z \end{aligned} \tag{3.7}$$

In the following we evaluate the dynamics for an initial state which is a simple product state. In this case all dynamics is purely due to the flip-flop terms and all decoherence results from H_{ff}. It is typically expected that applying a magnetic field B to the central spin system strongly suppresses the influence of flip-flop terms between the central spin system and the bath [30–35]. Here one usually assumes that whenever the magnetic field exceeds all other energy scales $B \gg A$, a complete neglect of their influence is justified. Consequently, a very large magnetic field should in general lead to highly coherent dynamics. In the following we show that it strongly depends on the inhomogeneity of the coupling constants to what extent H_{ff} causes decoherence. The more couplings are chosen to be equal to each other, the stronger H_{ff} acts as a source of decoherence.

To this end, in Figure 3.2 we consider the case $N_\mathrm{c} = 2$. We choose $S_i = I_i = 1/2$ and plot the spin dynamics for two integrable models ($A_j^{(1)} = A_j^{(2)} = A_j$, as explained above) with inhomogeneous and homogeneous coupling constants. In the first case the coupling constants A_j are chosen with respect to a non-uniform distribution so that $A_i \neq A_j$. As to be further explained in the second part of the present thesis, for an initial state which is not an element of the subspace with only a single spin flip, $N_\mathrm{D} = 1$, this case can only be accessed via exact diagonalization, which strongly restricts the size of the system [36, 37, 71, 72]. We therefore consider a comparatively small system with $N = 2N_\mathrm{D}^\mathrm{b} + 1$ and $N_\mathrm{D}^\mathrm{b} = 5$, where N_D^b denotes the number of spin flips exclusively in the bath. This corresponds to a very low bath polarization

$$p_b = \frac{N - 2N_\mathrm{D}^\mathrm{b}}{N} \tag{3.8}$$

of $p_b = 1/N$. The initial state of the central spin system is given by $|\Downarrow\Uparrow\rangle$. For details concerning the calculation of the spin dynamics the reader is referred to Appendix A. We checked the dynamics for much larger systems in the homogeneous case using a semi-analytical approach based on the work to be presented in Chapter 6. We did not find any qualitative differences. Moreover, non-integrable systems with fully inhomogeneous couplings $A_i^{(1)} \neq A_i^{(2)}$ show a qualitatively very similar behavior to the integrable case of inhomogeneous couplings, $A_i^{(1)} = A_i^{(2)}$ and $A_i \neq A_j$. Note that all results derived for the special case of $N_\mathrm{c} = 2$ and $S_i = I_i = 1/2$ in the following can be directly adapted to the general case of an arbitrary number of central spins and arbitrary spin lengths.

Although the magnetic field is in both cases larger than any other energy scale, the dynamics for the inhomogeneous case is completely coherent, whereas in the homogeneous case it still decays. This means that in the inhomogeneous case the flip-flop terms between

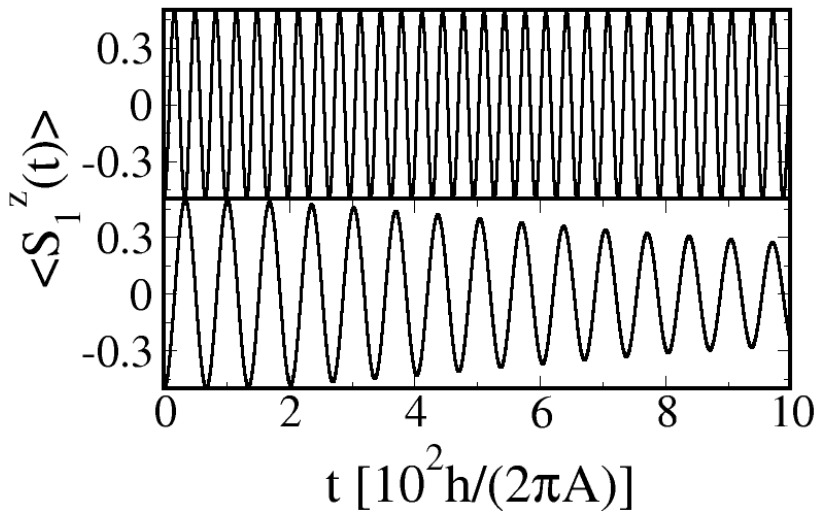

Figure 3.2: Spin dynamics for $N_\mathrm{c} = 2$, $N = 2N_\mathrm{D}^\mathrm{b} + 1 = 11$, where $S_i = I_i = (1/2)$, $B = 3.441A$, and $J_\mathrm{ex} = 0.023A$. The initial state of the system is given by $|\Downarrow\Uparrow\rangle \otimes \prod_{i=1}^{N_\mathrm{D}^\mathrm{b}} I_i^- |0\rangle$. We consider two integrable models fulfilling $A_i^{(1)} = A_i^{(2)} = A_i$ with either $A_i \neq A_j$ (upper panel), chosen due to a non-uniform distribution, or $A_i = A_j$ (lower panel). Although in both cases B is larger than any other energy scale, for homogeneous couplings the dynamics still decays.

the central spin system and the bath do not contribute to decoherence in any determinable way. The oscillations are completely due to the flip-flop terms between the two central spins. Indeed, this dynamical effect is not entirely trivial. A qualitative explanation of the dynamics shown in Figure 3.2 goes as follows: Flipping a spin in a magnetic field changes the energy E by $\Delta E \propto B$. In order to ensure energy conservation this change must be compensated. As indicated in the upper panel of Figure 3.3, for inhomogeneous couplings this has to be done by the energy change due to the flop of the respective bath spin and the one resulting from the central spin flip via the central spin coupling term. Hence, if the magnetic field exceeds any other energy scale, this is impossible and flip-flop processes are forbidden by energy conservation. If we instead consider homogeneous couplings, this restriction can be circumvented by simultaneous flip-flop processes on both of the central spins. Here the energy changes due to the central spin flips in the magnetic field and the bath spin flops compensate each other as depicted in the bottom panel of Figure 3.3. This is impossible for inhomogeneous couplings because the energy change depends on which bath spin is flipped.

The effect vanishes for initial states with a fully polarized central or bath spin system. However, from the above explanation it is clear that it will still occur if the couplings are varied away slightly from complete homogeneity. This means that the *more* the couplings approach the CSCO integrable limit, the *less* flip-flop terms are suppressed by a magnetic field applied to the central spin system. This leads to two different interpretations of the results, both of which indicate that it is not necessarily the integrability or non-integrability itself which is related to decoherence, as assumed in previous studies [41–46]: (a) As demonstrated above, the influence of a magnetic field applied to the central spin system on the

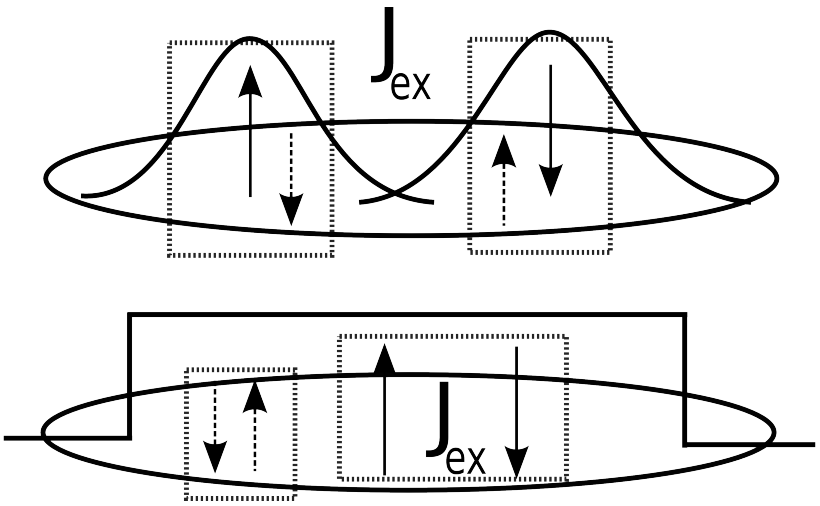

Figure 3.3: Sketch of flip-flop processes in a $N_c = 2$ central spin model. The solid lines drawn above the spins symbolize the coupling constants. Physically these are realized for example by the square modulus of the wave function of an electron confined in a semiconductor quantum dot (hyperfine interaction, see Part 2 of the present thesis). The inhomogeneous case is shown in the upper panel, the homogeneous one in the bottom panel. For homogeneous couplings the energy changes due to simultaneous flip-flop processes on both of the central spins can compensate each each other. This is not possible for inhomogeneous couplings because the energy changes of the processes differ for different bath spins.

decoherence properties strongly differs for models which are clearly non-integrable or integrable by Bethe ansatz and those which are near to the CSCO integrable limit. In the first case the dynamics becomes highly coherent, whereas in the second case it still decays. This suggests that it is the mathematical structure ensuring integrability which determines the reaction of a system on an external quantity applied to the central system with respect to the decoherence properties rather than the integrability or non- integrability itself. (b) An even more general interpretation results from the observation, described in Section 2.1, that if we apply a magnetic field to the central spin system, the non-integrable models as well as those integrable by Bethe ansatz keep the respective property, whereas it is lost in the CSCO case. Hence, the result suggests that if a model is close to a limit in which the integrability is broken by some external quantity applied to the central system, its decoherence properties will be stronger affected than those of a system near to a limit with stable integrability. It is therefore the *breaking* of integrability which has a negative effect on the decoherence properties and not the actual integrability or non-integrability.

3.4 Summary and outlook

In the present chapter we investigated integrability and its relation to decoherence for central spin models with more than a single central spin. Differing from the usual definitions introduced in Section 2.1, in the present chapter we considered a quantum system to be integrable provided it is possible to calculate the full eigensystem using operations with less complexity than the direct diagonalization of the Hamiltonian matrix. Based on this notion of integrability, an explicit relation between the *type* of integrability and decoherence has been derived. Here we applied a strong magnetic field to the central spin system and inves-

tigated its reaction with respect to decoherence. The results lead to new insights not only with respect to the relation between integrability and physical phenomena, but also justify the notion of quantum integrability introduced in the present chapter.

Of course our results have to be regarded as a first indication into the direction described above and it would be desirable to check them for more general external quantities on a wider class of systems. As explained above, in Equation (3.4) we can easily add a term describing an interaction between the different bath spins. Hence, in an immediate next step it would be interesting to check for which types of bath terms the Bethe ansatz integrability still holds and if we can find effects similar to those described in the present chapter. In this context see e.g. Reference [41, 42]. Furthermore, it would be an interesting question to what extent it is possible to reinterpret the data presented in previous works in terms of the relation derived in the present chapter. Here in particular interpretation (b) could be a valuable basis.

4 Unexpected systematic degeneracy in a system of two coupled Gaudin models with homogeneous couplings

Parts of this chapter have been published in collaboration with John Schliemann in Reference [73].

In Chapter 3 we investigated integrability and its relation to decoherence for central spin models with more than a single central spin, $N_c > 1$. No restrictions concerning the model parameters have been made. In the present chapter we proceed investigating basic properties of central spin models. However, here we specify a *non-integrable* system of two coupled Gaudin models with homogeneous couplings and investigate the spectral properties.

We begin with a numerical study of an inversion symmetric system. In order to lower the dimension of the problem, the baths of the two Gaudin models are replaced by single long spins, which does not change the set of eigenvalues of the Hamiltonian. Surprisingly, the spectrum exhibits systematically degenerate multiplets of consecutive total angular momentum and alternating parity. This is a situation somewhat similar to the degenerate multiplets of orbital angular momentum in the hydrogen atom, reviewed in Section 2.3. As explained there, degeneracies are extremely scarce. Hence, a new example for a an even *systematic* degeneracy is a remarkable result on its own right. Furthermore, as we briefly discuss below, it opens interesting perspectives with respect to solid state quantum information processing.

The outline of the chapter is as follows: The degeneracies in the spectrum of the coupled Gaudin models are first analyzed in a numerical approach in Section 4.1. In Section 4.2 we analytically construct the full subspace of degenerate states, which turns out to be located in the kernel of the commutator between the two Gaudin models and the coupling term. In Section 4.3 we furthermore investigate the role of the inversion symmetry and show that indeed there is a whole class of systems with spectra showing the same type of degeneracy.

4.1 Model and spectral properties

In the introduction of this thesis we defined the Gaudin model [12], important properties of which were reviewed in Section 2.1. It describes the coupling of a *single* central spin $\vec{S}_i$ to a set of N_i bath spins $\vec{I}_{i,j}$

$$H_{\mathrm{G}}^{(i)} = \vec{S}_i \cdot \sum_{j=1}^{N_i} A_j^{(i)} \vec{I}_{i,j} \tag{4.1}$$

via coupling constants $A_j^{(i)}$, which have the unit of energy. In the following we choose the couplings to be homogeneous, i.e. $A_j^{(i)} = A^{(i)}$. In this case the central spin couples to

a simple sum of spins, denoted by $\vec{I}_i = \sum_{j=1}^{N_i} \vec{I}_{i,j}$ from now on. Furthermore, we assume $S_i = 1/2$. Coupling together two such Gaudin models $H_{2\mathrm{G}} = H_{\mathrm{G}}^{(1)} + H_{\mathrm{G}}^{(2)}$ by

$$H_{\mathrm{c}} = J_{\mathrm{ex}} \vec{S}_1 \cdot \vec{S}_2 \tag{4.2}$$

yields the Hamiltonian subject to the investigations of the present chapter:

$$H_{2\mathrm{B}} = H_{2\mathrm{G}} + H_{\mathrm{c}} = A^{(1)} \vec{S}_1 \cdot \vec{I}_1 + A^{(2)} \vec{S}_2 \cdot \vec{I}_2 + J_{\mathrm{ex}} \vec{S}_1 \cdot \vec{S}_2.$$

Obviously the Hamiltonian conserves the total spin $\vec{J} = \vec{S}_1 + \vec{S}_2 + \vec{I}_1 + \vec{I}_2$ as well as $\vec{I}_1^2$ and $\vec{I}_2^2$.

The N_i bath spins couple to different values I_i of the total bath spin squared. In the following we study the spectrum of the Hamiltonian for $A^{(1)} = A^{(2)} = A$, where $A = (1/2)(A^{(1)} + A^{(2)})$, on subspaces $I_1 = I_2 = I$. On these subspaces, in addition to the symmetries mentioned above, $H_{2\mathrm{B}}$ is invariant under "inversions", meaning an interchange $1 \leftrightarrow 2$. It is clear that this is not the case globally, i.e. on the entire Hilbert space. However, subspaces with $I_1 = I_2$ lie fully in the kernel of the commutator $[H_{2\mathrm{G}}, \tau]$, where τ denotes the inversion operator. Just as the spatial inversion operator $\tau_{\vec{r}}$, which we introduced in Section 2.3, τ only has the two eigenvalues (± 1). In the following we again refer to this as positive and negative parity.

In order to reduce the dimension of the problem, we replace each bath by one single spin of length I. This neglects the quantum numbers associated with a certain Clebsch-Gordan decomposition of the respective bath and therefore changes the multiplicity of the eigenvalues, but not the set of eigenvalues itself (also see Equation (4.10)). Every energy in the resulting spectrum indeed appears $x_1 x_2$ times in the spectrum of $H_{2\mathrm{B}}$, where x_i denotes the number of multiplets with the quantum number I_i (so far $I_1 = I_2$). If for example $I_{i,j} = \frac{1}{2}$, we have [36]

$$x_i = \left[\binom{N_i}{\frac{N_i}{2} - I_i} - \binom{N_i}{\frac{N_i}{2} - I_i - 1} \right]. \tag{4.3}$$

However, it should be stressed again that the energy eigenvalues themselves remain unaltered.

In Figures 4.1 and 4.2 we show spectra obtained numerically for different values of the coupling constant J_{ex}, both for an even and an odd value of I. We plot the eigenenergies against the $\vec{J}^2$ quantum number J. Although the spectra are quite rich in detail, their global structure becomes already plausible from simple qualitative arguments. Obviously we always have four "branches" of energy levels, where, in particular for large J_{ex}, three of them form a bundle separated from the fourth one. The three former branches consist of states where the two central spins are predominantly coupled to a triplet (which has the eigenvalue $J_{\mathrm{ex}}/4$ under H_{c}), while in the latter branch the central spins are mainly in the singlet state (having the eigenvalue $-3J_{\mathrm{ex}}/4$ under H_{c}). The coupling of the central spin triplet and singlet to the bath spins then leads to the observed further energy splittings between and within the corresponding branches.

An unexpected particular feature, however, occurs in the triplet branch of intermediate energy. Here all multiplets are energetically completely degenerate with eigenvalue $(J_{\mathrm{ex}} - 2A)/4$. These multiplets have consecutive total spin between $J = 1$ and $J = 2I$ and alternating parity. Here positive (negative) parity corresponds to $2I - J$ being even (odd). The latter observation is reminiscent to the degenerate multiplets of orbital angular momentum $\vec{L}$ found in the hydrogen problem, which we reviewed in Section 2.3. As explained

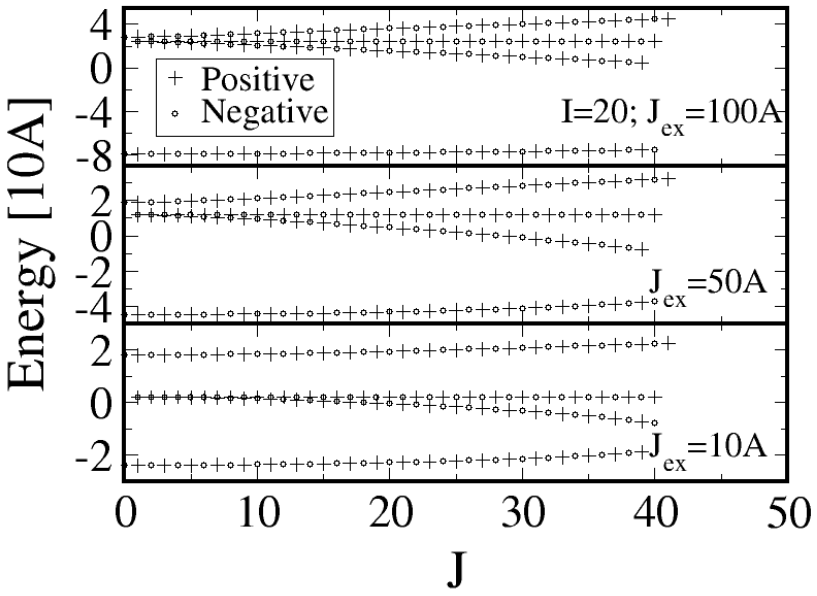

Figure 4.1: Spectrum of H_{2B} with baths replaced by two single spins of equal length $I = 20$ for different values of the coupling J_{ex}. The energies (in units of A) are plotted against the total spin J, i.e. each data point represents a multiplet of $2J + 1$ states. States of positive (negative) parity are signalled by a cross (circle). For all exchange couplings J_{ex} we have four "branches" of energy levels, where the above three ones originate from triplet states with respect to H_c and the lower one is associated with the singlet state. The triplet branch of intermediate energy consists of completely degenerate multiplets of alternating parity.

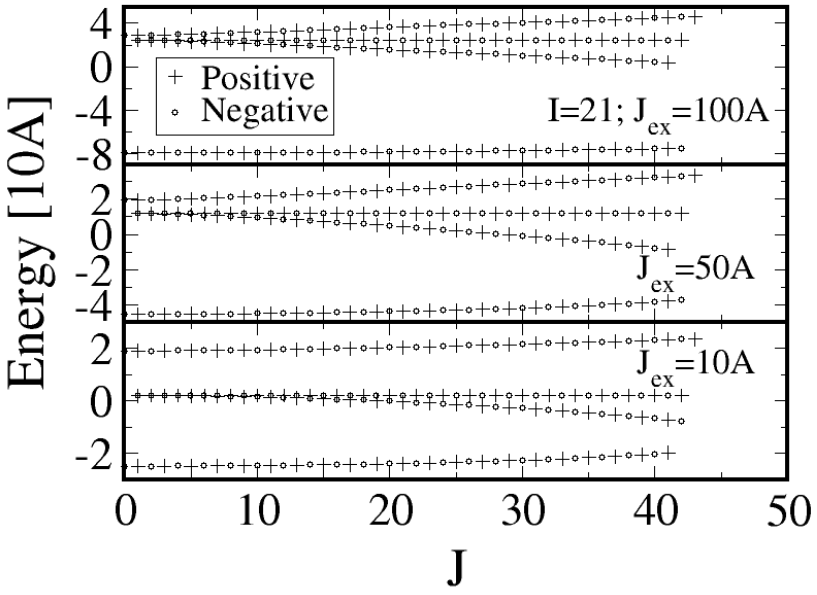

Figure 4.2: Analogous data as in Figure 4.1 for an odd spin length $I = 21$. Again we find a completely degenerate triplet branch.

there, this degeneracy is due to the existence of a hidden symmetry given by the quantum mechanical analogue of the Runge-Lenz vector $\vec{R}$ defined in Equation (2.27). In a very first attempt, the similarity between the two cases motivated us to consider $\vec{K} = \vec{J}_1 - \vec{J}_2$ with $\vec{J}_i = \vec{S}_i + \vec{I}_i$ as a possible candidate for the generating symmetry in our model. This results from the fact that the commutation relations

$$\left[J^i, J^j\right] = i\varepsilon_{ijk}J^k \tag{4.4a}$$
$$\left[K^i, K^j\right] = i\varepsilon_{ijk}J^k \tag{4.4b}$$
$$\left[K^i, J^j\right] = i\varepsilon_{ijk}K^k, \tag{4.4c}$$

are identical to those of $\vec{L}$ and $\vec{R}$ given in Equation (2.32). However, we have (note that $I_1 = I_2$)

$$\left[H_{2\mathrm{B}}, \vec{K}\right] = 2i\left(\vec{S}_1 \times \vec{S}_2\right), \tag{4.5}$$

which, as will become clear below, is not even zero on the degenerate subspace. So far we have not found the symmetry generating the detected degeneracy.

As explained in Section 2.3, such systematic degeneracies are extremely scarce, and hence our finding is interesting on its own right. Moreover, potential applications in, for example, solid state quantum information processing can be envisaged: It is clear that states with overlap exclusively in a degenerate subspace do not show any non-trivial time evolution. Therefore, such spaces have the potential to provide valuable implementations of long lived quantum memory, where the present one appears to be particularly suitable due to its *enormous* size. Note that even in the "thermodynamic limit" $I \gg 1$ approximately a fourth of the Hilbert space is degenerate: The dimension of the full Hilbertspace is $4(2I+1)^2$ and the degenerate subspace, denoted by $\mathcal{H}_{\mathrm{D}}$ from now on, has dimension $\sum_{n=1}^{2I}(2n+1) = 4I(I+1)$, yielding

$$\frac{I(I+1)}{(2I+1)^2} \approx \frac{1}{4}$$

if $I \gg 1$. Furthermore, the space of degenerate states detected here decomposes into subspaces of different parity which could also serve as a computational basis for quantum information processing.

4.2 Construction of the degenerate subspace

So far we have reported on numerical observations revealing an unexpected systematic degeneracy in the spectrum of the Hamiltonian $H_{2\mathrm{B}}$. In the following we analytically construct the subspace $\mathcal{H}_{\mathrm{D}}$ of these degenerate multiplets.

4.2.1 General ansatz and first consequences

As we shall see below, the degenerate states are simultaneous eigenstates of the Gaudin part $H_{2\mathrm{G}}$ of the Hamiltonian and the coupling between the two central spins H_{c}. In other words, $\mathcal{H}_{\mathrm{D}}$ lies entirely in the kernel of the commutator

$$[H_{2\mathrm{G}}, H_{\mathrm{c}}] = -iAJ_{\mathrm{ex}}\left(\vec{S}_1 \times \vec{S}_2\right) \cdot \left(\vec{I}_1 - \vec{I}_2\right). \tag{4.6}$$

Let us first turn to a single Gaudin Hamiltonian, $H_{\mathrm{G}}^{(i)} = A\vec{S}_i \cdot \vec{I}_i$, on subspaces $I_i = I$. In the following we omit the quantum numbers $\{S_i\}$ associated with some Clebsch-Gordan decomposition of the bath. The eigenvalues read

$$E_{\pm}(A, I) = \frac{A}{2}\left(\pm\left(I + \frac{1}{2}\right) - \frac{1}{2}\right) \tag{4.7}$$

and the eigenstates are given by a well-known Clebsch-Gordan decomposition [74]

$$|I \pm \frac{1}{2}, m_i\rangle = \mu^{\pm}(m_i)|\Uparrow\rangle|I, m_i - \frac{1}{2}\rangle \pm \mu^{\mp}(m_i)|\Downarrow\rangle|I, m_i + \frac{1}{2}\rangle, \tag{4.8}$$

where, apart from standard notation, we have introduced

$$\mu^{\pm}(m) = \sqrt{\frac{I \pm m + \frac{1}{2}}{2I + 1}}\,. \tag{4.9}$$

The eigenvalues of $H_{2\mathrm{G}} = H_{\mathrm{G}}^{(1)} + H_{\mathrm{G}}^{(2)}$ now follow immediately

$$H_{2\mathrm{G}}|+, m_1\rangle|+, m_2\rangle = AI|+, m_1\rangle|+, m_2\rangle \tag{4.10a}$$

$$H_{2\mathrm{G}}|+, m_1\rangle|-, m_2\rangle = -\frac{A}{2}|+, m_1\rangle|-, m_2\rangle \tag{4.10b}$$

$$H_{2\mathrm{G}}|-, m_1\rangle|+, m_2\rangle = -\frac{A}{2}|-, m_1\rangle|+, m_2\rangle \tag{4.10c}$$

$$H_{2\mathrm{G}}|-, m_1\rangle|-, m_2\rangle = -A(I+1)|-, m_1\rangle|-, m_2\rangle, \tag{4.10d}$$

where we abbreviated $|I \pm \frac{1}{2}, m_i\rangle = |\pm, m_i\rangle$. Obviously, the states $|\pm, m_1\rangle|\mp, m_2\rangle$ are degenerate with the eigenvalue being independent of I. As seen above, the highly degenerate eigenvalue in the subspace $\mathcal{H}_{\mathrm{D}}$ is $(J_{\mathrm{ex}} - 2A)/4$. Thus, eigenstates of $H_{2\mathrm{B}}$ with this eigenvalue can be constructed by simply combining the states $|\pm, m_1\rangle|\mp, m_2\rangle$ to triplet states with respect to the two central spins, meaning that they lie in the kernel of the commutator (4.6). At this point it is of course not clear that all eigenstates with the above eigenvalue are resulting through this approach. However, we will see that this is indeed the case. Note in this context that the action of the operator (4.5) on triplet states partly gives non-zero contributions. This means that, as explained above, $\vec{K}$ can not be the symmetry generating the detected systematic degeneracy.

In other words, our goal is to eliminate singlet contributions from suitable linear combinations of the states $|\pm, m_1\rangle|\mp, m_2\rangle$. To this end we use an ansatz already accounting for the conservation of J^z and the parity symmetry by superimposing states of the form

$$|+, m\rangle|-, M - m\rangle \pm |-, M - m\rangle|+, m\rangle\,, \tag{4.11}$$

where M denotes the eigenvalue of J^z. All following considerations are focused on $M \geq 0$ because states with $M < 0$ result simply by reversing every spin. In the following analysis one needs to distinguish the four different cases depending on whether M is even or odd and I is integer or half-integer. This case-by-case procedure can be nicely encapsulated and simplified as follows by introducing $i = 2I - M$ so that $i = 0, \ldots, 2I$: In Figure 4.3 the possible values of m_1 and m_2 are arranged on a grid. The diagonal lines mark the states of constant magnetization $M = 2I - i$, where we refer to the maximal value on such a diagonal as $m_{\max}$. Obviously, we have $m_{\max} = I - 1/2$ for $i = 2I$ and $m_{\max} = I + 1/2$

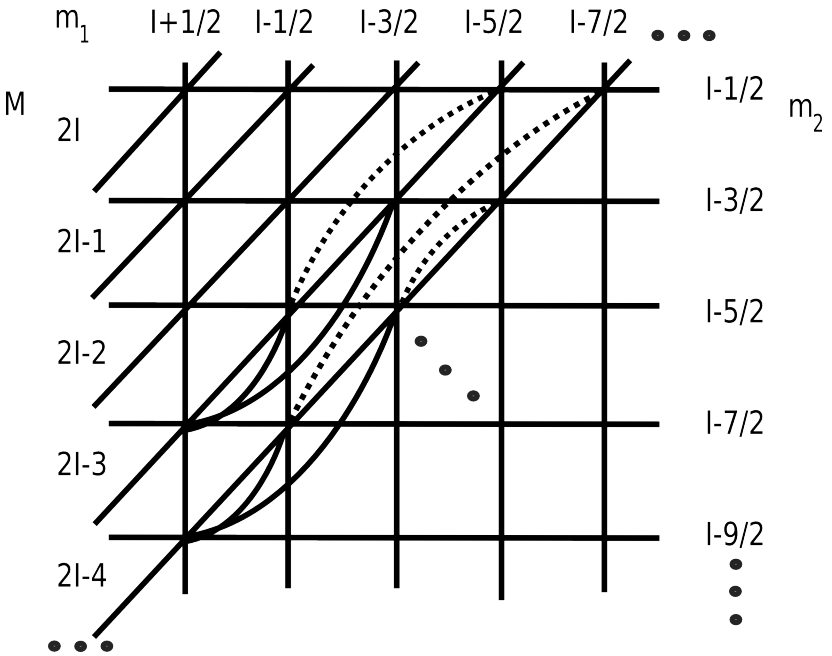

Figure 4.3: The different values of m_1 and m_2 arranged on a grid. The diagonal lines mark the states with constant magnetization. The dotted bended lines connect the states with interchanged magnetization, combined in our ansatz (4.12). The solid bended lines connect the states which are combined in order to construct the set of linearly independent eigenstates spanning the full eigenspace to the eigenvalue $(J - 2A)/4$.

otherwise. Following a line of constant magnetization starting from $m_{\max}$, one recognizes that from a certain value $m = m_{\min}$ on, all occurring states result from those with larger values of m by interchanging the respective magnetizations $(m, M - m)$. In Figure 4.3 these "complementary" states are connected by dotted bended lines. It is easy to see that if i is odd, we have $m_{\min} = (2I - i)/2$, whereas for an even value of i we have to add $(1/2)$ so that $m_{\min} = (2I - i + 1)/2$. It is now a simple fact that there are states which do not have a complement. This is the case for the states with $m = m_{\max}$ if $i \neq 2I$ and for those with $m = m_{\min}$ provided i is odd or equal to zero.

With respect to later considerations it turns out to be more convenient to use an ansatz which is a sum over pairs of complementary states, rather than a direct superposition of the states (4.11). Hence, we introduce coefficients α_m, α'_m for any state with $m \geq m_{\min}$ and its complement and combine them to a sum running from $m_{\min}$ to $m_{\max}$:

$$\begin{aligned} |\pm, i\rangle = \sum_{m=m_{\min}}^{m_{\max}} \big[& \alpha_m \left(|+, m\rangle|-, 2I - i - m\rangle \pm |-, 2I - i - m\rangle|+, m\rangle \right) \\ & + \theta(m)\alpha'_m \left(|+, 2I - i - m\rangle|-, m\rangle \pm |-, m\rangle|+, 2I - i - m\rangle \right) \big] \end{aligned} \tag{4.12}$$

The complements of the respective $m = m_{\max}$ states automatically vanish, whereas the function $\theta(m)$ accounts for the $m_{\min}$ states without a complement

$$\theta(m) = \Theta(m - m_{\min} - 1) + \delta_{i \bmod 2,0}\delta_{m,m_{\min}}. \tag{4.13}$$

Here $\Theta(x)$ denotes the Heaviside function, which is unity for any $x \geq 0$ and zero otherwise.

Clearly, the ansatz (4.12) is an eigenstate of $H_{2\mathrm{G}}$,

$$H_{2\mathrm{G}}|\pm,i\rangle = -\frac{A}{2}|\pm,i\rangle, \tag{4.14}$$

consisting of triplet and singlet terms. Eliminating the latter by demanding

$$\begin{aligned}
\sum_{m=m_{\min}}^{m_{\max}} \Big[& \big(\alpha_m \mu^+(m)\mu^+(2I-i-m) \mp \theta(m)\alpha'_m \mu^-(m)\mu^-(2I-i-m)\big) \\
& \times \left(\left| m-\frac{1}{2}, 2I-i-m+\frac{1}{2} \right\rangle \mp \left| 2I-i-m+\frac{1}{2}, m-\frac{1}{2} \right\rangle \right) && \text{(4.15a)} \\
& + \big(\alpha_m \mu^-(m)\mu^-(2I-i-m) \mp \theta(m)\alpha'_m \mu^+(m)\mu^+(2I-i-m)\big) \\
& \times \left(\left| m+\frac{1}{2}, 2I-i-m-\frac{1}{2} \right\rangle \mp \left| 2I-i-m-\frac{1}{2}, m+\frac{1}{2} \right\rangle \right) \Big] = 0, && \text{(4.15b)}
\end{aligned}$$

we arrive at an eigenstate of H_{c}. Note that the states in (4.15) are states of the two long bath spins $|I,m_1\rangle|I,m_2\rangle = |m_1,m_2\rangle$ and that the top (bottom) sign corresponds to positive (negative) parity.

Let us first consider the two particularly simple cases $i=0$ and $i=2I$. For $i=0$, i.e. $M=2I$, the sum consists of only one term $m=I+1/2$. For positive parity the unwanted singlet terms are automatically zero. As for $i=0$ the contributions related to $\alpha'_{I+1/2}$ in the terms (4.15a) and (4.15b) are vanishing, no further solution exists. This means that the largest degenerate multiplet with $J=2I$ always has positive parity, as demonstrated by our numerics.

In the other case $i=2I$, as corresponding to $M=0$, one easily sees that

$$\mu^+(m)\mu^+(-m) = \mu^-(m)\mu^-(-m)\,. \tag{4.16}$$

If i is even, this condition means that for every m the singlet terms can be eliminated by simply choosing $\alpha_m = \pm\alpha'_m$. Therefore, in this case we always have an equal number of multiplets with positive and with negative parity. As mentioned above, for an odd value of i the summand with $m=m_{\min}=0$ does not have a complement. However, for positive parity the unwanted terms vanish automatically so that the number of positive multiplets is larger by one than the number of negative multiplets. In total, we get $2I$ solutions as suggested by our numerics.

The solutions discussed above result from demanding that the terms in Equation (4.15) vanish separately for any value of m, while, strictly speaking, only their sum is required to be zero. However, it is indeed simple to see that there are no further solutions: Demanding that the total sum vanishes leads to the conditions

$$\begin{aligned}
&\mu^+(m)\mu^+(-m)\left(\alpha_m \mp \alpha'_m\right) \\
&= \pm\mu^+(m-1)\mu^+(-m+1)\left(\alpha_{m-1} \mp \alpha'_{m-1}\right),
\end{aligned}$$

and $\left(\alpha_{\frac{1}{2}} \mp \alpha'_{\frac{1}{2}}\right) = \left(\alpha_{I-\frac{1}{2}} \mp \alpha'_{I-\frac{1}{2}}\right) = 0$, which obviously give the same solutions as above. In summary, the resulting eigenstates at $i=2I$ ($M=0$) can be formulated most compactly as

$$\begin{aligned}
|\pm,2I,m\rangle \;=\; & |\Uparrow\Uparrow\rangle \left(\left| m-\frac{1}{2}, -m-\frac{1}{2} \right\rangle \pm \left| -m-\frac{1}{2}, m-\frac{1}{2} \right\rangle \right) \\
- \; & |\Downarrow\Downarrow\rangle \left(\left| m+\frac{1}{2}, -m+\frac{1}{2} \right\rangle \pm \left| -m+\frac{1}{2}, m+\frac{1}{2} \right\rangle \right). \qquad \text{(4.17)}
\end{aligned}$$

That $\mathcal{H}_\mathrm{D}$ lies *fully* in the kernel of the commutator (4.6) becomes clear at this point: There are $2I$ degenerate multiplets with alternating parity, each of which gives one state with $M = 0$. Above we constructed states which are superpositions of exactly those states and lie in kernel of the commutator (4.6). They can be combined to give eigenstates of $\vec{J}^2$, so that $\mathcal{H}_\mathrm{D}$ can be constructed simply by applying $J^\pm$. From $\left[\vec{J}, H_\mathrm{2G}\right] = \left[\vec{J}, H_\mathrm{c}\right] = 0$ it follows

$$\left[J^\pm, [H_\mathrm{2G}, H_\mathrm{c}]\right] = 0, \tag{4.18}$$

meaning that a state resulting from the application of $J^\pm$ to a state lying in the kernel of the commutator (4.6) again lies in the kernel of the commutator (4.6). Therefore the full degenerate subspace is located there.

4.2.2 Complete construction

Now we come to the construction of the full degenerate space $\mathcal{H}_\mathrm{D}$. In an immediate approach we follow the route described above and combine the states (4.17) to eigenstates of $\vec{J}^2$ such that $\mathcal{H}_\mathrm{D}$ can be generated by applying $J^\pm$. Unfortunately, the construction of $\vec{J}^2$ eigenstates is possible only up the solution of a homogeneous set of equations with a (in certain cases symmetric) tridiagonal coefficient matrix, which has to be carried out numerically. However, due to the simple tridiagonal shape of the matrix, such a problem has the very low complexity of $\mathcal{O}(2I)$. Hence, even systems of realistic size with respect to experimental situations in for example semiconductor quantum dots, $I \sim 10^6$, can be treated on conventional computers [75–78]. Nevertheless, in a second approach we construct a basis of $\mathcal{H}_\mathrm{D}$ in a fully analytical fashion. The resulting basis states are eigenstates of J^z and τ, but they are neither orthogonal nor do they satisfy the $\vec{J}^2$ symmetry. Nevertheless, for both applied as well as more mathematical future considerations it will be helpful to have closed analytical expressions at hand.

First approach: Construction of eigenstates of $\vec{J}^2$ with $M = 0$

As mentioned above, our first approach consists in using the particularly simple solutions for $i = 2I$, given in Equation (4.17), by combining them to eigenstates of $\vec{J}^2$ such that applying the ladder operators $J^\pm$ generates the full space $\mathcal{H}_\mathrm{D}$. Hence we demand

$$\begin{aligned} \vec{J}^2 \sum_{m=m_\mathrm{min}}^{I-\frac{1}{2}} \beta_m |\pm, 2I, m\rangle &= J(J+1) \sum_{m=m_\mathrm{min}}^{I-\frac{1}{2}} \beta_m |\pm, 2I, m\rangle \\ \Leftrightarrow \vec{J}^2 \sum_{m=m_\mathrm{min}}^{I-\frac{1}{2}} \beta_m |\pm, 2I, m\rangle - J(J+1) &\sum_{m=m_\mathrm{min}}^{I-\frac{1}{2}} \beta_m |\pm, 2I, m\rangle = 0. \end{aligned}$$

Explicitly this reads

$$
\begin{aligned}
|\Uparrow\Uparrow\rangle \sum_{m=m_{\min}}^{I-\frac{1}{2}} \beta_m \Bigg[& \left(2I(I+1) - 2\left(m+\frac{1}{2}\right)\left(m-\frac{1}{2}\right) - J(J+1)\right) \\
& \times \left(\left|m-\frac{1}{2}, -m-\frac{1}{2}\right\rangle \pm \left|-m-\frac{1}{2}, m-\frac{1}{2}\right\rangle\right) && \text{(4.19a)} \\
& + \nu^+\left(m-\frac{1}{2}\right)\nu^-\left(-m-\frac{1}{2}\right)\left(\left|m+\frac{1}{2}, -m-\frac{3}{2}\right\rangle \pm \left|-m-\frac{3}{2}, m+\frac{1}{2}\right\rangle\right) && \text{(4.19b)} \\
& + \nu^-\left(m-\frac{1}{2}\right)\nu^+\left(-m-\frac{1}{2}\right)\left(\left|m-\frac{3}{2}, -m+\frac{1}{2}\right\rangle \pm \left|-m+\frac{1}{2}, m-\frac{3}{2}\right\rangle\right)\Bigg] && \text{(4.19c)} \\
-|\Downarrow\Downarrow\rangle \sum_{m=m_{\min}}^{I-\frac{1}{2}} \beta_m \Bigg[& \left(2I(I+1) - 2\left(m+\frac{1}{2}\right)\left(m-\frac{1}{2}\right) - J(J+1)\right) \\
& \times \left(\left|m+\frac{1}{2}, -m+\frac{1}{2}\right\rangle \pm \left|-m+\frac{1}{2}, m+\frac{1}{2}\right\rangle\right) \\
& + \nu^+\left(m+\frac{1}{2}\right)\nu^-\left(-m+\frac{1}{2}\right)\left(\left|m+\frac{3}{2}, -m-\frac{1}{2}\right\rangle \pm \left|-m-\frac{1}{2}, m+\frac{3}{2}\right\rangle\right) \\
& + \nu^-\left(m+\frac{1}{2}\right)\nu^+\left(-m-\frac{1}{2}\right)\left(\left|m-\frac{1}{2}, -m+\frac{3}{2}\right\rangle \pm \left|-m+\frac{3}{2}, m-\frac{1}{2}\right\rangle\right)\Bigg] = 0,
\end{aligned}
$$

where $\nu^{\pm}(m) = \sqrt{I(I+1) - m(m\pm 1)}$ and hence

$$
\begin{aligned}
\nu^+\left(m-\frac{1}{2}\right)\nu^-\left(-m-\frac{1}{2}\right) &= \nu^+\left(m+\frac{1}{2}\right)\nu^-\left(-m+\frac{1}{2}\right) \\
\nu^-\left(m-\frac{1}{2}\right)\nu^+\left(-m-\frac{1}{2}\right) &= \nu^-\left(m+\frac{1}{2}\right)\nu^+\left(-m-\frac{1}{2}\right).
\end{aligned}
$$

This is plausible because the $|\Uparrow\Uparrow\rangle$ and $|\Downarrow\Downarrow\rangle$ terms must vanish separately. Note that all components with $|\Uparrow\Downarrow\rangle, |\Downarrow\Uparrow\rangle$ are equal to zero. It is now simple to see that the state in the term (4.19a) for some m is identical to the one in the tern (4.19b) for $(m+1)$ and to the one in the term (4.19c) for $(m+2)$. For an even value of i eliminating these terms gives the following set of equations

$$
\begin{aligned}
\beta_m\left[\nu^+\left(m-\frac{1}{2}\right)\nu^-\left(-m-\frac{1}{2}\right)\right] + \beta_{m+1}\left[2I(I+1) - 2\left(m+\frac{3}{2}\right)\left(m+\frac{1}{2}\right) - J(J+1)\right] & \\
+\Theta\left(I-\frac{3}{2}-m\right)\beta_{m+2}\left[\nu^+\left(m+\frac{3}{2}\right)\nu^-\left(-m-\frac{5}{2}\right)\right] = 0 & \\
\beta_{\frac{1}{2}}\left[2I(I+1) - J(J+1) \pm I(I+1)\right] + \beta_{\frac{3}{2}}\left[\nu^-(1)\nu^+(-2)\right] = 0, &
\end{aligned}
$$

where $m = 1/2, \ldots, I-3/2$. This yields a symmetric tridiagonal matrix. However, the symmetry of the matrix is destroyed if i is odd. In this case we have

$$
\begin{aligned}
\beta_m(1\pm\delta_{m,0})\left[\nu^+\left(m-\frac{1}{2}\right)\nu^-\left(-m-\frac{1}{2}\right)\right] + \beta_{m+1}\left[2I(I+1) - 2\left(m+\frac{3}{2}\right)\left(m+\frac{1}{2}\right) - J(J+1)\right] & \\
+\Theta\left(I-\frac{3}{2}-m\right)\beta_{m+2}\left[\nu^+\left(m+\frac{3}{2}\right)\nu^-\left(-m-\frac{5}{2}\right)\right] = 0 & \\
\beta_0\left[2I(I+1) - J(J+1) - \frac{1}{2}\right] + \beta_1\left[\nu^-\left(\frac{1}{2}\right)\nu^+\left(-\frac{3}{2}\right)\right] = 0, &
\end{aligned}
$$

where $m = 0, \ldots, I - 1/2$. The two above systems now have to be solved numerically for the different values of J.

Second approach: Explicit elimination of singlet contributions for $2I > M > 0$ via ansatz

Our second approach, which in contrast to the one described above leads to closed analytical expressions for the degenerate eigenstates, consists in *directly* determining the constants α_m and α'_m for a given value of M. In Subsection 4.2.1 we already considered $i = 0, 2I$ so that here we concentrate on the remaining cases $0 < i < 2I$, which correspond to $2I > M > 0$. As already used above, considering the term (4.15a) for some m and the term (4.15b) for $(m-1)$, one sees that the respective states become identical up to a factor (∓ 1). The idea is now to eliminate these terms systematically so that we get a sufficient number of linearly independent eigenvectors. As indicated in Figure 4.3 by the solid bended lines, this can be done by simply superposing an increasing number of successive terms and choosing all other constants to be equal to zero. Of course these solutions are by no means unique. We just choose the most compact ones. For an odd value of i this yields the following (still quite cumbersome) solutions

$$\alpha_{I+\frac{1}{2}-\lambda} = (-1)^{\kappa-\lambda}(\mp 1)^{\kappa-\lambda-1} N_\kappa \Big[\mu^+\left(I+\frac{1}{2}-\lambda\right)\mu^+\left(I-i-\frac{1}{2}+\lambda\right) \mp \mu^-\left(I+\frac{1}{2}-\lambda\right)\mu^-\left(I-i-\frac{1}{2}+\lambda\right)\Big]^{-1}, \tag{4.20}$$

where $\lambda = 0, \ldots, (\kappa - 1)$ and

$$N_\kappa = \begin{cases} \left[\mu^-(I+\frac{1}{2}-\kappa)\mu^-(I-i-\frac{1}{2}+\kappa) - \frac{\left(\mu^+(I+\frac{1}{2}-\kappa)\mu^+(I-i-\frac{1}{2}+\kappa)\right)^2}{\mu^-(I+\frac{1}{2}-\kappa)\mu^-(I-i-\frac{1}{2}+\kappa)}\right]\alpha_{I+\frac{1}{2}-\kappa} \\ \left[(\mu^+(I-\frac{i}{2}))^2 \mp (\mu^-(I-\frac{i}{2}))^2\right]\alpha_{I-\frac{i}{2}}. \end{cases} \tag{4.21}$$

Here the first line refers to $\kappa = 1, \ldots, (i-1)/2$ and the second line applies to $\kappa = (i+1)/2$. For even i and negative parity the solution coincides with the first line of Equation (4.21), where now $\kappa = 1, \ldots, i/2$. Considering positive parity we get

$$N_\kappa = \begin{cases} \left[\mu^-(I+\frac{1}{2}-\kappa)\mu^-(I-i-\frac{1}{2}+\kappa) - \frac{\left(\mu^+(I+\frac{1}{2}-\kappa)\mu^+(I-i-\frac{1}{2}+\kappa)\right)^2}{\mu^-(I+\frac{1}{2}-\kappa)\mu^-(I-i-\frac{1}{2}+\kappa)}\right]\alpha_{I+\frac{1}{2}-\kappa} \\ \left[\mu^+(I-\frac{i}{2}+\frac{1}{2})\mu^+(I-\frac{i}{2}-\frac{1}{2}) - \mu^-(I-\frac{i}{2}+\frac{1}{2})\mu^-(I-\frac{i}{2}-\frac{1}{2})\right]\alpha_{I-\frac{i}{2}+\frac{1}{2}} \end{cases} \tag{4.22}$$

with $\kappa = 1, \ldots, (i-2)/2$ for the first line and $\kappa = i/2$ for the second one. Due to the presence of an $\alpha'_{m_{\min}}$ term, in contrast to the case of an odd i, here we have an additional solution. This results by simply choosing all constants to be equal to zero except for $\alpha_{m_{\min}}$ and $\alpha'_{m_{\min}}$, which are determined by eliminating the (4.15b) term:

$$\alpha'_{I-\frac{i}{2}+\frac{1}{2}} = \mp\frac{\mu^-(I-\frac{i}{2}+\frac{1}{2})\mu^-(I-\frac{i}{2}-\frac{1}{2})}{\mu^+(I-\frac{i}{2}+\frac{1}{2})\mu^+(I-\frac{i}{2}-\frac{1}{2})}\alpha_{I-\frac{i}{2}+\frac{1}{2}} \tag{4.23}$$

Note that in all cases there is one remaining constant. This is determined by the normalization condition.

Let us give a brief discussion of the above results. With respect to subspaces of fixed i the degeneracies shown in Figures 4.1 and 4.2 yield the pattern shown in Table 4.1. Obviously, for any i there are $(i+1)$ states. If i is odd, there is an equal number of states with positive and with negative parity, whereas for an even value of i the number of states with positive parity is larger by one than the number of states with negative parity. This is perfectly reproduced by our solutions: For an odd i the index κ in Equation (4.21) runs up to $(i+1)/2$ for each parity, meaning that there are $(i+1)$ solutions in total. If i is even, Equation (4.22) yields $(i/2)$ solutions for both parities and an additional one for positive parity.

i	τ
0	+
1	+-
2	+-+
3	+-+-
...	

Table 4.1: Numerically detected degeneracy pattern.

4.3 The role of the inversion symmetry

In the preceding section we have constructed the full degenerate subspace by determining the coefficients in the ansatz (4.12) so that we arrive at triplet states of the two central spins. Obviously, such a construction is still possible if the inversion symmetry is broken. Note that if $I_1 \neq I_2$, additional labels for the spin length have to be introduced in the coefficients (4.9) for the then following calculations. However, it is simple to see that in general our states are no longer eigenstates with respect to $H_{2\mathrm{G}}$ because the degeneracy between the $H_{2\mathrm{G}}$ eigenstates $|\pm, m_1\rangle|\mp, m_2\rangle$ is lifted. Indeed, this can be easily recovered by demanding $E_+(A^{(1)}, I_1) + E_-(A^{(2)}, I_2) = E_-(A^{(1)}, I_1) + E_+(A^{(2)}, I_2)$, which yields the quite remarkable relation

$$A^{(1)}\dim(\mathcal{H}_1) = A^{(2)}\dim(\mathcal{H}_2)\,, \tag{4.24}$$

where $\dim(\mathcal{H}_i) = 2I_i + 1$ denotes the dimension of the Hilbert space associated with I_i. Note that the bath spins $\sum_{j=1}^{N_i} \vec{I}_{i,j}$ couple to different values of I_i so that, by a corresponding choice of $A^{(1)}$ and $A^{(2)}$, several different degenerate subspaces can be implemented.

Relation (4.24) means that the inversion symmetric case is only an example of a whole class of systems exhibiting the same type of systematic degeneracy. In Figure 4.4 we plot the relevant part of the spectrum for $I_1 \neq I_2$ with $I_2 > I_1$. In the upper panel the couplings violate the relation (4.24) and consequently the degeneracy between the multiplets is lifted. In the bottom panel it is recovered by choosing $A^{(1)}$ and $A^{(2)}$ according to Equation (4.24), which gives

$$A^{(1)} = \frac{1+2I_2}{I_1+I_2+1}A \tag{4.25a}$$

$$A^{(2)} = \frac{1+2I_1}{I_1+I_2+1}A. \tag{4.25b}$$

In direct analogy to the inversion symmetric case the branch begins at (I_1+I_2) and ends at (I_2-I_1+1).

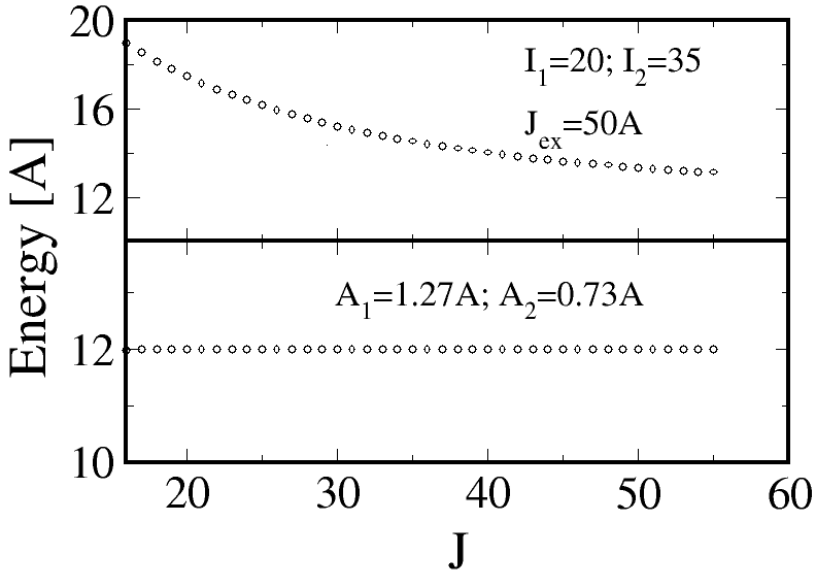

Figure 4.4: Formerly degenerate branch of the spectrum for $I = 20$ and $J_{\mathrm{ex}} = 25A$. The inversion symmetry is broken by choosing $I_1 \neq I_2$. The deviation from the degenerate case is stronger for multiplets with a small value of the quantum number J than for those with a large value. The bottom panel shows the spectrum with the degeneracy recovered by choosing $A^{(1)} \neq A^{(2)}$ due to Equation (4.24).

The relation (4.24) has a concrete physical meaning: Consider a semiconductor double quantum dot. As explained in detail in Chapter 5, here the electron spins interact with the surrounding nuclear spins via the hyperfine interaction, yielding a system of two coupled Gaudin models. The role of the couplings $A^{(1)}$ and $A^{(2)}$ is played by the overall coupling strengths of the respective dots, given by the sum of all hyperfine coupling constants (which depends on the properties of the respective material and the dot geometry). The size of the two Hilbert spaces results from the spatial extent of the respective electron wave function. If it is e.g. stretched over a larger area, each individual coupling decreases, but the sum remains unaltered. Hence, in an approximative sense, the relation (4.24) can always be realized by properly adjusting the electron wave functions.

With respect to possible future applications of $\mathcal{H}_{\mathrm{D}}$ it is important to note that for parameters only weakly violating Equation (4.24), the multiplets are still *nearly* degenerate: Let us fix $A^{(1)} = A^{(2)}$ and vary I_1 and I_2 so that Equation (4.24) is violated. From the eigenvalues of $H_{2\mathrm{G}}$ it is clear that the degeneracy is lifted in a continuous way. Furthermore, as can be seen very well in the upper panel of Figure 4.4, the influence of $I_1 \neq I_2$ on multiplets with small quantum numbers J is much stronger than on those with large values of J. This is also the case if we analogously choose $A^{(1)} \neq A^{(2)}$.

4.4 Summary and outlook

In summary we have reported an unexpected systematic degeneracy in an inversion symmetric system of two coupled Gaudin models with homogeneous couplings, as physically corresponding to separate spin baths in an e.g. semiconductor double quantum dot. This

leads to a degenerate subspace of macroscopic size. We have constructed the complete degenerate subspace, which is fully located in the kernel of the commutator between the two Gaudin models and their coupling term. Furthermore, we have studied the role of the inversion symmetry. Indeed, it turns out that the inversion symmetric case is only an example for a whole family of systems all of which share the same type of systematic degeneracy. This exclusively originates from the degeneracy of two eigenspaces of the Gaudin part of the Hamiltonian, yielding a remarkable relation between the dimension of the bath Hilbert spaces and the couplings.

Nevertheless, so far we have not been able to detect the (possibly continuous) symmetry underlying this remarkable degeneracy, i.e. a set of generating operators that would connect the highly degenerate multiplets. This question remains as an important but probably rather intricate problem for further studies. Furthermore, it would be fruitful to study applications of the degenerate space, especially in the context of solid state quantum information processing.

Part II

Hyperfine induced spin dynamics

5 Basics of hyperfine interaction

In the introduction we gave a list of three points motivating the study of central spin models. In the first part of this thesis we basically focused on the first and the last point and investigated very basic properties of central spin models from a rather abstract point of view. In the present part we come to the remaining point. Here we consider central spin models as a description of the hyperfine interaction between the electron and the nuclear spins in mainly III-V semiconductor double quantum dots and investigate the hyperfine induced spin dynamics. As already mentioned in the introduction, here one has to distinguish between the case of a strong and the case of a weak magnetic field applied to the central spin system. The first case is well-understood. Therefore we focus on the case of a zero magnetic field, which (as explained below) restricts our investigations to exact methods.

In Section 3.2 we demonstrated that any central spin model with homogeneous couplings is integrable via complete sets of commuting operators. In Chapter 6 we make advantage of this fact and evaluate the electron spin dynamics in a model of two exchange coupled electron spins interacting with a common bath of nuclear spins via homogeneous couplings in an almost analytical fashion. Focusing predominantly on the detrimental aspects of the hyperfine interaction, we in particular derive a scaling law for the decoherence time. Then, in Chapter 7, we come back to the system of two coupled Gaudin models with homogeneous couplings investigated in Chapter 4 with respect to its spectral properties. Here we focus on the *advantages* of the hyperfine interaction and, regarding the electron spins as an effective coupling between the two nuclear baths, study the nuclear spin dynamics. We demonstrate that for weakly coupled baths of realistic size it is possible to perform a nuclear swap, but not for smaller ones. Furthermore, we indicate that it should be possible to fully entangle the baths under the same conditions. Interestingly, the systematic degeneracy described in Chapter 4 seems to have a clear dynamical signature in these processes.

In the present chapter we give the basics necessary for the following chapters. In Sections 5.1 and 5.2 we introduce the hyperfine interaction mainly focusing on III-V semiconductor quantum dots and demonstrate that it is described by a central spin model. Then, in Section 5.3, we present solid state quantum information proposals based on quantum dot spin qubits and describe the role of the hyperfine interaction. Here the detrimental as well as the advantageous aspects of the hyperfine interaction are stressed. Although mainly focused on III-V semiconductor quantum dots, the results to be presented in Chapters 6 and 7 are also of interest with respect to a large variety of other important nanostructures in the context of spin based solid state quantum information processing. In Section 5.5 we briefly list the most important ones.

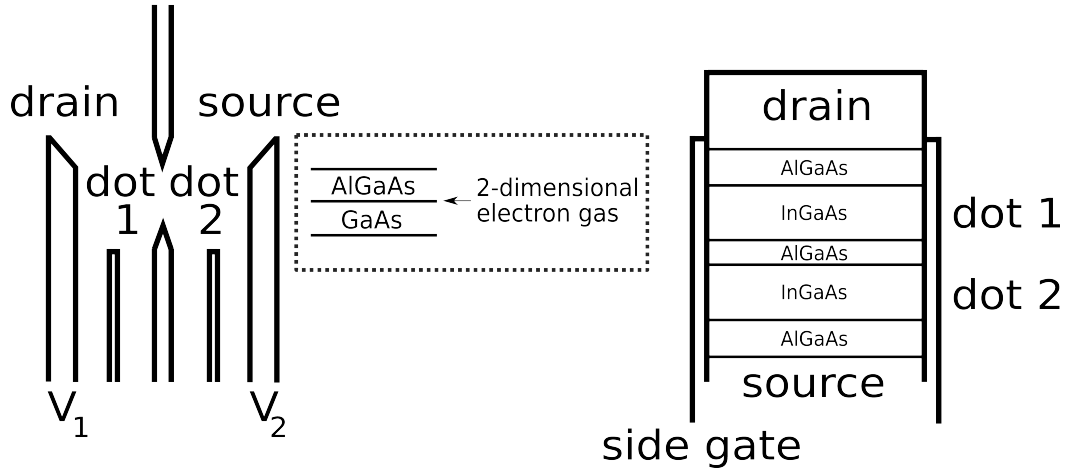

Figure 5.1: Sketch of electrostatically defined III-V semiconductor double quantum dots in lateral (left panel) and vertical (right panel) geometry after References [75, 77] and [79, 80]. The three-dimensional spatial confinement is achieved through local depletion of a two-dimensional electron gas formed at the interface between two layers of semiconductors with different Fermi energies and band gaps. The lateral dot is drawn in top view. The inset shows the used layer structure. The dots and, in the lateral case, the gate voltages are marked as corresponding to the explanations in Section 5.3.

5.1 III-V semiconductor quantum dots

Quantum dots are nanostructures in which particles are confined in all three spatial dimensions. As this leads to discrete energy levels, quantum dots are also referred to as artificial atoms. There are numerous ways to achieve the three dimensional confinement. At the time being, the most important experiments use electrostatically defined quantum dots based on III-V semiconductors. Here a two dimensional electron gas is locally depleted by electrical gates as depicted in Figure 5.1 for lateral geometry in the left [75, 77] and for vertical geometry in the right panel [79, 80].

A two dimensional electron gas is formed at the interface between semiconductors with different Fermi energies and band gaps like for example AlGaAs/GaAs and AlGaAs/InGaAs as in the two cases shown in Figure 5.1. Bringing together layers of these materials, electrons move from the material with the higher to the material with the lower Fermi energy, until the two Fermi energies are balanced. This is sketched in the upper panel of Figure 5.2. The electrons leave behind positively charged donors. Locally, this gives rise to an electrostatic potential, causing the bands to bend as shown in the bottom panel of Figure 5.2. Provided the electrostatic potential is large enough, the conduction band of the narrow gap material is bended below the Fermi energy. Consequently, at the heterojunction we have electrons free to move in two spatial dimensions.

The electronic properties of a bulk semiconductor are usually calculated using the so-called $\vec{k} \cdot \vec{p}$ method [81, 82]. Here one starts from the Schrödinger equation for an electron in a periodic potential $V_0(\vec{r})$. The eigenfunctions are Bloch functions $\psi_{n\vec{k}} = e^{i\vec{k}\vec{r}} u_{n\vec{k}}$, where $u_{n\vec{k}}$ is a lattice periodic function, $\vec{k}$ is an element of the first Brillouin zone and n is the band index.

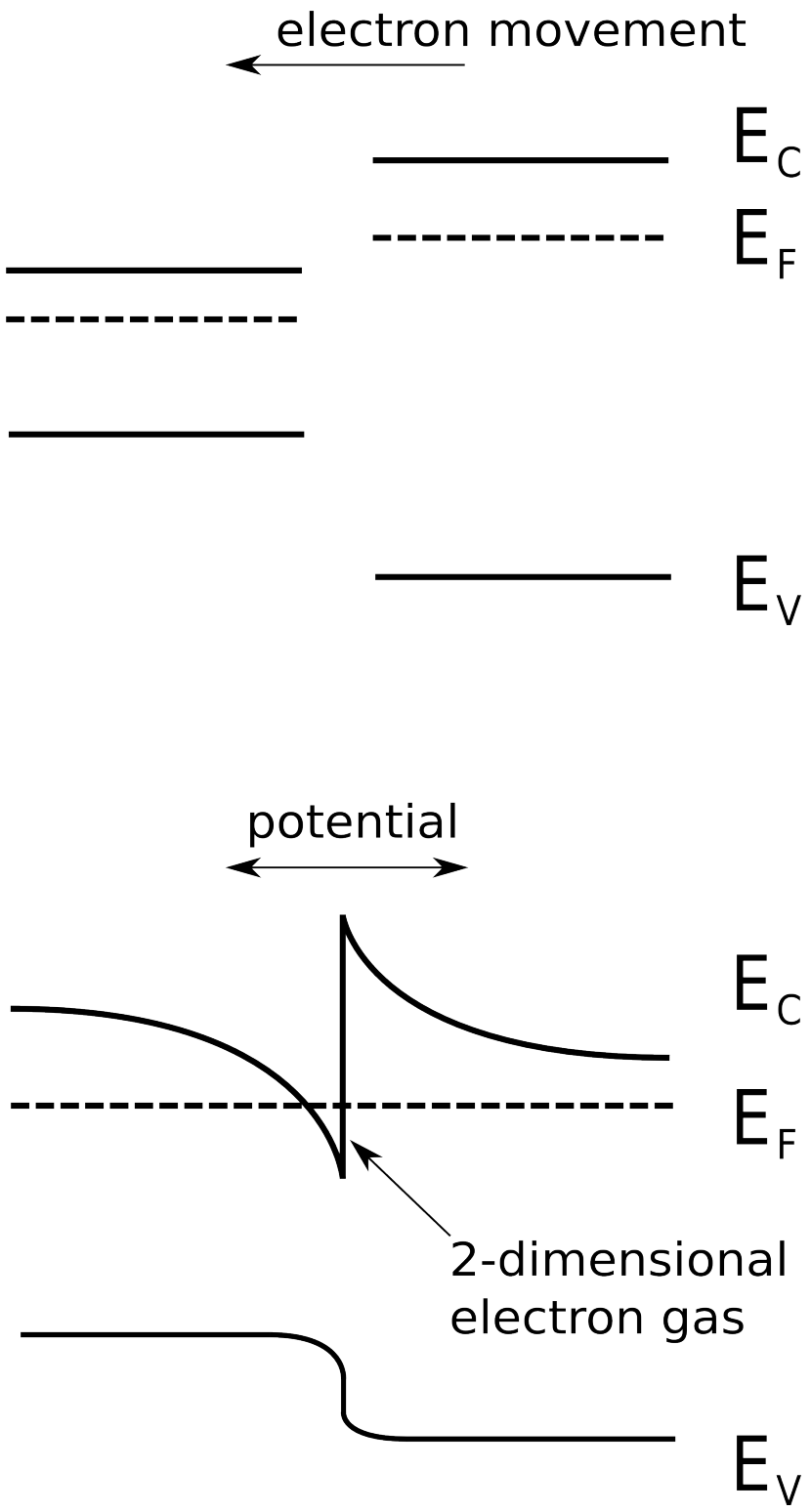

Figure 5.2: The formation of a two-dimensional electron gas is sketched. As schematically shown in the upper panel, two layers of semiconductors with different Fermi energies E_F and band gaps are brought together. Here E_V denotes the valence band energy and E_C the conduction band energy. Electrons move from the material with the higher to the one with the lower Fermi energy. This gives rise to an electrostatic potential, causing the bands to bend as shown in the bottom panel. If the electrostatic potential is large enough, the conduction band of the narrow gap material is bended below the Fermi energy so that a two-dimensional electron gas is formed.

Inserting this into the Schrödinger equation yields the following relation for the lattice periodic functions

$$\left(\frac{\vec{p}^2}{2m_\mathrm{e}} + V_0(\vec{r}) + \frac{\hbar^2 k^2}{2m_\mathrm{e}} + \frac{\hbar}{m_\mathrm{e}}\vec{k}\cdot\vec{p}\right) u_{n\vec{k}} = E_n(\vec{k})u_{n\vec{k}}, \tag{5.1}$$

where we used the notation introduced in Equation (2.22). Typically, properties near local extrema of the band structure are of particular interest. For III-V semiconductors the extrema of relevance are at the Γ point, corresponding to $\vec{k} = 0$. It is simple to solve (5.1) at the Γ point. The lattice periodic functions for non-zero values of $\vec{k}$ can be expressed through the functions at the Γ point:

$$u_{n\vec{k}}(\vec{r}) = \sum_\nu c_{n\nu}(\vec{k})u_{\nu 0}(\vec{r}) \tag{5.2}$$

Inserting this ansatz into (5.1) leads to an eigenvalue problem for the coefficients $c_{n\nu}(\vec{k})$, where bands with different indices n and m are coupled via the term $\vec{k}\cdot\vec{p}$. Most of the III-V semiconductors have zincblende structure. A group theoretical analysis shows that for this symmetry 14 bands (seven bands with two spin states each) are coupled by $\vec{k}\cdot\vec{p}$. The resulting 14×14 matrix is called the extended Kane model. It is now possible to derive effective Hamiltonians for certain subsets of the 14 bands. To this end it is assumed that the bands of interest are only weakly coupled to the other bands via $\vec{k}\cdot\vec{p}$. Then they can be decoupled to an arbitrary order in $\vec{k}\cdot\vec{p}$ using quasi-degenerate perturbation theory [81, 82]. If only a single band is considered, the so-called effective mass Hamiltonian results. This is identical to the Hamiltonian of a free particle with the rest mass being replaced by a 3×3 effective mass tensor. The effective mass approximation is typically sufficient to describe conduction bands and consequently the state of an electron in a III-V semiconductor quantum dot.

However, in an electrostatically defined quantum dot there is a confining potential $V(\vec{r})$, which breaks the translational symmetry, so that already (5.1) is not valid anymore. An approach to this problem is given by the so-called envelope function method. Here one assumes that the potential varies slowly on the length scale of the lattice constant and consequently makes the ansatz

$$\psi(\vec{r}) = \sum_n a_n(\vec{r})\psi_{n0}(\vec{r}), \tag{5.3}$$

where $\vec{k} = 0$ is again chosen with respect to III-V materials. Inserting this into the Schrödinger equation then yields an eigenvalue problem for the coefficients $a_n(\vec{r})$ quite similar to the one for the coefficients $c_{n\nu}(\vec{k})$, where in particular different bands are again coupled via $\vec{k}\cdot\vec{p}$. It is therefore possible to solve the problem with basically the same considerations as described above.

Typically, the confinements [83, 84] are adequately described by Gaussian wells

$$V(\vec{r}) = -v_0 e^{-\frac{r}{r_\mathrm{D}}} \tag{5.4}$$

Pöschl-Teller potentials

$$V(\vec{r}) = -v_0 \cosh^{-2}(-r^2/r_\mathrm{D}^2), \tag{5.5}$$

or simple parabolic potentials (here: $|r| \leq r_\mathrm{D}$):

$$V(\vec{r}) = -v_0 + \frac{v_0}{r_\mathrm{D}} r^2 \tag{5.6}$$

Here r_D denotes the radius of the quantum dot and v_0 is depth of the potential. All the potentials have in common that they are rotational invariant. Consequently, in an approximative sense, the states can be assigned a certain value of the orbital angular momentum quantum number L. The ground state of conduction band electrons will be s-type, the first exited state p-type.

5.2 Hyperfine interaction

In the following we derive the Hamiltonian of the hyperfine interaction [22, 23], demonstrating that it is described by a central spin model. Here we mainly follow [23]. The Dirac Hamiltonian of an electron in an electromagnetic field reads

$$H_\mathrm{D} = \vec{\alpha} \cdot \vec{\pi} + \beta m_\mathrm{e} c^2 - e\varphi(\vec{r}), \tag{5.7}$$

with $\vec{\pi} = c\left(\vec{p} + e\vec{A}(\vec{r})\right)$. Here $\vec{A}(\vec{r})$ is the vector and $\varphi(\vec{r})$ is the scalar potential of the electromagnetic field. In the standard representation of the Dirac algebra $\vec{\alpha}$ and β are given by

$$\alpha_i = \begin{pmatrix} 0 & \sigma_i \\ \sigma_i & 0 \end{pmatrix} \tag{5.8}$$

$$\beta = \begin{pmatrix} \mathbb{1} & 0 \\ 0 & -\mathbb{1} \end{pmatrix}, \tag{5.9}$$

where $i = 1, 2, 3$, σ_i denotes the i-th Pauli matrix and $\mathbb{1}$ is the 2×2 unit matrix. The Dirac Hamiltonian acts on a bispinor Ψ of two two-component spinors χ_1 and χ_2:

$$\Psi = \begin{pmatrix} \chi_1 \\ \chi_2 \end{pmatrix} \tag{5.10}$$

The time-independent Dirac equation $H_\mathrm{D}\Psi = E\Psi$, with $E = m_\mathrm{e}c^2 + \epsilon$, yields the following set of coupled equations for the two spinors χ_1 and χ_2:

$$-\left(\epsilon + e\varphi(\vec{r})\right)\chi_1 + \vec{\sigma} \cdot \vec{\pi}\chi_2 = 0 \tag{5.11}$$

$$\vec{\sigma} \cdot \vec{\pi}\chi_1 - \left(2m_\mathrm{e}c^2 + e\varphi(\vec{r}) + \epsilon\right)\chi_2 = 0 \tag{5.12}$$

Solving the second identity for χ_2 and inserting the result in the first equation yields:

$$\underbrace{\left(\vec{\sigma} \cdot \vec{\pi} \frac{1}{2m_\mathrm{e}c^2 + e\varphi(\vec{r}) + \epsilon} \vec{\sigma} \cdot \vec{\pi} - e\varphi(\vec{r})\right)}_{=H_1} \chi_1 = \epsilon\chi_1 \tag{5.13}$$

In a strict sense, H_1 can not be regarded as a Hamiltonian for the spinor χ_1. This manifests itself in H_1 containing non-hermitian terms and is due to the fact that the two spinors χ_1 and χ_2 are not decoupled. A decoupling of χ_1 and χ_2 in orders of (v/c), where v is the velocity of the electron, can be achieved by applying a series of so-called Foldy-Wouthuysen

transformations [74, 85]. This procedure results in a correct Hamiltonian for χ_1 to arbitrary order in (v/c).

However, already H_1 contains the correct spin-dependent terms, as becomes apparent by inserting the definition of $\vec{\pi}$ and using the vector identity

$$(\vec{\sigma}\cdot\vec{x})\,(\vec{\sigma}\cdot\vec{y}) = \vec{x}\cdot\vec{y} + i\vec{\sigma}\cdot(\vec{x}\times\vec{y})\,. \tag{5.14}$$

The spin-dependent terms are given by the isotropic hyperfine interaction, the anisotropic hyperfine interaction and the spin-orbit interaction:

$$H_{\mathrm{ihf}} = \frac{e^2\hbar c^2}{\left(2m_{\mathrm{e}}c^2 + e\varphi(\vec{r}) + \epsilon\right)^2}\left(\vec{E}(\vec{r})\times\vec{A}(\vec{r})\right)\cdot\vec{\sigma} \tag{5.15}$$

$$H_{\mathrm{ahf}} = \frac{e\hbar c^2}{2m_{\mathrm{e}}c^2 + e\varphi(\vec{r}) + \epsilon}\left(\vec{\nabla}\times\vec{A}(\vec{r})\right)\cdot\vec{\sigma} \tag{5.16}$$

$$H_{\mathrm{so}} = \frac{e\hbar c^2}{\left(2m_{\mathrm{e}}c^2 + e\varphi(\vec{r}) + \epsilon\right)^2}\left(\vec{E}(\vec{r})\times\vec{p}\right)\cdot\vec{\sigma} \tag{5.17}$$

Here we introduced the electric field $\vec{E}(\vec{r}) = -\vec{\nabla}\varphi(\vec{r})$. We now focus on the electromagnetic field of a nucleus with charge Ze, where $Z \in \mathbb{N}$. Here we have

$$\varphi(\vec{r}) = \frac{1}{4\pi\varepsilon_0}\frac{Ze}{r} \tag{5.18a}$$

$$\vec{E}(\vec{r}) = \frac{1}{4\pi\varepsilon_0}\frac{Ze\vec{r}}{r^3} \tag{5.18b}$$

$$\vec{A}(\vec{r}) = \frac{\mu_0}{4\pi}\frac{\vec{\mu}\times\vec{r}}{r^3}, \tag{5.18c}$$

where $\vec{\mu}$ is the nuclear magnetic moment and μ_0 is the magnetic constant. In the following we consider the isotropic hyperfine interaction, to which we simply refer as the hyperfine interaction from now on. We derive an effective spin Hamiltonian for an electron confined in a III-V semiconductor quantum dot, which turns out to have the form of a central spin model. Note that the following derivations are in fact very generic. Still, we always have in mind an electron in a III-V semiconductor quantum dot.

Inserting the electromagnetic quantities (5.18) in H_{ihf} and applying the vector identity

$$\vec{x}\times(\vec{y}\times\vec{z}) = \vec{y}\cdot(\vec{x}\cdot\vec{z}) - \vec{z}\cdot(\vec{x}\cdot\vec{y}) \tag{5.19}$$

yields:

$$H_{\mathrm{ihf}} = \frac{1}{4\pi\varepsilon_0}\frac{Ze^3\hbar c\mu_0}{4\pi\left(2m_{\mathrm{e}}c^2 + e\varphi(\vec{r}) + \epsilon\right)^2}\left(\frac{\vec{\sigma}\cdot\vec{\mu} - (\vec{\sigma}\cdot\vec{e}_r)\,(\vec{\mu}\cdot\vec{e}_r)}{r^4}\right) \tag{5.20}$$

Here $\vec{e}_r$ denotes the unit vector in the direction of $\vec{r}$. We now assume ϵ to be negligible against the rest energy contribution $m_{\mathrm{e}}c^2$. Introducing

$$d = \frac{1}{4\pi\varepsilon_0}\frac{Ze^2}{2m_{\mathrm{e}}c^2} \tag{5.21}$$

and the Bohr magneton $\mu_{\mathrm{B}} = \hbar e/(2m_{\mathrm{e}})$, we arrive at

$$H_{\mathrm{ihf}} = \frac{\mu_0\mu_{\mathrm{B}}}{4\pi}\frac{d}{1+(d/r)}\left(\frac{\vec{\sigma}\cdot\vec{\mu} - (\vec{\sigma}\cdot\vec{e}_r)\,(\vec{\mu}\cdot\vec{e}_r)}{r^4}\right). \tag{5.22}$$

Let us now assume that the electron is confined in a III-V semiconductor quantum dot and that it is in some state $|\psi_i\rangle$ as resulting from the envelope function method described in Section 5.1. Taking the respective expectation value of H_{ihf} yields

$$\langle\psi_i|H_{\mathrm{ihf}}|\psi_i\rangle = \frac{\mu_0\mu_{\mathrm{B}}}{4\pi}\int_0^\infty dr\frac{d}{(r+d)^2}g(\vec{r}) \tag{5.23}$$

with

$$g(\vec{r}) = \int d\Omega|\psi_i(\vec{r})|^2(\vec{\sigma}\cdot\vec{\mu} - (\vec{\sigma}\cdot\vec{e}_r)\,(\vec{\mu}\cdot\vec{e}_r))\,. \tag{5.24}$$

Obviously, the radial integration is dominated by the contribution on distances $r \leq d$. As d is of the order 10^{-15}m, it is adequate to approximate

$$\langle\psi_i|H_{\mathrm{ihf}}|\psi_i\rangle = \frac{\mu_0\mu_{\mathrm{B}}}{4\pi}g(\vec{r})|_{r=0}, \tag{5.25}$$

which can be easily evaluated yielding:

$$\langle\psi_i|H_{\mathrm{ihf}}|\psi_i\rangle = \frac{4}{3}\mu_0\mu_{\mathrm{B}}\gamma_I|\psi_i(0)|^2\vec{S}\cdot\vec{I} \tag{5.26}$$

Here we introduced $\vec{S} = (1/2)\vec{\sigma}$ and $\vec{\mu} = \gamma_I\vec{I}$ with γ_I being the nuclear gyromagnetic ratio. Note that γ_I depends on the nuclear species. So far, the origin of the coordinate system has been chosen with respect to the nucleus, meaning that the strength of the hyperfine interaction is proportional to the value of the electronic wave function *at the site of the nuclear spin*. If we now generalize the Hamiltonian (5.26) to an arbitrary number of electrons and nuclei, we arrive at the effective Hamiltonian which is the basis for all analyses in the present part of the thesis:

$$H_{\mathrm{HF}} = \langle\psi_i|H_{\mathrm{ihf}}|\psi_i\rangle = \sum_{i=1}^{N_{\mathrm{c}}}\vec{S}_i\cdot\sum_{j=1}^{N}A_j^{(i)}\vec{I}_j + \sum_{i<j}J_{\mathrm{ex}}^{(ij)}\vec{S}_i\cdot\vec{S}_j \tag{5.27}$$

A magnetic field can be included by adding a Zeeman term as given in Equation (1.2). Obviously, H_{HF} has the form of a central spin model as given in Equation (1.1). Here N_{c} and N denote the number of electron or nuclear spins, respectively. We introduced

$$A_j^{(i)} = (4/3)\mu_0\mu_{\mathrm{B}}\gamma_{I_j}|\psi^{(i)}(\vec{r}_j)|^2, \tag{5.28}$$

where $\psi^{(i)}(\vec{r})$ is the wave function of the i-th electron and $\vec{r}_j$ is the site of j-th nucleus. Note that $|\psi_i\rangle$ is the state of an electron confined in a quantum dot and not an atomic state. Hence, also excited states lead to a non-zero hyperfine interaction. This is in contrast to excited atomic states, which have a zero at the site of the nucleus. Just like in the first part of the thesis, we define an overall hyperfine coupling strength $A = (1/N_{\mathrm{c}})\sum_{i=1}^{N_{\mathrm{c}}}\sum_{j=1}^{N}A_j^{(i)}$. The second term in (5.27) accounts for an exchange coupling between the different electron spins. Obviously, H_{HF} conserves the total spin $\vec{J} = \sum_{i=1}^{N_{\mathrm{c}}}\vec{S}_i + \sum_{i=1}^{N}\vec{I}_i$.

5.3 Hyperfine interaction and quantum information proposals

In the preceding section we introduced the hyperfine interaction with respect to an electron spin confined in a III-V semiconductor quantum dot. Indeed, the III-V materials most

intensively studied at the present time, as exemplified in Figure 5.1, consist of entirely spin carrying isotopes. Therefore the hyperfine interaction will play an important role in these nanostructures.

Most of the work into this direction is clearly motivated by the so-called Loss-DiVincenzo proposal, where the electron spins are utilized as qubits [21]. It can be shown that single qubit manipulations together with a XOR gate can be assembled to perform any quantum computation [86]. Within the Loss-DiVincenzo proposal two-qubit operations are realized by pulsing the electrostatic barrier between two different quantum dots. This leads to a time-dependent exchange coupling between the respective electron spins:

$$H(t) = J_{\mathrm{ex}}(t)\vec{S}_1 \cdot \vec{S}_2 \tag{5.29}$$

It is now simple to see that provided $(1/\hbar)\int_{t'=0}^{t_{\mathrm{swap}}} dt' J(t') = \pi$ the application of the time evolution operator

$$U = Te^{-\frac{i}{\hbar}\int_{t'=0}^{t_{\mathrm{swap}}} dt' H(t')}, \tag{5.30}$$

where T denotes the time ordering operator, interchanges the states of the two electron spins. This operation is called swap. Pulsing for only half the time, $(t_{\mathrm{swap}}/2)$, yields the so-called square-root of swap operation. This can be embedded in a series of single qubit manipulations to constitute a XOR gate. Hence, taking single qubit manipulations to be given, any quantum operation can be realized using quantum dot spin qubits. Loss and DiVincenzo suggested to use electron spin resonance in order to realize single electron spin rotations. Until today, many new solid state quantum information proposals utilizing electron spins confined in semiconductor quantum dots as qubits have been developed. The crucial differences to the Loss-DiVincenzo proposal lie in the experimental feasibility of the single qubit manipulations. A particularly interesting approach in this context suggests a set-up of three quantum dots, enabling to perform one and two-qubit gates using an exchange coupling exclusively.

With respect to a point of view as described above, the hyperfine interaction has a clearly detrimental character, as it provides a decohering environment. The character of the hyperfine interaction changes if it is considered as an efficient way to access the nuclear spins. There are various proposals for using the nuclear bath in a semiconductor quantum dot for quantum information purposes, which are essentially motivated by the long decoherence times of the nuclear spins [24–29]. In the following we describe the basic concepts shared by most of the approaches. To this end we consider two instructive examples given in References [25, 26]. The first one uses the nuclear spins in order to store quantum states of the electron spin, whereas the second one utilizes two collective nuclear spin states as the qubit.

Let us consider the basic idea of the first proposal [25]. As demonstrated in Equation (3.7), for a general central spin model, the Hamiltonian (5.27) consists of a flip-flop part H_{ff} and a z term. The latter can be regarded as an effective magnetic field. It is possible to compensate this by the external magnetic field B so that the dynamics is governed exclusively by H_{ff}. Assuming the bath to be fully polarized initially, i.e. $N_{\mathrm{D}}^{\mathrm{b}} = 0$, the time evolution induced by H_{ff} can be used to map an arbitrary electron spin state coherently into the nuclear bath:

$$(a|\Uparrow\rangle + b|\Downarrow\rangle)\,|N_{\mathrm{D}}^{\mathrm{b}} = 0\rangle \rightarrow |\Uparrow\rangle\left(a|N_{\mathrm{D}}^{\mathrm{b}} = 0\rangle + b|N_{\mathrm{D}}^{\mathrm{b}} = 1\rangle\right) \tag{5.31}$$

Here $|N_{\mathrm{D}}^{\mathrm{b}} = 0\rangle$ denotes the fully polarized nuclear state and $|N_{\mathrm{D}}^{\mathrm{b}} = 1\rangle$ the state with one spin flip as resulting from the action of the time evolution operator (corresponding to H_{ff}) for a very short time t. As the nuclear spins have long decoherence times, in principle the electron spin state can be stored for a long time on this way.

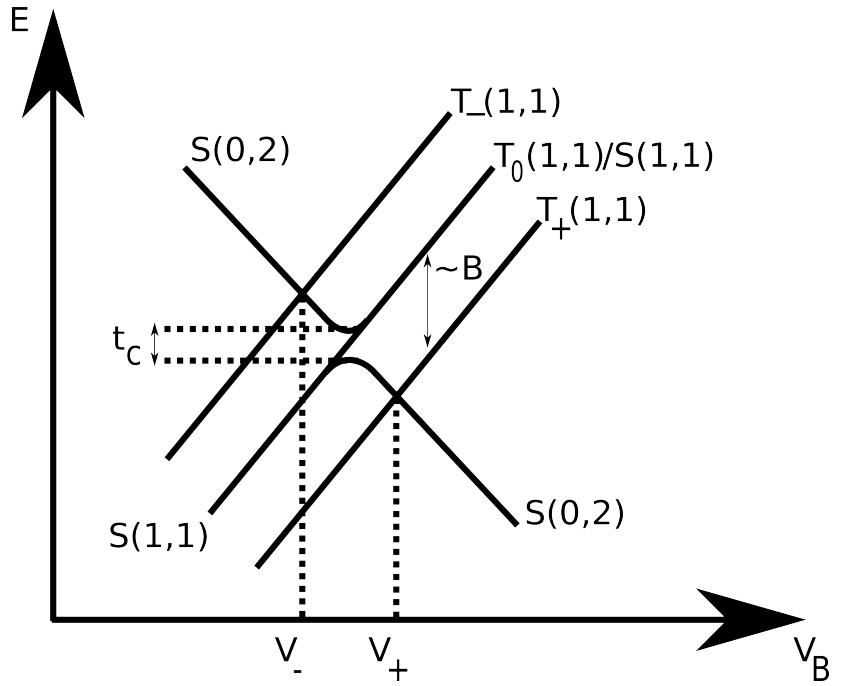

Figure 5.3: Sketch of the energy dispersion of a double quantum dot near to a $(0,2) \rightarrow (1,1)$ charge transition. Here (n,m) denotes the number of electrons in the first and the second dot. The influence of the hyperfine interaction is not included. The energy is plotted against the bias $V_\mathrm{B} = (V_2 - V_1)$. The states $|S(n,m)\rangle$, $|T_i(n,m)\rangle$, where $i = +,0,-$, denote the electron spin singlet and triplet states with both electrons being in the second dot for $(0,2)$ or one electron being in each dot for $(1,1)$.

The second of the above mentioned proposals [26] now considers the states $|N_\mathrm{D}^\mathrm{b} = 0\rangle$ and $|N_\mathrm{D}^\mathrm{b} = 1\rangle$ as the qubit. One-qubit gates are implemented by mapping the nuclear state to the electron which is then manipulated via e.g. electron spin resonance. The resulting state is mapped back to the nuclear ensemble. The two-qubit operations are simply realized by mapping the nuclear state to the electron and then transferring it to a second quantum dot. This approach combines the possibility to efficiently manipulate the electron spin state with the long decoherence times of the nuclear spins.

5.4 Experimental and theoretical approaches

In the preceding sections we introduced the hyperfine interaction mainly focusing on III-V semiconductor quantum dots and described its vice and virtue with respect to different important solid state quantum information proposals. Within the last decade, these have caused enormous experimental and theoretical effort with respect to the experimental implementation of the proposals as well as in understanding the different spin interactions, in particular the hyperfine interaction [36, 37, 71, 72, 87].

5.4.1 Experimental implementations

Indeed, one and two qubit gates [75] have been successfully implemented in GaAs quantum dots. The single spin rotations have been realized via electron spin resonance as well as by means of optical manipulation [76, 88, 89]. Furthermore, very high nuclear spin polarizations

up to 80% have been realized [80, 90–92], which are of key importance for the nuclear spin baths to act as a ressource of quantum information processing. Rather than giving a detailed review on all aspects of these experiments, in the following we describe, from a rather heuristic point of view, a typical initialization procedure as demonstrated in Reference [75] and a recent polarization experiment published in Reference [80]. These experiments contain most of the key ingredients of all experiments in the given context and are of direct importance for the work to be presented in the following chapters.

In Figure 5.3 a typical energy dispersion for a double quantum dot in a magnetic field near to a $(0,2) \rightarrow (1,1)$ charge transition is sketched. Here (n,m) gives the number of electrons in dot 1 and dot 2, as marked in Figure 5.1. The dispersion can be calculated using a simple Hubbard model (see e.g. [93]). The influence of the hyperfine interaction is not included. The energy is plotted against the bias $V_\mathrm{B} = (V_2 - V_1)$. Here V_j is the voltage applied to the j-th dot via either the gates, in lateral geometry, or the source-drain voltage if a vertical geometry is considered (see again Figure 5.1). The states $|S(n,m)\rangle, |T_+(n,m)\rangle, |T_0(n,m)\rangle, |T_-(n,m)\rangle$ denote the electron spin singlet and triplet states

$$|T_+\rangle = |\Uparrow\Uparrow\rangle \tag{5.32a}$$

$$|T_0\rangle = \frac{1}{\sqrt{2}}\left(|\Uparrow\Downarrow\rangle + |\Downarrow\Uparrow\rangle\right) \tag{5.32b}$$

$$|T_-\rangle = |\Downarrow\Downarrow\rangle \tag{5.32c}$$

$$|S\rangle = \frac{1}{\sqrt{2}}\left(|\Uparrow\Downarrow\rangle - |\Downarrow\Uparrow\rangle\right) \tag{5.32d}$$

with either both electrons being in the second dot for $(0,2)$ or one electron being in each dot for $(1,1)$. The $(0,2)$ triplet states are much higher in energy and therefore excluded in what follows. The parameter t_c denotes the tunnel coupling.

Obviously, the two electrons are immediately in the state $|S(0,2)\rangle$ when inserted into the second of the two quantum dots. The charging of the dots is detected via a quantum point contact (see e.g. [94]). This is a small constriction in the two-dimensional electron gas as shown in Figure 5.4. The larger the gate voltages, the less electrons can pass the constriction. If one of the gate electrodes is connected to one of the quantum dots, the charging can be detected by measuring the current through the quantum point contact.

If the bias is decreased strong enough, the initial state $|S(0,2)\rangle$ is transferred into the spatially separated singlet $|S(1,1)\rangle$. With $|T_+(1,1)\rangle$ and $|T_-(1,1)\rangle$ being splitted off by a magnetic field of the order of 100mT, the states $|T_0(1,1)\rangle$ and $|S(1,1)\rangle$, which are degenerate for large and small values of V_B as sketched in Figure 5.3, form an effective two level system. It is simple to see that the hyperfine interaction (5.27) couples $|T_0(1,1)\rangle$ and $|S(1,1)\rangle$. This leads to dephasing of the initial singlet state $|S(1,1)\rangle$, which can be used to initialize the electron spin system in different superpositions of $|T_0(1,1)\rangle$ and $|S(1,1)\rangle$, say $(\alpha_1|T_0(1,1)\rangle + \alpha_2|S(1,1)\rangle)$, by varying the passage speed. Therefore, in the investigations presented in Chapter 6 and 7 we mainly focus on initial electron spin states of this type.

It is possible to measure the square moduli of the coefficients α_i, allowing to determine the spin state resulting from a certain passage speed up to a relative phase of an integer multiple of π. In Figure 5.3 it can be seen that, increasing the bias after the initialization, the state $|T_0(1,1)\rangle$ can not be transferred back into a $(0,2)$ configuration. Hence, $|\alpha_2|^2$ and consequently $|\alpha_1|^2 = 1 - |\alpha_2|^2$ can be determined over many experimental runs by measuring the "returning probability" of the separated electron into the original dot using

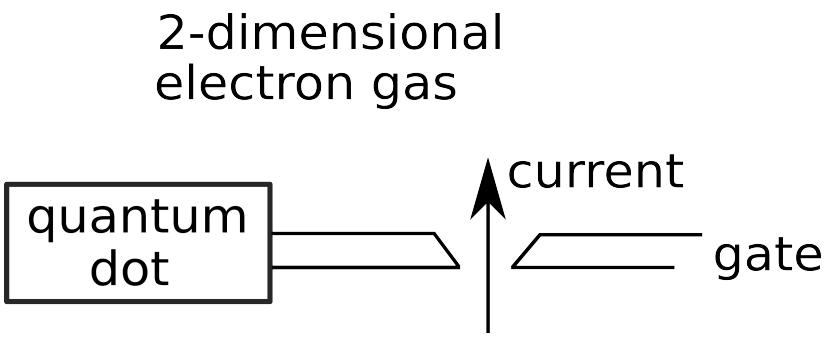

Figure 5.4: Sketch of a quantum point contact. We have a small constriction between two gates in a two-dimensional electron gas. The larger the gate voltages, the less electrons can pass the constriction. If one of the gates is connected to a quantum dot (as depicted), the charging of the dot can be determined by measuring the current through the quantum point contact.

the quantum point contact. If for example in one half of the runs the electron returns, we have $|\alpha_i|^2 = (1/2)$, meaning that the state has been initialized in $(1/\sqrt{2})(|T_0(1,1)\rangle \pm |S(1,1)\rangle)$.

With the above considerations it is now simple to understand the polarization experiment. Here one starts in a $(1,1)$ configuration. At $V_\pm$ shown in Figure 5.3, the $|T_\pm(1,1)\rangle$ states are degenerate with $|S(1,1)\rangle$. Consequently, here a $|T_\pm(1,1)\rangle$ state can make a transition into $|S(1,1)\rangle$ via the hyperfine interaction. This leads to a change of the bath polarization by (∓ 1). On this way the bath can be polarized through many runs just by properly adjusting V_B.

5.4.2 Different spin interactions

In the preceding sections we introduced different spin interactions with a special focus on the hyperfine interaction. Indeed, it turns out that the hyperfine interaction is the leading decoherence mechanism of an electron spin in a III-V semiconductor quantum dot: As demonstrated in Section 5.2, besides the hyperfine interaction interaction we have the anisotropic hyperfine and the spin orbit interaction. It can be shown that the first one mainly reduces to a weak dipole-dipole interaction [37]. For localized states the spin-orbit interaction does not lead to decoherence in zero magnetic field. However, in Reference [95] it is demonstrated that even for comparatively large magnetic fields the decoherence time induced by the spin-orbit interaction is of the order of microseconds, which is much larger than the typical time scales of the hyperfine interaction. Apart from the above mentioned decoherence mechanisms, there are processes which lead to dynamics within the nuclear baths, like e.g. dipolar and quadrupolar interactions and the coupling between the electron orbital degree of freedom and the nuclear spins [37]. The latter is of course weak for the s-type ground states. The fluctuations of the nuclear bath resulting from the other interactions influence the electron spin via the hyperfine interaction. However, as to be expected, the related time scales are much larger than those resulting from the direct electron-nuclear interaction [36, 37].

With respect to the theoretical treatment of the hyperfine interaction it turned out that one has to distinguish between the limit of a strong and the limit of a weak magnetic field as compared to the overall hyperfine coupling strength, meaning that either $B \geq A$ or $B < A$ [36, 37]. In the first case the flip-flop terms between the electron and nuclear spins H_{textff}, as given in Equation (3.7), are typically strongly suppressed. As already explained in Section 3.3, this can be easily understood thinking of first order time-dependent perturbation theory.

Flipping a spin in a magnetic field causes an energy change ΔE proportional to the magnetic field $\Delta E \propto B$. In order to assure energy conservation, this change has to be compensated by the simultaneous flop of a bath spin. Provided $B > A$, this is not possible and flip-flop terms are not allowed to contribute in first order. This enables to treat H_{ff} perturbatively or, assuming an extremely strong field $B \gg A$, to even completely neglect them [30–35]. However, considering for example a GaAs quantum dot, the condition $B \geq A$ means that $B \geq 1T$, which is, as explained above, much larger than any magnetic field used in the experiments [96, 97].

It is the purpose of the present part of the thesis to investigate the experimentally significant case of $B < A$. In the following investigations we restrict ourselves to the less intensively studied double quantum dot setup $N_{\mathrm{c}} = 2$, which, as explained in Section 5.3, is of central importance for the realization of two qubit operations. At the time being it is commonly accepted that the weak field case can be treated only via exact methods. Here one can follow three different routes:

- Restrictions to the hyperfine coupling constants [49, 98]
- Restriction to small system sizes enabling progress via exact numerical diagonalizations [36, 47]
- Restriction of the initial state to the one magnon sector [30, 31]

As explained in the introduction of the present chapter, in Chapter 6 we investigate the dynamics in a model with all hyperfine coupling constants being equal to each other, which has shown to be integrable in Section 3.2. This approach corresponds to the first point of the above list. In Chapter 7 we then revisit the two bath model introduced in Chapter 4. Here the two electron spins are considered to interact with individual nuclear spin baths via homogeneous couplings. Just as in Section 4.1 we reduce the dimension of the problem by approximating the two baths by single long spins and numerically study the nuclear spin dynamics of the resulting model. Hence, the work to be presented in Chapter 7 combines the first two points of the above list.

5.5 Alternative approaches to quantum information processing using spins

As described above, most of the work to be presented in the following chapters is motivated by the idea to use III-V semiconductor quantum dots for solid state quantum information purposes. However, many of the results are also of direct interest to other nanostructures important in the context of solid state quantum information processing. Therefore we want to close our motivating discussion by briefly describing other highly relevant nanostructures.

As we have discussed in the preceding sections, the hyperfine interaction is the leading decoherence mechanism with respect to the electron spin playing the role of the qubit. A natural approach in order to circumvent this problem is to look for host materials which do not carry a nuclear spin. Promising candidates in this recent approach are carbon structures like graphene, carbon nanotubes [99–102] and nitrogen-vacancy centers [103] as well as silicon [104]. While the graphene based approaches still suffer in particular from the Klein paradox, which makes it experimentally demanding to confine electrons, the last two

ideas have undergone substantial theoretical as well as experimental progress in particular in recent times [105–113].

Very similar situations as in the above mentioned structures occur in magnetic molecules. The main motivation to deal with these structures results from the fact that they carry a large ground state spin, e.g. $S = 10$ in Fe_8 and Mn_{12}, and are subject to high magnetic anisotropy [114, 115]. Via the hyperfine interaction, the spin of a magnetic molecule couples to a comparatively small number of nuclear spins of the crystal structures, in which the molecule is embedded in. However, this still turns out to be an important source of decoherence [116–119].

In the preceding section we have discussed that, apart from its detrimental character, the hyperfine interaction can be regarded as an efficient way to access the nuclear degrees of freedom. An approach of Kane, very similar to the Loss-DiVincenzo proposal, uses the hyperfine interaction between the electron spins and the nuclear spins of the phosphorus donors in a Si:P matrix in order to utilize the latter as qubits [120]. Clearly, this idea is motivated by the long decoherence times of nuclear spins. Although not as popular as the Loss-DiVincenzo proposal, also this idea is subject to huge experimental effort [121–124]. In a recent experimental attempt, very similar to the proposals described in Section 5.3 in the context of the advantages of the hyperfine interaction, the nuclear spins of the phosphorus donors have been utilized as quantum memory, whereas the electron spins acted as qubits [125].

6 Hyperfine induced spin and entanglement dynamics in Double Quantum Dots: A homogeneous coupling approach

Parts of this chapter have been published in collaboration with John Schliemann in Reference [126].

In Chapter 5 we introduced the hyperfine interaction and explained its importance in the context of quantum information processing using III-V semiconductor quantum dot spin qubits. We stressed that with respect to the electron spin utilized as the qubit, the hyperfine interaction acts as a source of decoherence and therefore has a clearly detrimental character. This changes if it is regarded as an efficient way to access the nuclear degrees of freedom. The work presented in the following focuses on the first point of view considering a double quantum dot. As demonstrated in Section 3.2, the Hamiltonian of any central spin model with homogeneous coupling constants can be embedded in a complete set of commuting operators. In the present chapter we make advantage of this fact and consider the case of a double quantum dot with homogeneous hyperfine coupling constants, corresponding to a flattened electronic wave function as illustrated in the bottom panel of Figure 3.3. Here the two electron spins are interacting with a common bath of nuclear spins as particularly realistic for two nearby quantum dots.

In Section 6.1 we introduce the model and derive analytical expressions for the electron spin and entanglement dynamics. In Section 6.2 we study the related time evolutions for different exchange couplings and bath polarizations. For the completely homogeneous case of the exchange coupling being the same as the hyperfine couplings we find an empirical rule describing the transition from low polarization electron spin dynamics to high polarization electron spin dynamics. The latter shows a jump in the amplitude when varying the exchange coupling away from complete homogeneity. This effect as well as features like the periodicity of the dynamics are explained by analyzing the level spacings and their contributions to the dynamics. In Section 6.3 we extract the decoherence time from the dynamics by investigating the scaling behaviour of the short time electron spin dynamics. The result turns out to be in good agreement with experimental findings.

6.1 Model and formalism

The hyperfine interaction in a system of two quantum dot spin qubits is given by the Hamiltonian (5.27) with $N_c = 2$

$$H_{\mathrm{HF}} = \vec{S}_1 \cdot \sum_{i=1}^{N} A_i^{(1)} \vec{I}_i + \vec{S}_2 \cdot \sum_{i=1}^{N} A_i^{(2)} \vec{I}_i + J_{\mathrm{ex}} \vec{S}_1 \cdot \vec{S}_2, \tag{6.1}$$

where $J_{\rm ex}$ denotes an exchange coupling between the two electron spins $\vec{S}_1$, $\vec{S}_2$ and $A_i^{(1)}$, $A_i^{(2)}$ are the coupling parameters for their hyperfine interaction with the surrounding nuclear spins $\vec{I}_i$. As explained in Section 5.2, the Hamiltonian obviously conserves the total spin $\vec{J} = \vec{S} + \vec{I}$, where $\vec{S} = \vec{S}_1 + \vec{S}_2$ and $\vec{I} = \sum_{i=1}^{N} \vec{I}_i$.

The model to be studied in this chapter now results by neglecting the spatial variation of the hyperfine coupling constants and choosing them to be equal to each other $A_i^{(1)} = A_i^{(2)} = A/N$, as illustrated in the bottom panel of Figure 3.3. Note that both, the square $\vec{S}^2$ of the total electron spin as well as the square $\vec{I}^2$ of the total bath spin are separately conserved quantities if homogeneous couplings are considered. Variation of the exchange coupling between the two electron spins $J_{\rm ex}$ then gives rise to an inhomogeneity in the system. Hence, the two electron spins are interacting with a common nuclear spin bath. Moreover, if small variations of the coupling constants would be included, degenerate energy levels would slightly split and give rise to a modified *long-time* behavior of the system. In our quantitative studies to be reported on below, however, we focus on the *short-time* properties where decoherence phenomena take place. Indeed, in Section 6.3 we obtain realistic decoherence time scales in an almost analytical fashion. As explained in Section 5.3, the hyperfine coupling constants depend on the respective nuclear species through the nuclear gyromagnetic ratio. In consistency with the homogeneous couplings we therefore choose the length of the bath spins to be equal to each other. For simplicity, we restrict the nuclear spins to $I_i = 1/2$. We expect our results to be of quite general nature, not strongly depending on this choice [61].

As already mentioned in the preceding chapter, considering the two electrons to interact with a common nuclear spin bath as in our model corresponds to a physical situation where the electrons are comparatively near to each other. This leads to the question whether our model is also adapted to the case of two electrons in one quantum dot, rather than in two nearby quantum dots. Assuming perfect confinement, in the former case one of the two electrons would be forced into the first excited state, which typically has p-character and consequently a zero around the dot center, as explained in Sections 5.1 and 5.2. Thus, the coupling constants near the very center of the dot would clearly be different for the two electrons. Therefore, our model is more suitable for the description of two electrons in two nearby quantum dots than for the case of two electrons in one dot.

Let us now turn to the exact solution of our homogeneous coupling model and calculate the spin and entanglement dynamics from the eigensystem. In what follows we shall work in subspaces of a fixed eigenvalue of J^z. Thus, the expectation values of the x and y components of the electron and nuclear spins vanish, and we only have to consider their z components.

If all hyperfine couplings are equal to each other $A_i^{(1)} = A_i^{(2)} = A/N$, the Hamiltonian (6.1) can be rewritten in the following way

$$H_{\rm 1B} = H_{\rm hom} + \left(J_{\rm ex} - \frac{A}{N} \right) \vec{S}_1 \cdot \vec{S}_2 \tag{6.2}$$

with

$$H_{\rm hom} = \frac{A}{2N} \left(\vec{J}^2 - \vec{S}_1^{\,2} - \vec{S}_2^{\,2} - \vec{I}^{\,2} \right). \tag{6.3}$$

Omitting the quantum numbers corresponding to a certain Clebsch-Gordan decomposition of the bath, the eigenstates are labeled by J, M, and S associated with the operators $\vec{J}^2, J^z$ and $\vec{S}^{\,2}$. The two electron spins couple to $S = 0, 1$. Hence, the eigenstates of $H_{\rm 1B}$ are given by triplet states $|J, M, 1\rangle$, corresponding to the coupling of a spin of length one to an

arbitrary spin, and a singlet state $|J, M, 0\rangle$. The explicit expressions are given in Equations (B.1), (B.3), and (B.4) in Appendix B.

The corresponding eigenvalues read as follows:

$$H_{1\mathrm{B}}|I+1, M, 1\rangle = \left(\frac{A}{N}I + \frac{J_{\mathrm{ex}}}{4}\right)|I+1, M, 1\rangle \tag{6.4a}$$

$$H_{1\mathrm{B}}|I, M, 1\rangle = \left(\frac{J_{\mathrm{ex}}}{4} - \frac{A}{N}\right)|I, M, 1\rangle \tag{6.4b}$$

$$H_{1\mathrm{B}}|I-1, M, 1\rangle = \left(-\frac{A}{N}I + \frac{J_{\mathrm{ex}}}{4} - \frac{A}{N}\right)|I-1, M, 1\rangle \tag{6.4c}$$

$$H_{1\mathrm{B}}|I, M, 0\rangle = -\frac{3}{4}J_{\mathrm{ex}}|I, M, 0\rangle \tag{6.4d}$$

Now we are ready to evaluate the time evolution of the electron spins and their entanglement from the eigensystem of the Hamiltonian. Here we adapt the general concept presented in Appendix A. We consider initial states $|\alpha\rangle$ of the form $|\alpha\rangle = |\alpha_{\mathrm{e}}\rangle|\alpha_{\mathrm{n}}\rangle$, where $|\alpha_{\mathrm{e}}\rangle$ is an arbitrary electron spin state and $|\alpha_{\mathrm{n}}\rangle$ is a product of N nuclear states $|\uparrow\rangle, |\downarrow\rangle$. The physical significance of this choice becomes clear by rewriting the electron-nuclear coupling parts of the Hamiltonian in terms of creation and annihilation operators as in (3.7). Obviously the z term does not contribute to the dynamics for initial states which are simple product states. Hence, by considering initial states of the above form, we mainly study the influence of the flip-flop part on the dynamics of the system. This is exactly the part which is eliminated by considering a strong magnetic field like in References [30–35], briefly reviewed in Section 5.4.

As the 2^N dimensional bath Hilbert space is spanned by the $\vec{I}^2$ eigenstates, every product state can be written in terms of these eigenstates. If $N_{\mathrm{D}}^{\mathrm{b}} \leq N/2$ is the number of down spins in the bath, it follows

$$|\underbrace{\downarrow \ldots \downarrow}_{N_{\mathrm{D}}^{\mathrm{b}}} \uparrow \ldots \uparrow\rangle = \sum_{k=0}^{N_{\mathrm{D}}^{\mathrm{b}}} \sum_{\{S_i\}} c_k^{\{S_i\}} \Big| \underbrace{\frac{N}{2} - k}_{I}, \frac{N}{2} - N_{\mathrm{D}}^{\mathrm{b}}, \{S_i\} \Big\rangle, \tag{6.5}$$

where the quantum numbers $\{S_i\}$ are due to a certain Clebsch-Gordan decomposition of the bath. In Equation (6.5) we assumed the first $N_{\mathrm{D}}^{\mathrm{b}}$ spins to be flipped, which is no loss of generality with respect to the dynamics due to the homogeneity of the couplings.

Using Equation (6.5) and inverting Equations (B.1), (B.3), and (B.4), the time evolution of the initial state can be calculated by writing $|\alpha\rangle$ in terms of the above eigenstates and applying the time evolution operator. Using Equations (B.1), (B.3), and (B.4) again and tracing out the bath degrees of freedom, we arrive at the reduced density matrix $\rho(t)$, which enables to evaluate the expectation value $\langle S_{1/2}^z(t)\rangle$ and the dynamics of the entanglement between the two electron spins. As a measure for the entanglement we use the concurrence [127]

$$C(t) = \max\{0, \sqrt{\lambda_1} - \sqrt{\lambda_2} - \sqrt{\lambda_3} - \sqrt{\lambda_4}\}, \tag{6.6}$$

where λ_i are the eigenvalues of the non-hermitian matrix $\rho(t)\tilde{\rho}(t)$ in decreasing order. Here $\tilde{\rho}(t)$ is given by $(\sigma_y \otimes \sigma_y)\,\rho^*(t)\,(\sigma_y \otimes \sigma_y)$, where $\rho^*(t)$ denotes the complex conjugate of $\rho(t)$. The coefficients $c_k^{\{S_i\}}$ in Equation 6.5 are of course products of Clebsch-Gordan coefficients,

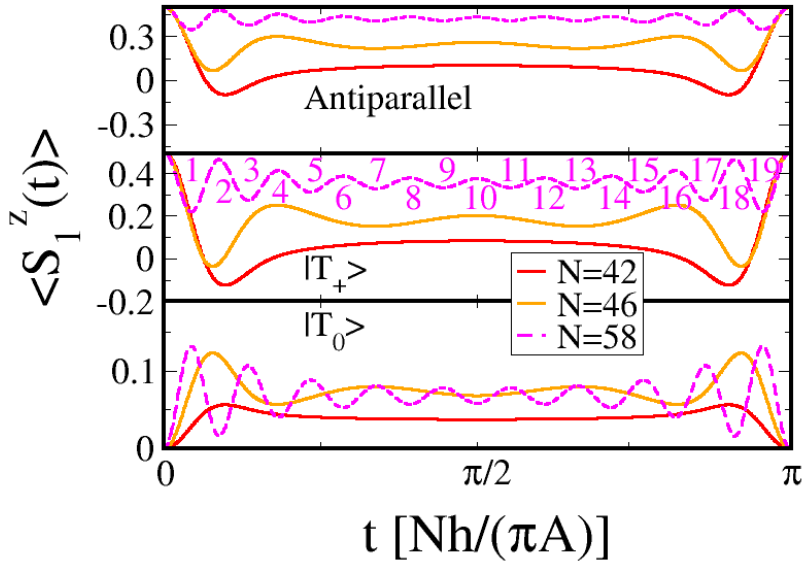

Figure 6.1: Spin dynamics for $|\alpha_e\rangle = |\Uparrow\Downarrow\rangle, |T_+\rangle, |T_0\rangle$ and different even values of N. The number of down spins in the bath is $N_D^b = 20$ in all plots, yielding bath polarizations $p_b \approx 5\% - 30\%$. Note that the time unit is rescaled according to the number of bath spins. We see periodicity with π. For $|\alpha_e\rangle = |T_0\rangle$ and $N = 58$ we count the number of local extrema on one period and find $N - 2N_D^b + 1 = 58 - 40 + 1 = 19$ as expected due to the rule (6.9).

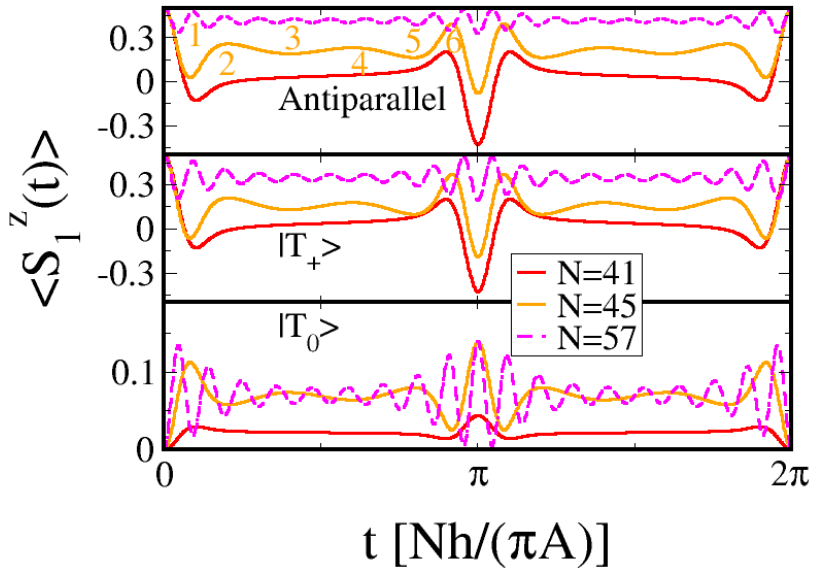

Figure 6.2: Spin dynamics for $|\alpha_e\rangle = |\Uparrow\Downarrow\rangle, |T_+\rangle, |T_0\rangle$ and an odd number of spins. The number of down spins in the bath is $N_D^b = 20$ in all plots, giving polarizations bath $p_b \approx 2\% - 30\%$. In contrast to the case of an even number of spins we see periodicity with 2π. For $|\alpha_e\rangle = |\Uparrow\Downarrow\rangle$ and $N = 45$ we count the number of local extrema on half the period and find $N - 2N_D^b + 1 = 45 - 40 + 1 = 6$ as expected due to the rule (6.9).

which enter the time evolution through the quantity

$$d_k = \sum_{\{S_i\}} \left(c_k^{\{S_i\}} \right)^2 \tag{6.7}$$

and usually have to be calculated numerically (also see Section 3.2). The main advantage in considering $I_i = 1/2$ is now that in this case a closed expression for d_k can be derived [98]:

$$d_k = \frac{N_\mathrm{D}^\mathrm{b}!(N - N_\mathrm{D}^\mathrm{b})!(N - 2k + 1)}{(N - k + 1)!k!} \tag{6.8}$$

For further details on the calculation of the time-dependent reduced density matrix and the dynamical quantities derived therefrom we refer the reader to Appendix C.

Already at this point of the investigation, it is a simple but remarkable difference between our one bath system with two electron spins and the homogeneous Gaudin model of a single electron spin, investigated in References [36, 98], that even if we choose $|\alpha_\mathrm{n}\rangle$ as an $\vec{I}^2$ eigenstate and hence fix k in Equation (6.5) to a single value, due to the higher number of eigenvalues the resulting dynamics can not be described by a single frequency.

6.2 Basic dynamical properties

We now give an overview on basic dynamical features of the system in consideration. Due to the homogeneous couplings, the dynamics of the two electron spins can be read off from each other. Hence, the following discussion of the electron spin dynamics will be restricted to $\langle S_1^z(t) \rangle$.

6.2.1 Electron spin dynamics

In Figures 6.1 and 6.2 we consider the completely homogeneous case $J_\mathrm{ex} = A/N$ and plot the dynamics for $|\alpha_\mathrm{e}\rangle = |\Uparrow\Downarrow\rangle, |T_+\rangle, |T_0\rangle$ and varying bath polarization, as defined in Equation (3.8), $p_\mathrm{b} \approx 2\% - 30\%$. A polarization of 30% does not seem to be particularly high, but the behavior typical for high polarizations occurs indeed already at such a value. We omit the singlet case because it is an eigenstate of the system. In Figure 6.1 the number of spins is even, whereas in Figure 6.2 an odd number is chosen. Note that we measure the time t in rescaled units $\hbar/(A/2N)$ which depends on the number of bath spins. Furthermore, we introduce a factor 2 on the time scale as compared to the "natural" time unit $\hbar/(A/N)$. This is convenient in order to compare our results with those for the homogeneous Gaudin model as investigated in Reference [98]. Similarly to that case [36, 98], from Figures 6.1 and 6.2 we see that the dynamics for an even number of spins is periodic with a periodicity of π (in rescaled time units), whereas an odd number of spins leads to a periodicity of 2π. These characteristics can of course be explained by analyzing the level spacings in the different situations. Consider for example an even number of bath spins. Here all level spacings are even multiples of $A/2N$, which results in dynamics periodic with π. However, if the number of spins is odd, we get even and odd level spacings (in units of $A/2N$), yielding a period of 2π. For the given case of completely homogeneous couplings the dynamics can be nicely characterized: The number of local extrema, for an even number of bath spins within a complete period as well as for an odd number of bath spins within half a period, is in both cases given by

$$N - 2N_\mathrm{D}^\mathrm{b} + 1. \tag{6.9}$$

This – so far empirical – rule holds for all initial electron spin states and is illustrated in Figures 6.1 and 6.2.

Let us now investigate the spin dynamics for varying exchange coupling, i.e. the case $J_{\mathrm{ex}} \neq A/N$. Note that for an initial electron spin state $|\alpha_{\mathrm{e}}\rangle$ which is an eigenstate of the central spin coupling term $\vec{S}_1 \cdot \vec{S}_2$ this inhomogeneity has no influence on the spin dynamics since

$$\left[H_{\mathrm{hom}}, \vec{S}_1 \cdot \vec{S}_2\right] = 0. \tag{6.10}$$

The dynamics for J_{ex} being any integer multiple of A/N are identical to the one of the completely homogeneous case. In Figure 6.3 the dynamics for $|\alpha_{\mathrm{e}}\rangle = |\Uparrow\Downarrow\rangle$ and varying exchange coupling is plotted. In the upper two panels we consider the case of low polarization $p_{\mathrm{b}} \approx 10\%$ for an even and an odd number of spins. The remaining two panels show the dynamics for high polarization $p_{\mathrm{b}} \approx 30\%$. In Figure 6.4 the plots are ordered likewise for a more general linear combination of $|T_0\rangle$ and $|S\rangle$ given by $|\alpha_{\mathrm{e}}\rangle = (1/\sqrt{13})\,(2|\Uparrow\Downarrow\rangle + 3|\Downarrow\Uparrow\rangle)$.

From Figures 6.3 and 6.4 we see that if the exchange coupling is an odd multiple of $A/2N$, the even-odd effect described above does not occur and we have periodicity of 2π. In both of the aforementioned situations of J_{ex} being an even or odd multiple of $A/2N$ the time evolutions are symmetric with respect to the middle of the period, which is a consequence of the invariance of the underlying Hamiltonian under time reversal. For a more general exchange coupling the periodicity, along with the mirror symmetry, of the dynamics is broken on the above time scales.

Considering the case of low polarization, neither the dynamics of initial states with a product nor the one of states with an entangled electron spin state show dramatic qualitative changes if J_{ex} is varied. However, if the polarization is high, the spin is oscillating with mainly one frequency proportional to J_{ex}. Furthermore, the amplitude of the oscillation is larger for the case $J_{\mathrm{ex}} \neq A/N$ than for the completely homogeneous case. This behaviour can be understood as follows: If the polarization is high, we clearly have $d_{N_{\mathrm{D}}^{\mathrm{b}}} \approx 1$, whereas $d_k \approx 0$ for $k \neq N_{\mathrm{D}}^{\mathrm{b}}$. This means that calculating the spin and entanglement dynamics, we only have to consider the term $k = N_{\mathrm{D}}^{\mathrm{b}}$. An evaluation of the coefficients for the different frequencies now shows that the main contribution results from $E_{T_0} - E_S = (A/N) - J_{\mathrm{ex}}$, where we used an obvious notation as corresponding to the eigenvalues (6.4b) and (6.4d). Hence, if the polarization is more and more increased, this is the only frequency left. If we choose $J_{\mathrm{ex}} = (A/N)$, the two associated eigenstates are degenerate so that in this case the main contribution to the dynamics is constant. This explains why the amplitude of the high polarization dynamics in Figures 6.3 and 6.4 is large compared to the one in Figures 6.1 and 6.2. For further details the reader is referred to Appendix C

6.2.2 Entanglement dynamics

In Figures 6.5 and 6.6 the concurrence dynamics $C(t)$ for $|\alpha_{\mathrm{e}}\rangle = |\Uparrow\Downarrow\rangle, |T_+\rangle$ is plotted with the same polarizations considered as in Figures 6.3 and 6.4 and varying exchange coupling.

Surprisingly, in the second case the concurrence drops to zero for certain periods of time. This is very similar for the case $|\alpha_{\mathrm{e}}\rangle = |T_0\rangle$ not explicitly shown. As already explained concerning the spin dynamics, the exchange coupling J_{ex} of course has no influence because $|T_+\rangle$ is an eigenstate of $\vec{S}_1 \cdot \vec{S}_2$.

It is an interesting fact now that for $|\alpha_{\mathrm{e}}\rangle = |\Uparrow\Downarrow\rangle$ and a small polarization, changing from $|J_{\mathrm{ex}}| > 1$ to $|J_{\mathrm{ex}}| < 1$ increases the maximum value of the function $C(t)$.

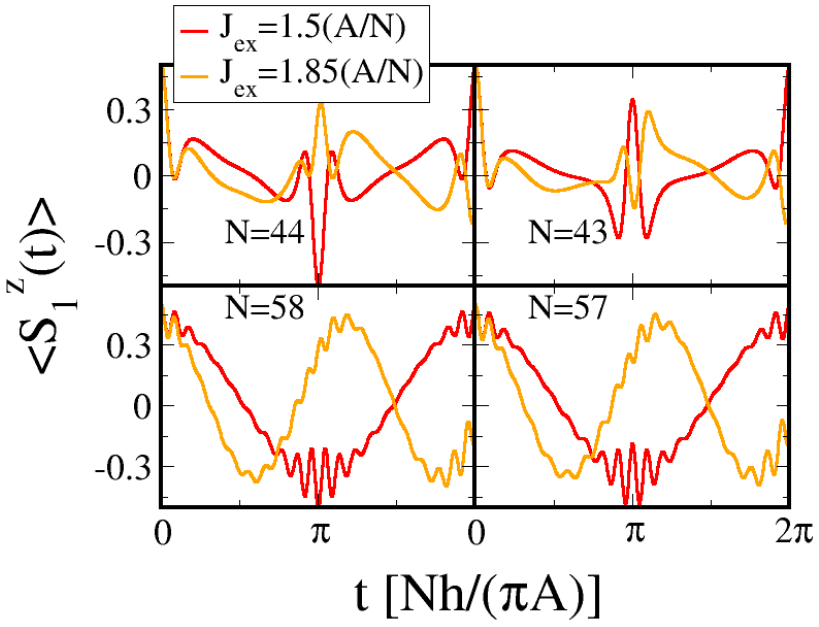

Figure 6.3: Spin dynamics for $|\alpha_e\rangle = |\Uparrow\Downarrow\rangle$ and $N_D^b = 20$, resulting in $p_b \approx 6\% - 30\%$. If J_{ex} is an odd multiple of $A/2N$, we see periodicity with 2π.

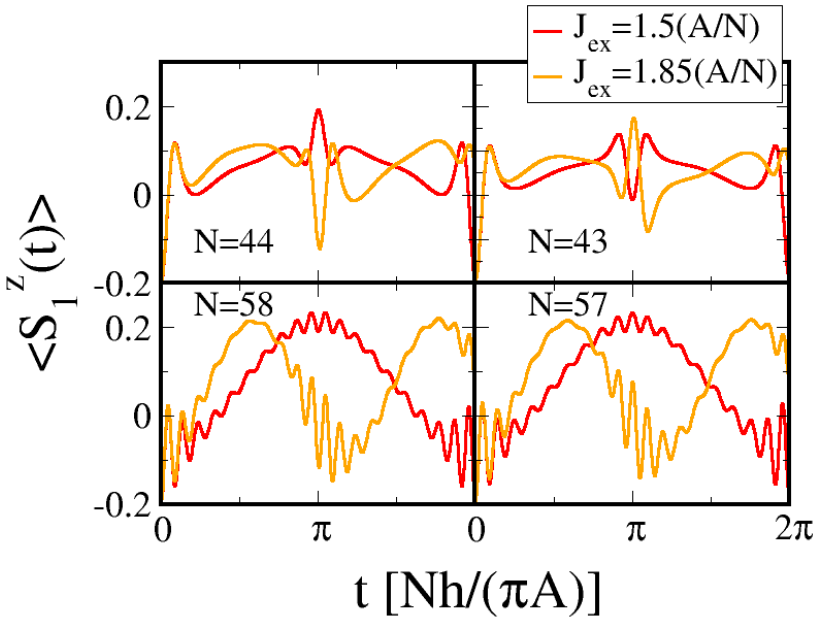

Figure 6.4: Spin dynamics for $|\alpha_e\rangle = (1/\sqrt{13})\,(2|\Uparrow\Downarrow\rangle + 3|\Downarrow\Uparrow\rangle)$ and $N_D^b = 20$, resulting in $p_b \approx 6\% - 30\%$. If J_{ex} is an odd multiple of $A/2N$, we see periodicity with 2π.

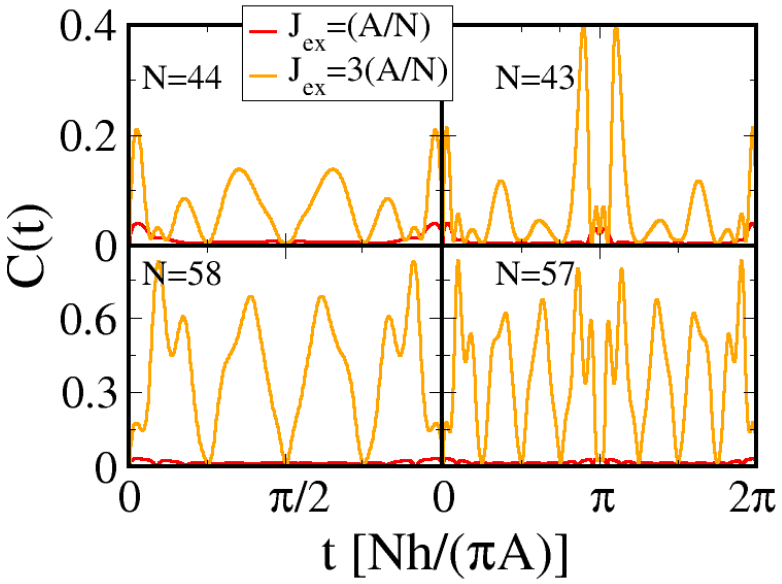

Figure 6.5: Entanglement dynamics for $|\alpha_e\rangle = |\Uparrow\Downarrow\rangle$ and $N_D^b = 20$, resulting in $p_b \approx 6\% - 30\%$. In the completely homogeneous case the amplitude is small even for high polarization. Generation of entanglement benefits from high polarization.

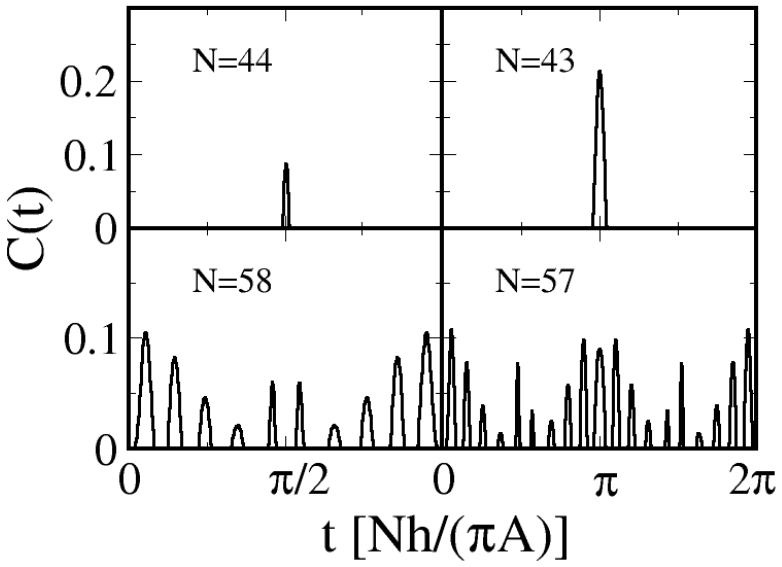

Figure 6.6: Entanglement dynamics for $|\alpha_e\rangle = |T_+\rangle$ and $N_D^b = 20$, resulting in $p_b \approx 6\% - 30\%$. Instead of an oscillating function we see discrete peaks. Variation of the exchange coupling has no influence because $|T_+\rangle$ is an eigenstate of the electron spin coupling term.

Furthermore, we see from Figure 6.5 that, surprisingly, the entanglement is much smaller for the completely homogeneous case $J_{\mathrm{ex}} = A/N$ than for $J_{\mathrm{ex}} \neq A/N$, even for low polarizations.

6.3 Decoherence and its quantification

Depending on the choice of the exchange coupling, the dynamics of the one bath model can either be symmetric and periodic or without any regularities on the considered time scales. It is now not entirely obvious to determine in how far these dynamics constitute a process of decoherence. Considering for example the spin dynamics for an integer J_{ex} (in units of $A/2N$) and an even number of bath spins as shown in Figure 6.1, one can either regard the decay of the spin as decoherence or, especially due to the symmetry of the function, as part of a simple periodic motion. In Reference [98] the first zero of $\langle S_1^z(t)\rangle$ has been considered as a measure for the decoherence time. In Figure 6.7 we illustrate examples of the spin dynamics on short time scales for $J_{\mathrm{ex}} \geq 0$ as well as $J_{\mathrm{ex}} < 0$ and a varying number of bath spins. For $J_{\mathrm{ex}} \geq 0$ this procedure is straightforward meaning that $\langle S_1^z(t)\rangle$ crosses the horizontal line $\langle S_1^z\rangle = 0$ before reaching its first minimum with $\langle S_1^z(t)\rangle < 0$. However, for $J_{\mathrm{ex}} < 0$ and a sufficiently small number of bath spins, as can be seen from the lower panel of Figure 6.7, such a first minimum is attained before the first actual zero $\langle S_1^z(t)\rangle = 0$. This first zero occurs indeed at much larger times t whose scaling behavior as a function of the system size N is clearly different from the zero positions found for $J_{\mathrm{ex}} \geq 0$, as we have checked in a detailed analysis. Thus, our evaluation scheme needs to be modified for $J_{\mathrm{ex}} < 0$. An obvious way out of this problem is to either consider large enough spin, baths where such an effect does not occur, or to evaluate the intersection with an alternative "threshold level" $\langle S_1^z\rangle > 0$. In Figure 6.7 we have chosen $\langle S_1^z\rangle = 0.2$, which will be the basis of our following investigation. As a further alternative, one could also consider the position of the first minimum of $\langle S_1^z(t)\rangle$. Hence, strictly speaking, it is not per se the first zero of $\langle S_1^z(t)\rangle < 0$ which is a measure for the decoherence time, but the scaling behavior of the dynamics on short time scales.

Following the route described above, in Figure 6.8 we plot the positions (measured in units of $\hbar/(A/2N)$) of the first zeros of $\langle S_1^z(t)\rangle$ for $J_{\mathrm{ex}} \geq 0$ and of the first intersections with the threshold level $\langle S_1^z\rangle = 0.2$, shown in Figure 6.7, for $J_{\mathrm{ex}} < 0$ on a double logarithmic scale. We choose a weakly polarized bath $N = 2N_{\mathrm{D}}^{\mathrm{b}} + 2 \Rightarrow p_{\mathrm{b}} = 2/N$, approaching the completely unpolarized case for $N \to \infty$. The absolute values of the positions for $J_{\mathrm{ex}} \geq 0$ and $J_{\mathrm{ex}} < 0$ differ slightly from each other, which results from the fact that the intersection with the threshold level at $\langle S_1^z\rangle = 0.2$ happens closer to $t = 0$ than with the usual threshold level $\langle S_1^z\rangle = 0$. Nevertheless, the scaling behavior is very similar in all cases, and each curve can nicely be fitted by a power law $\propto (N+2)^{\nu}$ with $\nu \approx -0.5$, a result similar to the one found for the homogeneous Gaudin model with only one electron spin [98].

In a GaAs quantum dot the electron spins usually interact with approximately $N = 10^6$ nuclei. Assuming the hyperfine coupling strength to be of the order of $A = 10^{-5}$eV, as realistic for GaAs quantum dots [36], this results in a time scale of $Nh/(\pi A) = 1.31 \cdot 10^{-4}$s. If we now use the above scaling behaviour $1/\sqrt{N+2}$, we get a decoherence time of 131ns, which fits quite well with the experimental data [75, 128–130]. This is an interesting result not only with respect to the validity of our model: As explained in Section 6.1 referring to (3.7), generally decoherence results "directly" from the electron-nuclear flip-flop terms and through the superposition of product states from the z terms.

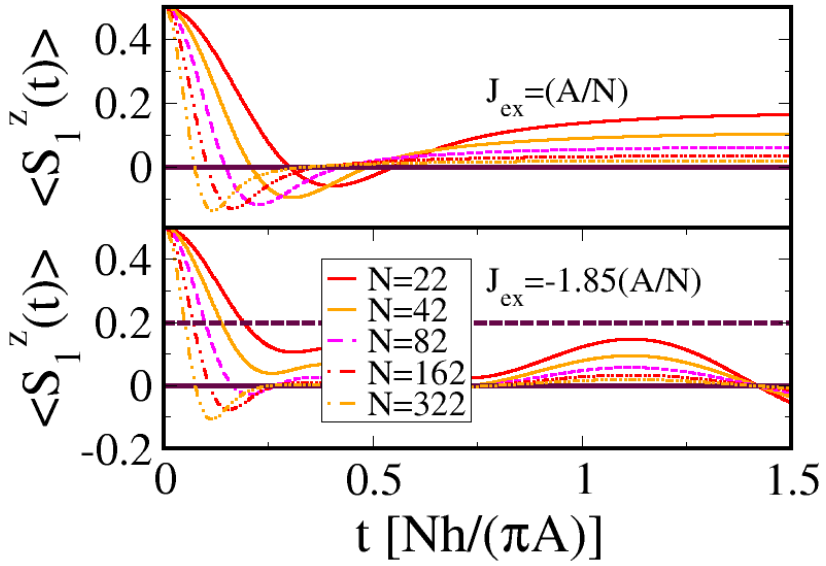

Figure 6.7: Spin dynamics on short time scales for $J_{\rm ex} \lesseqgtr 0$, $p_{\rm b} = 2/N$, and $|\alpha_{\rm e}\rangle = |\Uparrow\Downarrow\rangle$. The thick solid lines mark the zero level $\langle S_1^z\rangle = 0$, while the thick dashed line (lower panel) represents the threshold level $\langle S_1^z\rangle = 0.2$ as appropriate for $J_{\rm ex} < 0$ and small spin baths.

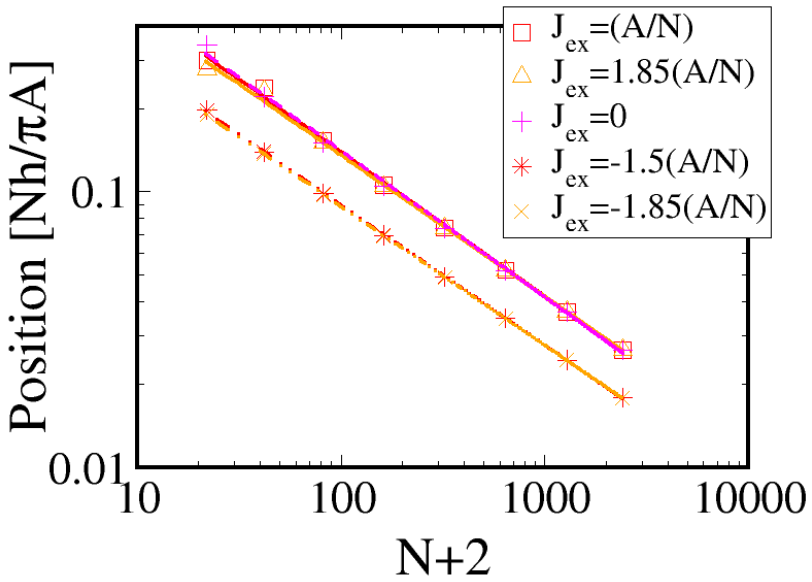

Figure 6.8: Position of the first zero of $\langle S_1^z(t)\rangle$ for $J_{\rm ex} \geq 0$ and the first intersection with the threshold level $\langle S_1^z\rangle = 0.2$ for $J_{\rm ex} < 0$ on a double logarithmic scale. We choose $|\alpha_{\rm e}\rangle = |\Uparrow\Downarrow\rangle$ and a polarization of $p_{\rm b} = 2/N \Leftrightarrow N = 2N_{\rm D}^{\rm b} + 2$. The curves are fitted to a power law $\propto (N+2)^{\nu}$ with $\nu = -0.52$ ($J_{\rm ex} = (A/N)$), $\nu = -0.51$ ($J_{\rm ex} = 1.85(A/N)$), $\nu = -0.53$ ($J_{\rm ex} = 0$), $\nu = -0.51$ ($J_{\rm ex} = -1.5(A/N)$), and $\nu = -0.50$ ($J_{\rm ex} = -1.85(A/N)$). Note that the parallel offset between the plots for $J_{\rm ex} \geq 0$ and $J_{\rm ex} < 0$ results from the fact that the intersection with the higher threshold level happens closer to $t = 0$.

Above we calculate the decoherence time for a product initial bath state, where the influence of the z terms is eliminated. The fact that we are able to reproduce the decoherence times suggests that the decoherence time caused by the flip-flop terms is equal or smaller than the one resulting from the z-parts of the Hamiltonian. It should be stressed that we calculate the decoherence time of an individual electron here. In Reference [131] the decoherence time of an ensemble of GaAs quantum dots with 10^5 nuclear spins each has been calculated yielding 1ns.

It is now a well-known fact for the Gaudin model that the decaying part of the dynamics decreases with increasing polarization [36]. A numerical evaluation shows that this is also the case for two electron spins. As explained in the context of Figures 6.1, 6.2, 6.3 and 6.4, the oscillations of our one bath model become more and more coherent with increasing polarization. Together with the above results for the decoherence times this means that, although the homogeneous couplings are a strong simplification of the physical reality, our homogeneous coupling model shows rather realistic dynamical characteristics on the relevant time scales. This is plausible because artifacts of the homogeneous couplings, like the periodic revivals, set in on longer time scales.

6.4 Summary and outlook

In conclusion we have studied in detail the hyperfine induced spin and entanglement dynamics of a double quantum dot model with homogeneous hyperfine coupling constants and varying exchange coupling, based on an exact analytical calculation.

We found the dynamics to be periodic and symmetric for J_{ex} being an integer multiple of A/N or an odd multiple of $A/2N$, where the period depends on whether the number of bath spins is even or odd. We explained this periodicity by analyzing the level spacings. For $J_{\mathrm{ex}} = A/N$ we found an empirical rule which characterizes the dynamics for varying polarization. We have seen that for low polarizations the exchange coupling has no significant qualitative influence, whereas in the high polarization case the dynamics mainly consists of one single frequency proportional to J_{ex}. It is not possible to entangle the electron spins completely in the setup considered in the present chapter.

Following Reference [98] we extracted the decoherence time by analyzing the scaling behaviour of the first zero. In the case of negative exchange coupling the dynamics strongly changes on short time scales and instead of the first zero we considered the intersection of the dynamics with another threshold level parallel to the time axis. Both cases yield the same result, which is in good agreement with experimental data. Hence, the scaling behaviour of the short time dynamics can be regarded as a good indicator for the decoherence time and the simple homogeneous one bath model adequately describes the short time dynamics of the realistic inhomogeneous case.

7 Swapping and entangling hyperfine coupled nuclear spin baths

Parts of this chapter have been published in collaboration with John Schliemann in Reference [132].

In Chapter 5 we introduced the hyperfine interaction and gave summary of its vice and virtue with respect to semiconductor spin qubit based quantum information processing. In Chapter 6 we mainly considered the first point of view and investigated the electron spin dynamics in a model of two exchange coupled electron spins interacting with a common bath of nuclear spins via homogeneous hyperfine couplings.

In the present chapter we focus on the advantageous character of the hyperfine interaction. To this end we revisit the homogeneous two bath model studied with respect to its spectral properties in Chapter 4. Here two exchange coupled electron spins are considered to interact with individual nuclear spin baths (again) via homogeneous couplings. In contrast to the one bath model studied in Chapter 6, physically this corresponds to spatially well-separated quantum dots. We investigate via exact numerical diagonalization to what extent it is possible to swap and entangle the nuclear spin baths, meaning that we aim at utilizing them as a resource of quantum information processing.

In Section 7.1 we briefly recapitulate the two bath model of Chapter 4 and introduce the methods. Usually exact numerical diagonalization is restricted to rather small system sizes. In order to go beyond these limits, we proceed as in the numerical calculations presented in Chapter 4 and reduce the dimension of the problem by replacing the two baths by two single long spins. The range of validity of this approximation is discussed in detail. In Section 7.2 we determine the optimal choice for the coupling constants with respect to a nuclear swap operation and investigate the time evolution of the nuclear baths within this parameter range. We distinguish between an inversion symmetric system and a system with broken inversion symmetry. The first (second) case corresponds to two quantum dots of identical (different) geometry. It turns out that a swap is possible for systems of realistic size, but not for smaller ones and that it is advantageous to combine quantum dots of different geometry to a double dot setup. As described in Chapter 4, the spectrum of inversion symmetric models exhibits systematically degenerate multiplets. We discuss to what extent the latter finding could be a dynamical signature of the occurrence of this large degenerate subspace. In Section 7.3 we indicate that, under the same conditions as for the swapping of nuclear spin states, it might even be possible to fully entangle the two baths.

7.1 Model and methods

The two bath Hamiltonian introduced in Chapter 4 reads:

$$H_{\mathrm{2B}} = \vec{S}_1 \cdot \sum_{i=1}^{N_1} A_i^{(1)} \vec{I}_{1,i} + \vec{S}_2 \cdot \sum_{i=1}^{N_2} A_i^{(2)} \vec{I}_{2,i} + J_{\mathrm{ex}} \vec{S}_1 \cdot \vec{S}_2, \tag{7.1}$$

where now $\vec{S}_i$ are the electron spins and $\vec{I}_{i,j}$ are the nuclear spins the i-th electron spin interacts with. For simplicity we consider $N_1 = N_2 = N$ in what follows. The parameter J_{ex} again denotes an exchange coupling between the two electron spins.

As discussed in Section 5.2, due to the spatial variation of the electronic wave function, the hyperfine couplings are clearly inhomogeneous. However, just as in the preceding chapter we consider them to be equal to each other within each bath, meaning that $A_j^{(i)} = A^{(i)}/N$. Then the Hamiltonian (7.1) conserves, apart from the total spin $\vec{J} = \vec{S}_1 + \vec{S}_2 + \vec{I}_1 + \vec{I}_2$ with $\vec{I}_i = \sum_{j=1}^{N_i} \vec{I}_{i,j}$, also the squares of the total bath spins $\vec{I}_1^2$ and $\vec{I}_2^2$:

$$\left[H_{\mathrm{2B}}, \vec{J}\right] = \left[H_{\mathrm{2B}}, \vec{I}_1^2\right] = \left[H_{\mathrm{2B}}, \vec{I}_2^2\right] = 0 \tag{7.2}$$

The first symmetry is helpful for exact numerical diagonalizations of the Hamiltonian matrix [36, 47], through which we obtain the dynamics in the following. As described in Appendix A, we compute the time-dependent density matrix by decomposing the initial state into energy eigenstates and applying the time evolution operator. Tracing out the electron degrees of freedom then yields the reduced density matrix of the nuclear baths $\rho_{\mathrm{n}}(t)$ from which we can calculate the time evolution of all the respective observables.

In Chapter 4 we numerically studied the spectral properties of the model (7.1). In order to lower the dimension of the problem, we replaced the sums $\vec{I}_i = \sum_{j=1}^{N_i} \vec{I}_{i,j}$ by single long spins of length I_i. Up to the multiplicity of the eigenvalues, this yields the exact spectrum on the respective subspaces. In the following we use the same numerical approach. Let us briefly discuss to which physical situation this corresponds. A general state of a bath is a superposition of states from different multiplets

$$|\beta_j\rangle = \sum_{I_j, m_j} \beta_j^{I_j, m_j} |I_j, m_j\rangle, \tag{7.3}$$

where the quantum numbers due to a certain Clebsch-Gordan decomposition of the bath have been omitted. The stronger the baths are polarized, the less multiplets contribute to the sum in the state (7.3). Considering very high polarizations we can therefore approximate the state (7.3) by $|\beta_j\rangle = |I, m_j\rangle$ with $m_j \approx \pm I$. Due to the commutation relations (7.2) all dynamics is then captured by the following simple Hamiltonian, to which we refer to as the long spin approximation Hamiltonian:

$$H_{\mathrm{LSA}} = \frac{A^{(1)}}{2I} \vec{S}_1 \cdot \vec{I}_1 + \frac{A^{(2)}}{2I} \vec{S}_2 \cdot \vec{I}_2 + J_{\mathrm{ex}} \vec{S}_1 \cdot \vec{S}_2 \tag{7.4}$$

The form of the couplings $A^{(i)}/2I$ results from the observation that the N bath spins can couple to $I = N/2, N/2-1, N/2-2, \ldots$. As we assume highly polarized baths, we consider the maximal value $I = N/2$. Solving for N then yields the coupling constants in the Hamiltonian (7.4). For later convenience, we define $A = A^{(1)} + A^{(2)}$, where in comparison to the overall

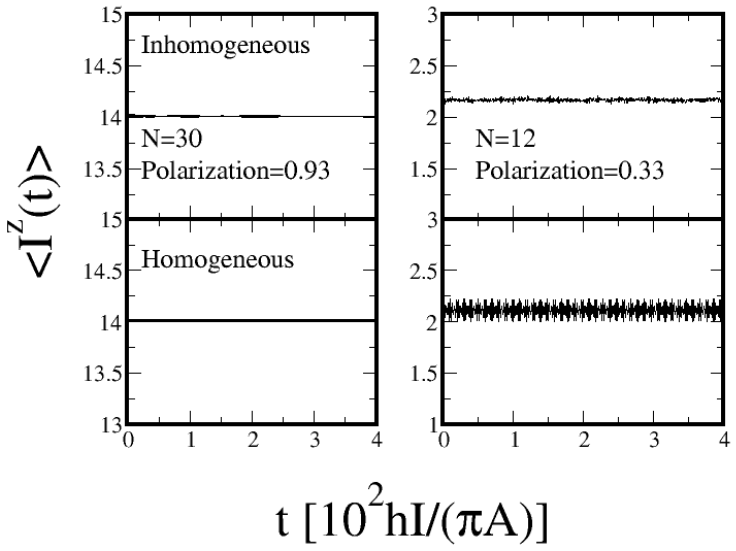

Figure 7.1: Nuclear spin dynamics of the Gaudin model for inhomogeneous (upper panels) and homogeneous (lower panels) hyperfine couplings. The bath state is initially randomly correlated [36, 47] and the electron spin is pointing upwards. The left column shows the case of $N = 30$ and a bath polarization (3.8) of $p_\mathrm{b} = 0.93$, while in the right column we have $N = 12$ and a bath polarization of $p_\mathrm{b} = 0.33$. Even in the latter case the bath dynamics for inhomogeneous and homogeneous couplings are still quite similar to each other.

coupling strength defined in Chapter 4 we drop a factor (1/2), as slightly more convenient with respect to the long time scales of the nuclear dynamics to be considered below.

High nuclear polarizations of up to 80% have been experimentally demonstrated in References [80, 90–92]. As described in Section 5.4, in Reference [80] it has been demonstrated that it is possible to polarize nuclear ensembles in different directions. However, a question concerning the long spin approximation arises from assuming the couplings to be homogeneous: As demonstrated in Chapter 6, this approximation is a good one for short time scales, whereas for longer times artifacts occur. As the nuclear dynamics are slow, it has to be questioned to what extent homogeneous couplings are adequate in order to evaluate nuclear spin dynamics. Therefore we numerically investigated the time evolution of the nuclear spins in the Gaudin model (2.1), as corresponding to one of the two first terms in the Hamiltonian (7.1). As a result from our numerics we find that the influence of inhomogeneities is suppressed with increasing polarization. This is illustrated in Figure 7.1, where we compare cases of high and of low polarization. Even in the latter case the dynamics for both types of couplings are very close to each other so that it is definitely justified to neglect the inhomogeneities at high polarizations.

7.2 Swapping nuclear spin polarizations

We now evaluate the nuclear spin dynamics within the long spin approximation and explore the possibility of swapping the states of oppositely polarized spin baths, $\langle I_1^z \rangle = -\langle I_2^z \rangle$. The initial state $|\alpha\rangle$ is considered to be a simple product state between the electron and the nuclear

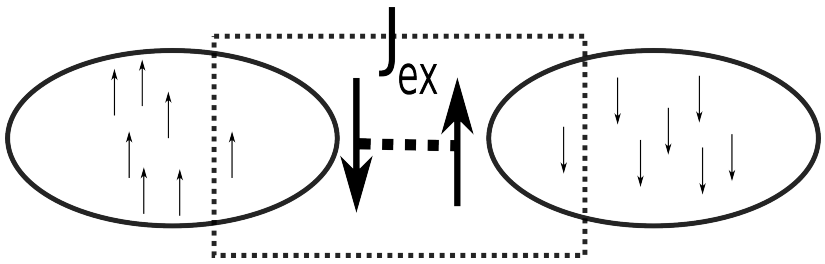

Figure 7.2: The nuclear baths are considered to consist of bath spins with length (1/2). The frame marks the long spin approximation system with the smallest possible bath spin length $I = 1/2$. Here the dynamics of all four spins are highly coherent provided the values of all couplings are close to each other, motivating the condition (7.5) (see text).

state $|\alpha\rangle = |\alpha_{\rm e}\rangle|\alpha_{\rm n}\rangle$, just as in Chapter 6. Since the two baths are spatially well-separated, the initial nuclear state is again a product state of the two long spins. The entanglement within the baths can not be considered within the long spin approximation. However, due to their high polarizations, correlations within the baths will be of minor importance. In what follows we always work in subspaces of a fixed value of the J^z quantum number M, where only the z component has a non-zero expectation value $\langle I_j^z(t)\rangle$. Note that (again) due to the high bath polarizations, it is realistic to assume that the initial bath has overlap exclusively in subspaces of fixed M. Moreover, we assume the z component of the total electron spin to be initially zero, i.e. the spins are antiparallel. Similar results as to be presented below are obtained for more general initial states of the electron spin system.

More importantly, we concentrate on exchange couplings being of the same order of magnitude as the hyperfine coupling strength

$$J_{\rm ex}/(A/2I) \approx 1, \tag{7.5}$$

meaning that the two electron spins are coupled as strongly to each other as they are coupled to the bath spins. This is motivated by the following observation. Let us consider the long spin approximation Hamiltonian (7.4) for the smallest possible value, $I = 1/2$. As shown by elementary numerics, the dynamics of all four spins are, under the condition (7.5), highly coherent and the nuclear spin states can nicely be swapped, i.e. at the end of the process the expectation values $\langle I_j^z(t)\rangle$ are, to a very good degree of accuracy, exchanged as compared to the initial state. Let us now consider the two baths in the original model (7.1) to consist of bath spins with length (1/2), as already assumed for the derivation of the couplings in the long spin approximation Hamiltonian (7.4). As depicted in Figure 7.2, the complete system can now be regarded as set of $I = 1/2$ models. Thus, from a heuristic point of view, the biggest chance to swap the full baths exists if all the subsystems are swapped. Hence, the exchange coupling has to be of the order of the coupling between the electron and the bath spins for *any* subsystem. For homogeneous couplings within the baths this means that $J_{\rm ex} \approx A/N$, which translates into the relation (7.5) for the long spin approximation, as already explained in the derivation of the coupling constants.

However, on the first sight, it does not seem to be possible to swap the initially antiparallel nuclear spins $I > 1/2$, even if the condition (7.5) is fulfilled. This is demonstrated in the upper panel of Figure 7.3, where we consider $I = 80$, $J_{\rm ex}/(A/2I) = 3.5$ and a zero "detuning" $\Delta = A^{(2)} - A^{(1)} = 0$. This corresponds to a situation in which the two quantum dots have the same geometries. We choose the comparatively generic electron spin state $|\alpha_{\rm e}\rangle = (1/\sqrt{13})\,(2|\Uparrow\Downarrow\rangle + 3|\Downarrow\Uparrow\rangle)$ (similar results occur for other choices) and plot the dynamics for

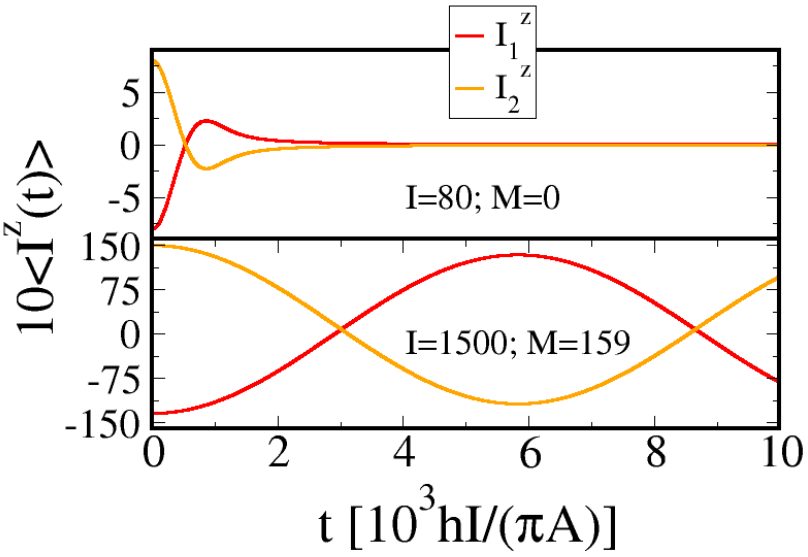

Figure 7.3: Nuclear spin dynamics for $J_{\rm ex}/(A/2I) = 3.5$, $\Delta = 0$ and $|\alpha\rangle = (1/\sqrt{13})\,(2|\Uparrow\Downarrow\rangle + 3|\Downarrow\Uparrow\rangle)\,|M-I,I\rangle$. The upper panel shows data for $I = 80$ and $M = 0$. Here the expectation values $\langle I_j^z(t)\rangle$ decay rapidly to zero. In the bottom panel we consider $I = 1500$ and $M = 159$ and observe an almost complete swap of the nuclear spins.

antiparallel nuclear spin configurations with the maximal possible z components $|\alpha_{\rm n}\rangle = |-I,I\rangle$. As can be seen from the figure, the expectation values of the bath spins decrease quite rapidly to zero and are far away from being properly swapped.

Surprisingly, this apparently negative result turns out to be related to the size of the baths in the following sense: Consider an initial state with the electron spins being in an arbitrary linear combination of $|\Uparrow\Downarrow\rangle$, $|\Downarrow\Uparrow\rangle$ and a nuclear state $|m_1,m_2\rangle$, where m_j denotes the I_j^z quantum number, fulfilling, say, $m_1 < 0$ and $m_2 > 0$ with $|m_1| < |m_2|$, meaning that the "magnetization" $M_{\rm r} = M/(2I+1)$ is nonzero, $M_{\rm r} = (|m_2| - |m_1|)/(2I+1) \neq 0$. Here we find that for magnetizations larger than a certain "critical" value $M_{\rm r}^{\rm c}$ (slightly depending on the electron spin state) the expectation value $\langle I_1^z(0)\rangle$ is, to an excellent degree of accuracy, completely reversed. As a representative example, in the left panel of Figure 7.4 we plot the quantity $\langle I_1^z(t)\rangle$ for $I = 200$ with, as before, $|\alpha_{\rm e}\rangle = (1/\sqrt{13})\,(2|\Uparrow\Downarrow\rangle + 3|\Downarrow\Uparrow\rangle)$ being the initial electron spin state. We consider two different initial nuclear states $|\alpha_{\rm n}\rangle = |M-I,I\rangle$, where the corresponding value of $M_{\rm r}$ is in one case exactly at, in the other case lower than the critical magnetization $M_{\rm r}^{\rm c}$. In the latter case the reversal of $\langle I_1^z(0)\rangle$ is slightly incomplete.

It is now a key observation that the critical magnetization is a function of the spin length $M_{\rm r}^{\rm c} = M_{\rm r}^{\rm c}(I)$ and that it *strongly decreases* with increasing spin length I. This is demonstrated in the right panel of Figure 7.4 for spin lengths up to $I = 600$, where a clear power law scaling is found:

$$M_{\rm r}^{\rm c} \approx e^{-\frac{1}{2}} \cdot I^{-\frac{1}{3}} \tag{7.6}$$

Hence, for a large enough value of I the critical magnetization $M_{\rm r}^{\rm c}$ is so close to zero that, up to irrelevant corrections, antiparallel nuclear spin configurations can indeed be swapped. To give a quantitative example, for $I = 10^6$, as typical for the nuclear spin bath of GaAs quantum dots, the above power law leads to $M_{\rm r}^{\rm c} = 0.006$, implying that baths with $I_1^z = -0.988 I_2^z$

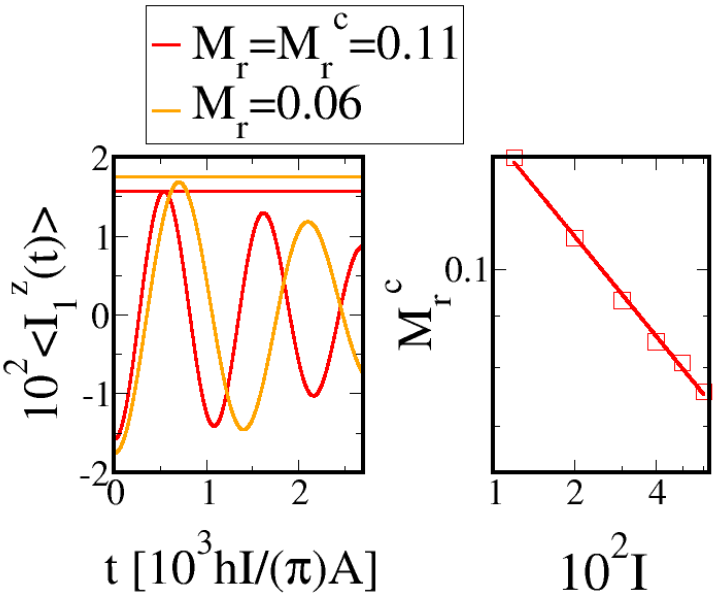

Figure 7.4: In the left panel $\langle I_1^z(t)\rangle$ is plotted for $J_{\rm ex}/(A/2I) = 3.5$, $\Delta = 0$ and $I = 200$. The initial state is $|\alpha\rangle = (1/\sqrt{13})\,(2|\Uparrow\Downarrow\rangle + 3|\Downarrow\Uparrow\rangle)\,|M-I, I\rangle$. Two values of the magnetization $M_{\rm r} = M/(2I+1)$ are considered, where $M_{\rm r} = 0.11$ corresponds to the critical value at $I = 200$. The vertical lines are guides to the eye indicating the value needed for a complete reversal of $\langle I_1^z(t)\rangle$. Obviously the swap for $M < M_{\rm r}^{\rm c}$ is slightly incomplete. In the right panel $M_{\rm r}^{\rm c}$ is plotted versus the spin length I for the same initial state as in the left panel. The fit results in a power law decrease $M_{\rm r}^{\rm c}(I) = e^{-0.5} I^{-0.33}$. Thus, for large enough spin baths antiparallel nuclear spin configurations can, to an excellent degree of accuracy, be swapped.

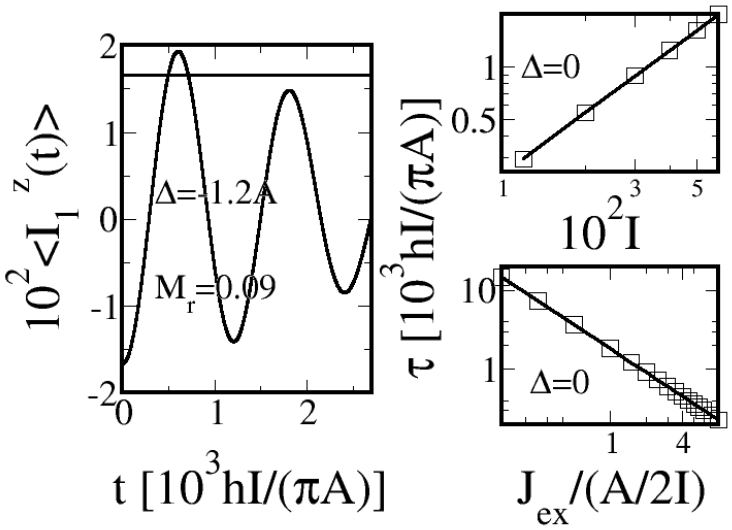

Figure 7.5: The left panel shows $\langle I_1^z(t)\rangle$ for the same situation as in the left panel of Figure 7.4, but with $\Delta = -1.2A$ and $M_\mathrm{r} = 0.09 < M_\mathrm{r}^\mathrm{c}$. Breaking inversion symmetry facilitates swapping the nuclear states. The right panels show the swap time τ at $\Delta = 0$ and $J_\mathrm{ex}/(A/2I) = 3.5$ as a function of I (upper panel), and at $I = 200$ as a function of $(J_\mathrm{ex}/(A/2I))$ (lower panel). In the first case we find a power law as $\tau = e^{0.015} I^{1.19}\,(hI/\pi A)$, in the second case $\tau = e^{7.51}\,[J_\mathrm{ex}/(A/2I)]^{-1.003}\,(hI/\pi A)$.

can be swapped. Finally, in the bottom panel of Figure 7.3 we plot $\langle I_1^z(t)\rangle$ and $\langle I_2^z(t)\rangle$ for $I = 1500$, which is about the largest system size accessible to our numerics. Obviously, we are very close to a full swap.

Moreover, the performance of such a swap process can be significantly improved by departing from the symmetric case $\Delta = 0$, i.e. considering different geometries for the two quantum dots: The left panel of Figure 7.5 shows $\langle I_1^z(t)\rangle$ for the same situation as in the left panel of Figure 7.4, but with $\Delta = -1.2A$ and $M_\mathrm{r} = 0.09$, which is lower than $M_\mathrm{r}^\mathrm{c} = 0.11$ found before for $\Delta = 0$. As can nicely be seen, $\langle I_1^z(0)\rangle$ is still fully reversed. Interestingly, this result turns out to be rather independent of the precise value of $\Delta \neq 0$ including its sign, which suggests that the observed increase of "swap performance" goes back to some qualitative change in the dynamical properties. In fact, as shown in Chapter 4, the spectrum of inversion symmetric systems exhibit a macroscopically large subspace of energetically degenerate multiplets. Although the initial states considered throughout this manuscript lie in energy quite far away from those degenerate levels, it is an interesting question to what extend both observations are related.

Finally, in the right panels of Figure 7.5 we analyze the duration τ of the swap process as a function of the spin length I as well as the ratio $J_\mathrm{ex}/(A/2I)$ for again $\Delta = 0$. In both cases we find power law dependencies leading for a realistic system size of $I = 10^6$ to a swap time τ of a few ten seconds.

As already briefly mentioned in Section 5.4, the nuclear bath is not static. The nuclear spins are interacting through e.g. dipolar and quadrupolar interactions [37]. These could be possible limitations to the phenomena described above. In order to circumvent the resulting problems, one would have to use additional techniques like e.g. refocusing [133].

7.3 Entangling the nuclear baths

In order to measure the entanglement between the long bath spins, we utilize the (logarithmic) negativity L (not to be mixed up with the $\vec{L}^{\,2}$ quantum number introduced in Section 2.3) defined by [134, 135]

$$L = \log_2 \left(\left\| \rho_{\mathrm{n}}^{(1)} \right\|_1 \right) , \tag{7.7}$$

where $\|.\|_1$ denotes the trace norm $\|A\|_1 = \mathrm{Tr}(\sqrt{A^+ A})$ and $\rho_{\mathrm{n}}^{(1)}$ is the partial transpose of ρ_{n} with respect to the first spin $\vec{I}_1$. Since

$$\left\| \rho_{\mathrm{n}}^{(1)} \right\|_1 = 1 + 2 \Big| \sum_i E_i^{<} \Big| , \tag{7.8}$$

where $E_i^{<}$ denote the energy eigenvalues smaller than zero, the negativity essentially measures to what extent the partial transpose fails to be positive, which indicates non-classical correlations [136].

In order to evaluate the dynamics of the negativity, $\rho_{\mathrm{n}}^{(1)}$ has to be diagonalized in each time step considered. This is a numerical effort which restricts us to system sizes somewhat smaller than those considered before. The left panels of Figure 7.6 show the entanglement dynamics for two spin lengths $I = 20, 80$ at comparatively high polarization $M_{\mathrm{r}} = 0.8$ and $\Delta = 0$. The initial state is the same as used before, $|\alpha\rangle = (1/\sqrt{13})\,(2|\Uparrow\Downarrow\rangle + 3|\Downarrow\Uparrow\rangle)\,|M-I, I\rangle$. In both cases the dynamics are rather similar to each other. A rapid increase of the negativity is followed by a more or less regular oscillation around a mean value which increases with the spin length I. In particular, the negativity does not return to zero on the considered time scales.

In order to quantify these observations, we introduce a relative negativity $L_{\mathrm{r}} = L/L_{\mathrm{max}}$, where $L_{\mathrm{max}} = \log_2(2I+1)$ is an upper bound of L (cf. Reference [137]), and analyze the maximum L_{r}^{200} of this quantity attained within a fixed time interval $[0, 200](hI/\pi A)$. The results are plotted in the right panel of Figure 7.6. While the spin lengths achievable here are too small to allow for a quantitatively meaningful fit, the data still shows a significant growth with increasing I (suggesting, in fact, a power law). This observation implies that, similarly as for swapping nuclear spin states, also entangling spin baths benefits from large bath sizes. We note that this effect is not due to the simple growth of the reduced density matrix with increasing I, since we are considering the relative negativity, where such influences are scaled out. On the other hand, by the same argument, the maximal relative negativity should decrease with increasing magnetization at fixed I. An example for this behavior is shown in the left panel of Figure 7.7.

In the right panel of Figure 7.7 we finally demonstrate the influence of a non-zero detuning for different spin lengths and magnetizations. Similarly to the results regarding a nuclear swap, the entanglement is enhanced by a non-zero detuning with its precise value being again of minor importance. This supports the conjecture that the systematic degeneracy reported in Chapter 4 has a clear dynamical signature. Interestingly, breaking the inversion symmetry has stronger influence for higher magnetizations.

7.4 Summary and outlook

In summary we have studied the spin and entanglement dynamics of the nuclear baths in a double quantum dot. Each of the two electron spins was considered to interact with an

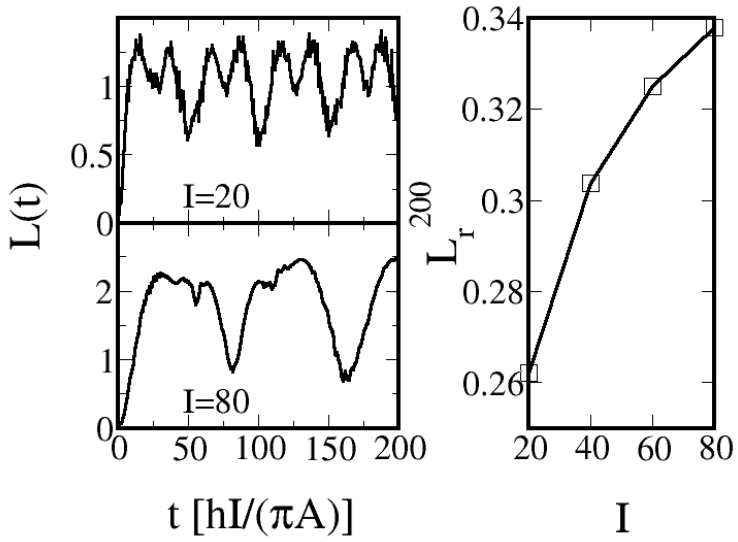

Figure 7.6: In the left panels the negativity $L(t)$ is plotted for the initial state $|\alpha\rangle = (1/\sqrt{13})\,(2|\Uparrow\Downarrow\rangle + 3|\Downarrow\Uparrow\rangle)\,|M-I,I\rangle$ with $M_\mathrm{r} = 0.8$. We consider $I = 20, 80$, $J_\mathrm{ex}/(A/2I) = 3.5$, and $\Delta = 0$. A rapid increase of $L(t)$ is followed by a "regular" oscillation. The negativity does not return to zero on the given time scales. The right panel shows the maximal relative negativity L_r^{200} in the time interval $[0, 200](hI/\pi A)$ as a function of the spin length I for otherwise identical parameters. We find a clearly increasing curve, indicating that for large enough sizes the baths can be fully entangled.

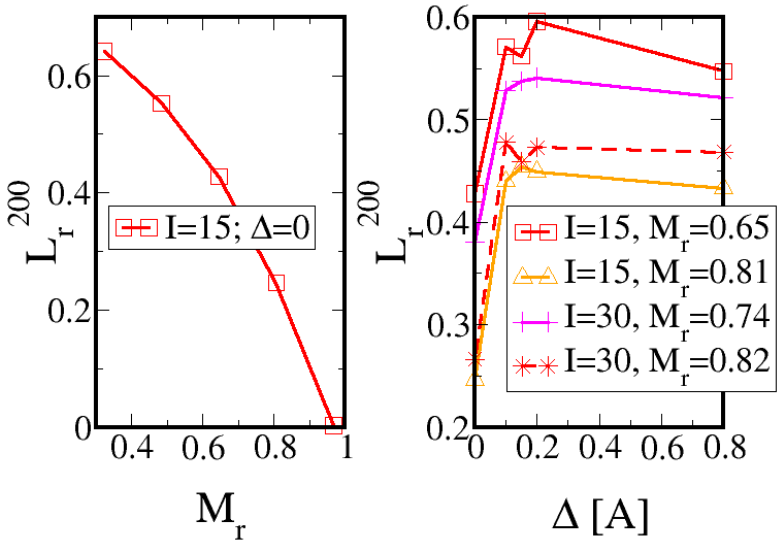

Figure 7.7: The left panel shows the maximal relative negativity L_r^{200} versus M_r for $I = 15$, $\Delta = 0$ and the same initial state as in Figure 7.6. As expected L_r^{200} is decreasing with increasing magnetization. In the right panel L_r^{200} is plotted as a function of the detuning Δ for various parameters. The relative negativity L_r^{200} is increased if the detuning is chosen to be different from zero. The precise value of the detuning is again of no particular importance.

individual bath of nuclear spins via homogeneous hyperfine couplings as in Chapter 4. In order to lower the dimension of the problem, both baths have been approximated by long spins. We focused on the virtue of the hyperfine interaction and regarded the electron spins as an effective coupling between the baths. We demonstrated that it is possible to swap them if they are weakly coupled and their size is large enough. Furthermore, we provided strong indication that, under the same conditions, it might be even possible to fully entangle them. Surprisingly, it turns out to be advantageous to use dots of *different* geometry (enabling for $\Delta \neq 0$) to built up the double quantum dot.

To which extent the described effects are limited by the intra-bath dynamics due to the dipolar and quadrupolar interaction remains an open question, which has to be addressed in future studies. However, even if these interactions turn out to be significant, the proposal could still be combined with additional techniques like refocusing in order to circumvent the resulting problems.

8 Conclusion

Central spin models describe the interaction of a set of central spins to a bath of other spin degrees of freedom. They are of importance in the context of quantum integrability including its relation to physical properties. Furthermore, central spin models describe the hyperfine interaction so that they play a significant role in quantum dot spin qubit based solid state quantum information processing. In the present thesis we studied different aspects of central spin models.

In the first part we focused on the basic properties from an abstract point of view, beginning with a brief introduction to quantum integrability [13–17] and a recapitulation of the systematic degeneracies in the spectrum of the hydrogen atom in Chapter 2. In Chapter 3 we established a new notion of quantum integrability and investigated the integrable structure of central spin models. We related our findings to the phenomenon of decoherence. On the one hand this justifies our approach to quantum integrability, on the other hand it gives new insights with respect to the relation between integrability and physical properties [41–46]. In Chapter 4 we then specified a model of two coupled Gaudin models with homogeneous couplings and studied its spectral properties. Surprisingly, the spectrum turns out to have the extremely scarce property of exhibiting systematically degenerate multiplets. We constructed the full degenerate subspace and discussed possible solid state quantum information perspectives.

As described in the introductory Chapter 5, the electron spin in a III-V semiconductor quantum dot interacts with a large number of nuclear spins via the hyperfine interaction [22, 23]. With respect to quantum information proposals utilizing the electron spin as the qubit the hyperfine interaction has a detrimental character as it provides a decohering environment [21]. However, it opens new quantum information perspectives if it is regarded as an efficient way to access the nuclear spin degrees of freedom [24–29]. The second part of the present thesis was devoted to the study of hyperfine induced spin dynamics in double quantum dots. In this context it has to be distinguished between the case of a strong and the case of a weak magnetic field (1.2) as compared to the strength of the hyperfine interaction. The first case has been subject to numerous theoretical studies and is well-understood [30–35]. We therefore concentrated on the experimentally much more realistic second case. At the time being it is commonly accepted that here one has to resort to exact methods [36, 37]. Motivated by the results of Chapter 3, in Chapter 6 we therefore considered two electron spins in zero magnetic field to interact with a common bath of nuclear spins via homogeneous hyperfine coupling constants, as corresponding to two nearby quantum dots. We investigated the electron spin dynamics and derived a scaling law for the decoherence time. In the next step, presented in Chapter 7, we revisited the two bath model introduced in Chapter 4, which corresponds to spatially well-separated quantum dots. Here we concentrated on the advantages of the hyperfine interaction and numerically studied in how far it enables to utilize

the nuclear ensembles for quantum information purposes. It turns out that it is possible to swap and entangle weakly coupled nuclear spin baths of realistic size, but not smaller ones.

In conclusion the present thesis provides a thorough study of *all* the important aspects of central spin models. Immediate next steps have already been mentioned in the summaries of the different chapters. The investigation of central spin models accounting for interactions within the spin bath (Chapters 3 and 7) as well as the search for hidden symmetries (Chapter 4) turned out to be of particular importance. Rather than dwelling upon possible outcomes of the related (most likely very comprehensive) studies, let us briefly describe two projects which already have been worked out to a large extent, but did not reach completion until the submission of the present thesis. They naturally complement the presented results and will be published in References [138, 139]. In the first project we evaluate the electron spin dynamics within the long spin approximation considered in Chapter 7. Here we distinguish between the case of an exchange coupling which is of the order of the coupling between the electron and the nuclear spins as in Chapter 7 and the case in which it is much larger. The latter is the limit in which the two bath model comes closest to the one bath model considered in Chapter 6. Although the one bath model yields e.g. accurate values for the decoherence times, it is of course an extreme case with respect to a system of two nearby quantum dots. Considered in the above strong coupling limit, the two bath model provides a complementary extreme case. Consequently, together the one and two bath model give a thorough picture of the realistic situation.

As explained in Section 5.4, at the present time it is commonly accepted that the weak field limit can only be considered via exact methods [36, 37]. This imposes strong limitations on the initial state of the system, the system size or the hyperfine coupling constants. Therefore a perturbative approach for the weak field case would be highly desirable. A first step has been presented recently in References [96, 97], where a well-controlled perturbative treatment of the flip-flop terms with $(A/\sqrt{N}B)$ being the small parameter has been established for the Gaudin model. Here A again denotes the overall hyperfine coupling strength. This suggests that for large enough system sizes the weak field limit can be treated perturbatively. Motivated by this result, in the second project we consider homogeneous couplings and investigate the scaling of the flip-flop contributions to the dynamics with N and B for $N_\mathrm{c} = 1$ and $N_\mathrm{c} > 1$, exemplified by $N_\mathrm{c} = 2, 3$. The results suggest perturbative parameters for the two cases, which significantly differ from each other and from the one used in References [96, 97]. In particular they clearly indicate that it is possible to go beyond the weak field limits imposed by $(A/\sqrt{N}B)$. The explicit construction of the associated perturbation theories of course requires a dedicated analysis.

Let us now close the thesis with a final interesting perspective for future research projects. In Section 5.5 we explained that the results of the present thesis are also of great interest with respect to other important nanostructures in the context of spin based solid state quantum information processing. Nitrogen-vacancy centers [103] have been introduced as a structure subject to particularly substantial experimental progress [105–108]. However, so far it has not been managed to bring two of these centers into contact with each other [109, 140, 141]. The particular advantage of carbon structures like nitrogen-vacancy centers is the absence of a large number of nuclear spins, which lead to decoherence of the spin utilized as the qubit. However, even highly purified carbon still contains C^{13} impurities. In Chapter 6 we investigated two electron spins interacting with a *common* bath of nuclear spins. In particular we considered initial states with respect to which the exchange coupling does not have any influence on the dynamics. Consequently, the generated entanglement between the

electron spins resulted exclusively from their interaction through the common bath of nuclear spins. It would now be highly interesting to pursue this route and furthermore investigate to what extent it is possible to adapt the results to the case of two nitrogen-vacancy centers interacting with each other through a small number of C^{13} impurities. Just as the results presented in Chapter 7, this would turn vice into virtue and regard the hyperfine interaction as a resource of quantum information processing.

A Time evolution from full eigensystem

Let H be a time-independent Hamiltonian acting on a product Hilbert space $\mathcal{H} = \otimes_{i=1}^{N} \mathcal{H}_i$. We assume that the Hamiltonian is diagonalized. This can be done numerically as in Chapters 3 and 7 or analytically as in Chapter 6. We denote the eigenvectors by $|\psi_i\rangle$ and the corresponding eigenvalues by E_i. In the following we calculate the time-dependent reduced density matrix for an initial state which is a pure state and derive the time evolution $\langle O_i(t)\rangle$ associated with an operator O_i acting on $\mathcal{H}_i$.

As the eigenstates of H span the whole Hilbertspace $\mathcal{H}$, the initial state $|\alpha\rangle$ of the system described by H can be written as

$$|\alpha\rangle = \sum_i \alpha_i |\psi_i\rangle. \tag{A.1}$$

The time evolution of the initial state results from the application of the time evolution operator $U = e^{-\frac{i}{\hbar}Ht}$. It follows:

$$\begin{aligned} |\alpha(t)\rangle\langle\alpha(t)| &= |U\alpha\rangle\langle U\alpha| \\ &= \sum_{ij} \alpha_i \alpha_j^* |U\psi_i\rangle\langle U\psi_j| \\ &= \sum_{ij} \alpha_i \alpha_j^* e^{-\frac{i}{\hbar}(E_i - E_j)t} |\psi_i\rangle\langle\psi_j| \end{aligned} \tag{A.2}$$

As O_i acts on $\mathcal{H}_i$, the other degrees of freedom have to be traced out

$$\rho_i(t) = \mathrm{Tr}_{\mathcal{H}\setminus\mathcal{H}_i} \left(|\alpha(t)\rangle\langle\alpha(t)| \right),$$

finally giving the time evolution of the expectation value of the operator O_i:

$$\langle O_i(t)\rangle = \mathrm{Tr}_{\mathcal{H}_i} \left(\rho_i(t) O_i \right) \tag{A.3}$$

B Diagonalization of the homogeneous coupling one bath model

In the following we calculate the eigenstates of the homogeneous coupling one bath model $H_{1\mathrm{B}}$ as defined in Equation (6.2). The eigenstates of H_{hom}, defined in Equation (6.3), can be found directly by iterating the well known expressions for coupling a spin of arbitrary length to a spin $S = 1/2$ as given in Equation (4.8) [74]. Two of these states lie fully in the triplet sector

$$\begin{aligned}
|I+1, M, 1\rangle &= \sqrt{\frac{I+M+1}{2I+2} \cdot \frac{I+M}{2I+1}} |I, M-1\rangle|T_+\rangle \\
&+ \sqrt{\frac{I+M+1}{I+1} \cdot \frac{I-M+1}{2I+1}} |I, M\rangle|T_0\rangle \\
&+ \sqrt{\frac{I-M+1}{2I+2} \cdot \frac{I-M}{2I+1}} |I, M+1\rangle|T_-\rangle \qquad \text{(B.1a)} \\
|I-1, M, 1\rangle &= \sqrt{\frac{I-M}{2I} \cdot \frac{I-M+1}{2I+1}} |I, M-1\rangle|T_+\rangle \\
&- \sqrt{\frac{I-M}{I} \cdot \frac{I+M}{2I+1}} |I, M\rangle|T_0\rangle \\
&+ \sqrt{\frac{I+M}{2I} \cdot \frac{I+M+1}{2I+1}} |I, M+1\rangle|T_-\rangle \qquad \text{(B.1b)}
\end{aligned}$$

and are consequently also eigenstates of $H_{1\mathrm{B}}$. As already mentioned in the text of Section 6.1, the states are labeled by the quantum numbers J, M, and S corresponding to the operators $\vec{J}^2, J^z$, and $\vec{S}^2$. The rest of the quantum numbers due to a certain Clebsch-Gordan decomposition of the bath is omitted. For the eigenstates of the central spin term $\vec{S}_1 \cdot \vec{S}_2$ we used the standard notation introduced in Equation (5.32).

The remaining two eigenstates of H_{hom} are superpositions of singlet and triplet states. As the expressions are rather cumbersome, it is convenient to introduce the following notation in order to abbreviate the Clebsch-Gordan coefficients:

$$\begin{aligned}
\{\mu_1^1, \mu_2^1, \mu_3^1, \mu_4^1\} = \Bigg\{ &\sqrt{\frac{I+m}{2I} \cdot \frac{I-m+1}{2I+1}}, \sqrt{\frac{I+m}{2I} \cdot \frac{I+m}{2I+1}}, \\
&\sqrt{\frac{I-m}{2I} \cdot \frac{I-m}{2I+1}}, \sqrt{\frac{I-m}{2I} \cdot \frac{I+m+1}{2I+1}} \Bigg\} \\
\{\mu_1^2, \mu_2^2, \mu_3^2, \mu_4^2\} = \Bigg\{ &\sqrt{\frac{I-m+1}{2I+2} \cdot \frac{I+m}{2I+1}}, \sqrt{\frac{I-m+1}{2I+2} \cdot \frac{I-m+1}{2I+1}}, \\
&\sqrt{\frac{I+m+1}{2I+2} \cdot \frac{I+m+1}{2I+1}}, \sqrt{\frac{I+m+1}{2I+2} \cdot \frac{I-m}{2I+1}} \Bigg\}
\end{aligned}$$

With these definitions the superposition states can be written as:

$$\begin{aligned} |a\rangle &= \mu_1^1|I,m-1\rangle|T_+\rangle + \frac{\mu_3^1-\mu_2^1}{\sqrt{2}}|I,m\rangle|T_0\rangle \\ &- \mu_4^1|I,m+1\rangle|T_-\rangle + \frac{\mu_3^1+\mu_2^1}{\sqrt{2}}|I,m\rangle|S\rangle \end{aligned}$$

$$\begin{aligned} |b\rangle &= \mu_1^2|I,m-1\rangle|T_+\rangle + \frac{\mu_2^2-\mu_3^2}{\sqrt{2}}|I,m\rangle|T_0\rangle \\ &- \mu_4^2|I,m+1\rangle|T_-\rangle - \frac{\mu_3^2+\mu_2^2}{\sqrt{2}}|I,m\rangle|S\rangle \end{aligned}$$

These states are degenerate with respect to H_{hom}. Hence, in order to find the remaining eigenstates of $H_{1\mathrm{B}}$, we are left with the simple task to find a superposition of $|a\rangle$ and $|b\rangle$ which eliminates $|I,m\rangle|S\rangle$. Obviously, this is given by

$$|I,m,1\rangle = \frac{1}{N_T}\left(\frac{\sqrt{2}}{\mu_2^1+\mu_3^1}|a\rangle + \frac{\sqrt{2}}{\mu_2^2+\mu_3^2}|b\rangle\right), \tag{B.2}$$

where $N_T = \sqrt{-(I+1)^{-1}+I^{-1}+4}$ is the normalization constant. Inserting $|a\rangle$ and $|b\rangle$, the state (B.2) reads:

$$\begin{aligned} |I,m,1\rangle &= \frac{1}{N_T}\sum_{i=1}^{2}\left(\frac{\sqrt{2}\mu_1^i}{\mu_2^i+\mu_3^i}|I,m-1\rangle|T_+\rangle\right. \\ &+ (-1)^{i+1}\frac{\mu_3^i-\mu_2^i}{\mu_2^i+\mu_3^i}|I,m\rangle|T_0\rangle \\ &- \left.\frac{\sqrt{2}\mu_4^i}{\mu_2^i+\mu_3^i}|I,m+1\rangle|T_-\rangle\right) \end{aligned} \tag{B.3}$$

Together with the singlet state

$$|I,m,0\rangle = |I,m\rangle|S\rangle \tag{B.4}$$

this solves our problem of diagonalizing the one bath homogeneous coupling Hamiltonian $H_{1\mathrm{B}}$. Furthermore, the states (B.1) and (B.3) give a solution to the very general problem of coupling a spin of arbitrary length to a spin $S = 1$.

C Calculation of the time-dependent reduced density matrix for the homogeneous coupling one bath model

In the following we calculate the time-dependent reduced density matrix for the homogeneous coupling one bath model $H_{1\mathrm{B}}$ defined in Equation (6.2). Following the general scheme presented in Appendix A, we have to write the initial state in terms of energy eigenstates first. As explained in the text of Section 6.1, we consider $|\alpha\rangle = |\alpha_\mathrm{e}\rangle|\alpha_\mathrm{n}\rangle$, where $|\alpha_\mathrm{e}\rangle$ is an arbitrary central spin state and $|\alpha_\mathrm{n}\rangle$ is a product state in the bath Hilbertspace, denoted by $\mathcal{H}_\mathrm{N}$ in the following. Using Equation (6.5) it follows:

$$|\alpha_\mathrm{e}\rangle|\alpha_\mathrm{n}\rangle = \sum_{k=0}^{N_\mathrm{D}^\mathrm{b}} \sum_{\{S_i\}} c_k^{\{S_i\}} |\alpha_\mathrm{e}\rangle \Big| \frac{N}{2} - k, \frac{N}{2} - N_\mathrm{D}^\mathrm{b}, \{S_i\} \Big\rangle \tag{C.1}$$

The eigenstates (B.1), (B.3), and (B.4) are given in terms of product states between an $\vec{S}_1 \cdot \vec{S}_2$ eigenstate as defined in Equation (5.32) and an $\vec{I}^2$ eigenstate. Hence, we can find the coefficients of (A.1) by solving Equations (B.1), (B.3), and (B.4) for these states and inserting them into (C.1). If we arrange the coefficients of the states (B.1), (B.3), and (B.4) into a 4×4 matrix W according to

$$W = \left(\begin{array}{c|cccc} & |T_+'\rangle & |T_0'\rangle & |T_-'\rangle & |S'\rangle \\ \hline |I+1, M, 1\rangle & \ddots & & & \\ |I, M, 1\rangle & & \ddots & & \\ |I-1, M, 1\rangle & & & \ddots & \\ |I, M, 0\rangle & & & & \ddots \end{array} \right), \tag{C.2}$$

this is simply done by transposing W. Here $|T_+'\rangle = |T_+\rangle|I, M-1\rangle$ and analogously for the other states. In order to abbreviate the following expressions, we denote the energy eigenstates by $|\psi_i\rangle$ as in the general considerations in Appendix A and number with respect to (C.2). Analogously we introduce the shorthand notation $|i\rangle$ for the basis states (5.32).

In order to avoid further coefficients, we choose $|\alpha_\mathrm{e}\rangle$ to be the j-th element of (5.32) and find the following expression for the decomposition of the initial state into energy eigenstates

$$|j\rangle|\alpha_\mathrm{n}\rangle = \sum_{l=1}^{4} \sum_{k=0}^{N_\mathrm{D}^\mathrm{b}} \sum_{\{S_i\}} c_k^{\{S_i\}} W_{jl}^T |\psi_l\rangle, \tag{C.3}$$

where it is has to be noted that the elements W_{jl}^T as well as the eigenstates $|\psi_l\rangle$ depend on the quantum numbers the sums run over. Hence, in our case the coefficients α_i and the eigenstates $|\psi_i\rangle$ of Equation (A.1) in fact have more than one index.

Using Equation (C.3) and the eigenstates (B.1), (B.3), and (B.4) in (A.2) and tracing out the bath degrees of freedom, we finally arrive at the reduced density matrix of the two central spins:

$$\rho(t) = \mathrm{Tr}_{\mathcal{H}_\mathrm{N}} \left(|\alpha(t)\rangle\langle\alpha(t)| \right) =$$
$$\sum_{k=0}^{N_\mathrm{D}^\mathrm{b}} \underbrace{\sum_{\{S_i\}} \left(c_k^{\{S_i\}} \right)^2}_{d_k} \sum_{l,m,n,o=1}^{4} W_{jl}^T W_{jm}^T W_{ln} W_{mo} e^{-\frac{i}{\hbar}(E_l - E_m)t} |n\rangle\langle o| \tag{C.4}$$

If we now choose $O_1 = S_1^z$, we have to trace out the second central spin. Inserting the result into (A.3) then gives rise to the time evolution $\langle S_1^z(t) \rangle$. As pointed out in the text of Section 6.2, for high polarizations there is a jump in the amplitude when J_ex is varied away from complete homogeneity. From Equation (C.4) the explanation given in the text becomes more transparent. Clearly, for high polarizations we have $d_k \approx 0$ if $k \neq N_\mathrm{D}^\mathrm{b}$. Fixing l and m, we can calculate the contribution of the different frequencies. It turns out that all of them are suppressed except for $E_2 - E_4 = E_{T_0} - E_S$.

References

[1] P. Zeeman, Phil. Mag. **43**, 226 (1897).

[2] P. Zeeman, Phil. Mag. **44**, 55 (1897).

[3] P. Zeeman, Nature **55**, 347 (1897).

[4] M. Böhm and A. Scharmann, *Höhere Experimentalphysik*, VCH, Weinheim, 1992.

[5] W. Gerlach and O. Stern, Z. Phys. **9**, 349 (1922).

[6] W. Gerlach and O. Stern, Z. Phys. **9**, 353 (1922).

[7] W. Pauli, Z. Phys. **43**, 601 (1927).

[8] P. A. M. Dirac, Proc. R. Soc. Lond. A **117**, 610 (1928).

[9] P. A. M. Dirac, Proc. R. Soc. Lond. A **118**, 351 (1928).

[10] V. I. Arnold, *Mathematical Methods of Classical Mechanics*, Springer, New York, 1978.

[11] F. Göhmann, private communication, 2010.

[12] M. Gaudin, J. Phys. (Paris) **37**, 1087 (1976).

[13] H. Bethe, Z. Phys. **71**, 205 (1931).

[14] K. Yosida, *Theory of Magnetism*, Springer, Berlin, 1996.

[15] L. D. Faddeev, arXiv:9605187, 1995.

[16] A. Klümper, Integrability of Quantum Chains: Theory and Applications to the Spin-1/2 XXZ Chain, in *Quantum magnetism*, edited by U. Schollwöck, volume 645 of *Lect. Notes Phys.*, page 349, Springer, Berlin, 2004.

[17] E. K. Sklyanin and T. Takebe, Phys. Lett. A **219**, 217 (1996).

[18] D. Deutsch and R. Jozsa, Proc. R. Soc. Lond. A **439**, 553 (1992).

[19] L. K. Grover, A fast quantum mechanical algorithm for database search, in *Proceedings, 28th Annual ACM Symposium on the Theory of Computing (STOC)*, page 212, 1996.

[20] P. Shor, SIAM J. Sci. Statist. Comput. **26**, 1484 (1997).

[21] D. Loss and D. P. DiVincenzo, Phys. Rev. A **57**, 120 (1998).

[22] E. Fermi, Z. Phys. **60**, 320 (1930).

[23] A. M. Stoneham, *Theory of Defects in Solids*, Claredon Press, Oxford, 1975.

[24] J. M. Taylor, A. Imamoglu, and M. D. Lukin, Phys. Rev. Lett. **91**, 246802 (2003).

[25] J. M. Taylor, C. M. Marcus, and M. D. Lukin, Phys. Rev. Lett. **90**, 206803 (2003).

[26] J. M. Taylor et al., arXiv:cond-mat/0407640v2, 2004.

[27] H. Schwager, J. I. Cirac, and G. Giedke, Phys. Rev. B **81**, 045309 (2010).

[28] H. Schwager, J. I. Cirac, and G. Giedke, New. J. Phys. **12**, 043026 (2010).

[29] Z. Kurucz, M. W. Sorensen, J. M. Taylor, M. D. Lukin, and M. Fleischhauer, Phys. Rev. Lett. **103**, 010502 (2009).

[30] A. V. Khaetskii, D. Loss, and L. Glazman, Phys. Rev. Lett. **88**, 186802 (2002).

[31] A. V. Khaetskii, D. Loss, and L. Glazman, Phys. Rev. B **67**, 195329 (2003).

[32] W. A. Coish and D. Loss, Phys. Rev. B **70**, 195340 (2004).

[33] W. A. Coish and D. Loss, Phys. Rev. B **72**, 125337 (2005).

[34] D. Klauser, W. A. Coish, and D. Loss, Phys. Rev. B **73**, 205302 (2006).

[35] D. Klauser, W. A. Coish, and D. Loss, Phys. Rev. B **78**, 205301 (2008).

[36] J. Schliemann, A. V. Khaetskii, and D. Loss, J. Phys.: Condens. Mat. **15**, R1809 (2003).

[37] W. A. Coish and J. Baugh, phys. stat. sol. (b) **246**, 2203 (2009).

[38] R. Steinigeweg, J. Gemmer, and M. Michel, Europhys. Lett. **75 (3)**, 406 (2006).

[39] L. F. Santos and A. Mitra, arXiv:1105:0925, 2011.

[40] C. Emary and T. Brandes, Phys. Rev. Lett. **90**, 044101 (2003).

[41] J. Lages, V. V. Dobrovitski, M. I. Katsnelson, H. A. D. Raedt, and B. N. Harmon, Phys. Rev. E **72**, 026225 (2005).

[42] A. Relano, J. Dukelsky, and R. A. Molina, Phys. Rev. E **76**, 046223 (2007).

[43] S. R. Dahmen, J. Links, R. H. McKenzie, and H.-Q. Zhou, J. Stat. Mech. , P10019 (2004).

[44] K. Kudo and T. Deguchi, Phys. Rev. B **68**, 052510 (2003).

[45] R. M. Angelo, K. Furuya, M. C. Nemes, and G. Q. Pellegrino, Phys. Rev. E **60**, 5407 (1999).

[46] T. Gorin and T. H. Seligman, Phys. Lett. A **309**, 61 (2003).

[47] J. Schliemann, A. V. Khaetskii, and D. Loss, Phys. Rev. B **66**, 245303 (2002).

[48] H. Frahm, J. Phys. A: Math Gen. **26**, L473 (1993).

[49] B. Erbe and H.-J. Schmidt, J. Phys. A: Math. Theor. **43**, 085215 (2010).

[50] A. Ballesteros and O. Ragnisco, J. Phys. A: Math. Theor. **31**, 3791 (1998).

[51] A. Ballesteros, F. Musso, and O. Ragnisco, J. Phys. A: Math. Theor. **35**, 8197 (2002).

[52] A. Ballesteros and A. Blasco, J. Phys. A: Math. Theor. **41**, 304028 (2008).

[53] V. G. Drinfel'd, Quantum groups, in *Proceedings of the International Congress of Mathematicians; Berkeley, California, USA, 1986*, edited by A. M. Gleason, page 798, 1987.

[54] V. Chari and A. Pressley, *A guide to quantum groups*, Univ. Press, Cambridge, 1994.

[55] Y. Manin, On the Mathematical Work of Vladimir Drinfel'd.

[56] D. Garajeu and A. Kiss, J. Math. Phys. **42**, 3497 (2001).

[57] T. Guhr, A. Müller-Groeling, and H. A. Weidenmüller, Phys. Rep. **299**, 189 (1998).

[58] M. L. Mehta, *Random matrices*, Acad. Press, San Diego, 1991.

[59] F. Haake, *Qantum Signatures of Chaos*, Springer, Berlin, 2001.

[60] O. Bohigas, M. J. Giannoni, and C. Schmit, Phys. Rev. Lett. **52**, 1 (1984).

[61] J. Schliemann, Phys. Rev. B **81**, 081301(R) (2010).

[62] J. von Neumann and E. Wigner, Phys. Z. **30**, 467 (1929).

[63] L. D. Landau and M. E. Lifschitz, *Quantum mechanics*, Butterworth Heinemann, Amsterdam, 2005.

[64] W. Pauli, Z. Phys. **36**, 336 (1926).

[65] G. A. Baker, Phys. Rev. **103**, 1119 (1956).

[66] F. D. M. Haldane, Z. N. C. Ha, J. C. Talstra, D. Bernard, and V. Pasquier, Phys. Rev. Lett. **69**, 2021 (1992).

[67] B. Erbe and J. Schliemann, Phys. Rev. Lett. **105**, 177602 (2010).

[68] F. H. L. Essler, H. Frahm, F. Göhmann, A. Klümper, and V. E. Korepin, *The one-dimensional Hubbard model*, Cambridge Univ. Press, Cambridge, 2005.

[69] R. Steinigeweg and H.-J. Schmidt, Math. Phys. Anal. Geom. **12**, 19 (2009).

[70] J. A. D. Loera and T. B. McAllister, Exp. Math. **15**, 7 (2006).

[71] W. Zhang, N. Konstantinidis, K. A. Al-Hassanieh, and V. V. Dobrovitski, J. Phys.: Condens. Mat. **19**, 083202 (2007).

[72] J. M. Taylor et al., Phys. Rev. B **76**, 035315 (2007).

[73] B. Erbe and J. Schliemann, J. Phys. A: Math. Theor. (Fast Track Communication) **43**, 492002 (2010).

[74] F. Schwabl, *Quantum Mechanics*, Springer, Berlin, 2002.

[75] J. R. Petta et al., Science **309**, 2180 (2005).

[76] F. H. L. Koppens et al., Nature (London) **442**, 766 (2006).

[77] L. P. Kouwenhoven, J. R. Petta, S. Tarucha, and L. M. K. Vandersypen, Rev. Mod. Phys. **79**, 1217 (2007).

[78] P. F. Braun et al., Phys. Rev. Lett. **94**, 116601 (2005).

[79] S. Amaha et al., Solid State Comm. **119**, 183 (2001).

[80] R. Takahashi, K. Kono, S. Tarucha, and K. Ono, arXiv:1012.4545, 2010.

[81] P. Y. Yu and M. Cardona, *Fundamentals of Semiconductors*, Springer, Heidelberg, 2005.

[82] R. Winkler, *Spin-orbit Coupling Effects in Two-Dimensional Electron and Hole Systems*, Springer, Berlin, 2003.

[83] L. Jacak, P. Hawrylak, and A. Wojs, *Quantum Dots*, Springer, Berlin, 1998.

[84] X. Wen-Fang, Commun. Theor. Phys. (Beijing, China) **42**, 923 (2004).

[85] L. L. Foldy and S. A. Wouthuysen, Phys. Rev. **78**, 29 (1950).

[86] A. Barenco et al., Phys. Rev. A **52**, 3457 (1995).

[87] D. Klauser, W. A. Coish, and D. Loss, Electron and hole spin dynamics and decoherence in quantum dots, in *Semiconductor Quantum Bits*, edited by O. Benson and F. Henneberger, World Scientific, 2008.

[88] J. Berezovsky, M. H. Mikkelsen, N. G. Stoltz, L. A. Coldren, and D. D. Awschalom, Science **320**, 349 (2008).

[89] D. Press, T. D. Ladd, B. Zhang, and Y. Yamamoto, Nature **456**, 218 (2008).

[90] P. Maletinsky, *Polarization and Manipulation of a Mesoscopic Nuclear Spin Ensemble Using a Single Confined Electron Spin*, PhD thesis, Eidgenössische Technische Hochschule Zürich, 2008.

[91] J. Baugh, Y. Kitamura, K. Ono, and S. Tarucha, Phys. Rev. Lett. **99**, 096804 (2007).

[92] J. Baugh, Y. Kitamura, K. Ono, and S. Tarucha, phys. stat. sol (c) **5**, 302 (2008).

[93] H. Ribeiro and G. Burkard, Phys. Rev. Lett. **102**, 216802 (2009).

[94] H. van Houten and C. W. J. Beenakker, Physics Today **49**, 22 (1996).

[95] V. N. Golovach, A. V. Khaetskii, and D. Loss, Phys. Rev. Lett. **93**, 016601 (2004).

[96] L. Cywinski, W. M. Witzel, and S. D. Sarma, Phys. Rev. Lett. **102**, 057601 (2009).

[97] L. Cywinski, W. M. Witzel, and S. D. Sarma, Phys. Rev. B **79**, 245314 (2009).

[98] M. Bortz and J. Stolze, J. Stat. Mech. , P06018 (2007).

[99] B. Trauzettel, D. V. Bulaev, D. Loss, and G. Burkard, Nature Physics **3**, 192 (2007).

[100] J. Fischer, B. Trauzettel, and D. Loss, Phys. Rev. B **80**, 155401 (2009).

[101] M. Stobinska, G. J. Milburn, and L. Stobinski, arXiv:0912.3547, 2009.

[102] P. Recher and B. Trauzettel, Nanotechnology **21**, 302001 (2010).

[103] F. Jelezko and J. Wrachtrup, phys. stat. sol. (a) **203**, 3207 (2006).

[104] J. L. Truitt et al., Si/SiGe Quantum Devices, Quantum Wells, and Electron-Spin Coherence, in *Electron Spin Resonance and Related Phenomena in Low-Dimensional Structures*, edited by M. Fanciulli, Springer, Heidelberg, 2009.

[105] J. Schliemann, Physik Journal, 9. Jhg., Oktober 2010.

[106] P. Neumann et al., Science **329**, 542 (2010).

[107] D. M. Toyli, C. D. Weis, G. D. Fuchs, T. Schenkel, and D. D. Awschalom, Nano Lett. **10**, 3168 (2010).

[108] E. Togan et al., Nature **466**, 730 (2010).

[109] W. Yang, Z. Xu, M. Feng, and J. Du, New J. Phys. **12**, 113039 (2010).

[110] Q. Li, L. Cywinski, D. Culcer, X. Hu, and S. D. Sarma, Phys. Rev. B **81**, 085313 (2010).

[111] D. Culcer, L. Cywinski, Q. Li, X. Hu, and S. D. Sarma, Phys. Rev. B **82**, 155312 (2010).

[112] M. Raith, P. Stano, and J. Fabian, arXiv:1101.3858, 2011.

[113] A. Wild et al., New J. Phys. **12**, 113019 (2010).

[114] M. Leuenberger and D. Loss, Nature **410**, 789 (2001).

[115] J. Tejada, E. Chudnovsky, E. del Barco, J. Herandez, and T. Spiller, Nanotechnology **12**, 181 (2001).

[116] N. V. Prokof'ev and P. C. E. Stamp, Phys. Rev. Lett. **80**, 5794 (1998).

[117] W. Wernsdorfer et al., Phys. Rev. Lett. **84**, 2965 (2000).

[118] W. Wernsdorfer, R. Sessoli, A. Caneschi, D. Gatteschi, and A. Cornia, Europhys. Lett. **50**, 552 (2000).

[119] A. Ardavan et al., Phys. Rev. Lett. **98**, 057201 (2007).

[120] B. E. Kane, Nature **393**, 133 (1998).

[121] S. R. Schofield et al., Phys. Rev. Lett. **91**, 136104 (2003).

[122] D. N. Jamieson et al., Appl. Phys. Lett. **86**, 202101 (2005).

[123] A. Morello et al., Nature **467**, 687 (2010).

[124] L. Dreher et al., Phys. Rev. Lett. **106**, 037601 (2011).

[125] J. J. L. Morton et al., Nature **455**, 1085 (2008).

[126] B. Erbe and J. Schliemann, Phys. Rev. B **81**, 235324 (2010).

[127] W. K. Wootters, Phys. Rev. Lett **80**, 2245 (1998).

[128] J. M. Kikkawa and D. Awschalom, Phys. Rev. Lett. **80**, 4313 (1998).

[129] F. H. L. Koppens et al., Science **309**, 1346 (2005).

[130] F. H. L. Koppens, K. C. Nowack, and L. M. K. Vandersypen, Phys. Rev. Lett. **100**, 236802 (2008).

[131] I. A. Merkulov, A. L. Efros, and M. Rosen, Phys. Rev. B **65**, 205309 (2002).

[132] B. Erbe and J. Schliemann, arXiv:1101.6011, 2011.

[133] C. Deng and X. Hu, IEEE Trans. Nanotechnology **4**, 35 (2005).

[134] G. Vidal and R. F. Werner, Phys. Rev. A **65**, 032314 (2002).

[135] M. Plenio, Phys. Rev. Lett. **95**, 090503 (2005).

[136] A. Peres, Phys. Rev. Lett. **77**, 1413 (1996).

[137] A. Datta, S. Flammia, and C. Caves, Phys. Rev. A **72**, 042316 (2005).

[138] B. Erbe and J. Schliemann, Hyperfine induced electron spin and entanglement dynamics in double quantum dots: The case of separate baths, in preparation, 2011.

[139] B. Erbe and J. Schliemann, Perturbative regimes in central spin models, in preparation, 2011.

[140] H. Fedder, private communication, 2011.

[141] P. Neumann et al., Nature Physics **6**, 249 (2010).

Acknowledgements

In the following I want to thank a number of people, who directly or indirectly contributed to the present thesis.

- First of all I would like to thank my supervisor John Schliemann. He not only shared his deep physical understanding with me, but also taught me a purposeful and efficient style of scientific working, without limiting my independence. Apart from that, he made it possible for me to attend many valuable conferences and supported me in every vocational respect.
- I would like to thank Jaroslav Fabian for acting as the co-referee to the present thesis.
- For proofreading the thesis I want to express my gratitude to Christian Neupert, Andreas Scholz, and Maxim Trushin.
- I want to thank Lizy Lazar for constant support in administrative issues and beyond.
- I would like to express my gratitude to all colleagues and friends I was allowed to meet during the time of my PhD studies in Regensburg. In particular I want to mention Carmen and Clemens Vierheilig, Christoph Schenke, Manohar Awasthi, Sergey Smirnov, Johannes Hausinger, Alexander Lopez, Andreas Scholz, Martin Raith, Francisco Mireles, Markus Leitl, Hans-Jürgen Möstl as well as the 3.1.09-diploma crew (including the non-Grifoni parts).
- Financial support through the SFB 631: "Solid-State Based Quantum Information Processing" is gratefully acknowledged.

My biggest thanks goes to my parents for their care and endless support.
This thesis is dedicated to them.